POTENTIALS OF POLYLACTIDE- CHITIN COMPOSITES AS FEMORAL SCAFFOLD IN ORTHOPAEDICS

By

GBENEBOR Oluwashina Philips
B.Sc. (Hons Lagos), M.Sc. (Lagos)
(010406057)

A Thesis submitted to the School of Postgraduate Studies, University of Lagos in partial fulfillment of the requirements for the award of the degree of Doctor of Philosophy (Ph.D.)

Metallurgical and Materials Engineering

DEPARTMENT OF METALLURGICAL AND MATERIALS ENGINEERING,
UNIVERSITY OF LAGOS, NIGERIA

OCTOBER, 2017
SCHOOL OF POST UATE STUDIES
UNIVERSITY OF LAGOS, AKOKA, LAGOS

CERTIFICATION

This is to certify that the thesis

POTENTIALS OF POLYLACTIDE-CHITIN COMPOSITES AS FEMORAL SCAFFOLD IN ORTHOPAEDICS

Submitted to the School of Postgraduate Studies, University of Lagos in partial fulfillment of the award of the degree of Doctor of Philosophy (Ph.D.) is a record of original research carried out

By

GBENEBOR Oluwashina Philips

In the Metallurgical and Materials Engineering

……	…….	....……..
AUTHOR'S NAME	SIGNATURE	DATE
……	…….	....……..
FIRST SUPERVISOR'S NAME	SIGNATURE	DATE
……	…….	....……..
SECOND SUPERVISOR'S NAME	SIGNATURE	DATE
……	…….	....……..
1st INTERNAL EXAMINER'S NAME	SIGNATURE	DATE
……	…….	....……..
2nd INTERNAL EXAMINER'S NAME	SIGNATURE	DATE
……	…….	....……..
EXTERNAL EXAMINER'S NAME	SIGNATURE	DATE
……	…….	....……..

DEDICATION

I dedicate this to Almighty God

ACKNOWLEDGEMENTS

I express my profound gratitude to God Almighty who has been my source of strength and sustenance throughout the course of this study.

My sincere gratitude goes to my supervisor Prof. S.O. Adeosun who has been a father to me in all ramifications for his patience, guidance and constructive criticism with infallible contributions to this work. My second supervisor, Prof. G.I. Lawal who also has been a father to me, deserves my gratitude for being there when necessary. The encouragement and support of Prof. S.B. Hassan, the Head of the Department is greatly acknowledged. I appreciate the tremendous supports offered by Dr. M.O.H Amuda, the Departmental Postgraduate coordinator and his assistant, Dr. H. Mgbemere. The encouragement of Prof. D.E. Esezebor and Dr. J.O. Agunsoye cannot be quantified. I am also grateful to Dr. M. Bodude, Dr. O.I. Sekunowo, Dr. L.O. Osoba, Dr. B.O. Bolasodun, Dr. W. Ayoola, Dr. (Mrs.) F. Ochulor, Dr. (Mrs.) E.O. Obidiegwu, Dr. (Mrs.) T. Oladoye, A. Agbeleye, S.I. Durowaye, H.O. Onovo, who contributed immensely and remarkably towards the success of this work. The contributions of the technologists in the Metallurgical and Materials Engineering Laboratory; Messrs Sulyman, Oduaran, Ugwuozor, Pogoson, Alonge, Surakat and Mrs Cole, University of Lagos is greatly acknowledged. Mrs. Opomulero, Adenusi, Ibeh, Kemi, Otseumeno, Bamgbelu and Mr. Iyiade were of great help towards the success of this work. I also appreciate the contributions of my numerous friends including Dr. E.I. Akpan, Mr. Seyi Taiwo, etc. I am grateful to my dear parents Engr. and Mrs. F.E. Gbenebor, my brother and sister, Tunde and Esther Gbenebor for their assistance, cooperation and prayers. I am also thankful to my Father and mother in-laws, Warrant Officer. and Mrs. G. Aiyegoro for their goodwill and interest shown that enabled the completion of the work. My sincere gratitude goes to my wife, Mrs. A.D. Gbenebor and son, Eromosele Gbenebor for their understanding and cooperation; I appreciate their prayers and patience.

The assistance rendered by University of Lagos- Nigeria, Redeemer's University- Nigeria, Covenant University- Nigeria and Soochow University- China are thankfully acknowledged for making their facilities available for this study.

Above all, I am grateful to God the Father, the Son and the Holy Ghost. He has spoken and also fulfilled.

ABSTRACT

Over the last two decades, several materials such as metals, polymers and composites have been used as implants in the body. Metallic implants have proven to cause stress shielding, toxic corrosion products and necessity for re-surgery. On the other hand, synthetic polymers possess poor stiffness and cause inflammation. The quest in making up for the disadvantages of these materials has culminated in a paradigm shift to the use of biodegradable and biocompatible polymers such as polylactide (PLA). However, PLA is hydrophobic and displays very low elastic modulus (1.9 - 4.1 GPa) compared to that of bone human (10 – 30 GPa). The low elastic modulus inhibits load transfer to the healing bone while hydrophobicity induces low affinity for living tissues. Therefore, this study is aimed at increasing the elastic modulus of PLA and making it hydrophilic by reinforcing with α-chitin (a structural polysaccharide), which is biodegradable and biocompatible. Chemical treatment method was employed in extracting chitin from crab and shrimp exoskeletons with the use of 0.4, 0.8 and 1.2M concentrations of both HCl and NaOH for demineralization and deproteinization processes respectively. Characterizations such as Fourier Transform Infrared Spectroscopy (FTIR), thermogravimetric analysis (TGA), Scanning Electron Microscope (SEM) and X-ray diffraction (XRD) were carried out on the extracted samples. The PLA-chitin composites were produced via slip casting where PLA was dissolved in dichloromethane (DCM) at room temperature (32 ^{0}C) and 10, 20 and 30 wt. % α-chitin with the lowest acetylation degree (DA) were added. In vitro degradation examination was carried out by immersing samples in phosphate buffered solution (PBS) maintained at pH 7.4 and at 37 ^{0}C for designated periods. Biodegradation of samples were studied by determining times of hydrolysis T_H and diffusion T_D. The presence of two amide I peaks formed between 1661-662 cm^{-1} and 1626-1628cm^{-1} in the FTIR spectra of treated shells revealed that chitin extracted from these two sources have α-form. Increasing concentrations of HCl and NaOH reduced DA from 99.4 - 63.7%. X- Ray reflections were observed on (021), (110), (120) and (013) planes. The crystalline index (Crl) ranged between 65.5 and 87.4 %, while thermal stabilities measured from activation energy (E_a) were between 100.12 and 139.63kJ/mol. There was reduction of hydrogen bond energy (E_H) from 5.25 - 4.52 kCal for α-chitin samples with increase in concentrations of HCl and NaOH. The addition of α-chitin to PLA increased its elastic modulus from 3.64 GPa to 10.1- 33 GPa. Composites of PLA-chitin degraded via bulk hydrolysis as $T_H >> T_D$ where 16.13-11.8 x 10^6 s and 33.67-15.00 m^2/s were measured for T_H and T_D respectively. Hydrolysis of PLA was accelerated on addition of hydrophilic chitin with weight loss from 16.22 - 66.02 %. The results of this study also showed non-toxic degradation products as the pH of PBS stood between 7.4 and 7.37 at 37 ^{0}C, which is similar to human physiological conditions. Thus, PLA-chitin composites can serve as a potential substitute for metallic and fossil based polymers as femoral scaffolds in orthopaedic applications.

Keywords: Biodegradation, hydrolysis, In-vitro, polylactide-chitin composite, phosphate buffered solution

TABLE OF CONTENTS

LIST OF FIGURES

LIST OF TABLES

LIST OF ABBREVATIONS

CH_3COOH	Acetic acid
DCM	Dichloromethane
DMA	Dynamic mechanical analysis
DSC	Differential Scanning Calorimetry
EDS	Energy Dispersive X-Ray Analysis
FTIR	Fourier Transform Infrared Spectroscopy
GPC	Gel Penetration Chromatography
HCl	Hydrochloric acid
HCOOH	Formic acid
HNO_3	Nitric acid
hr/hrs	Hour/hours
NaOH	Sodium hydroxide
PB	Polybutylenessuccinate
PBC	Polybutylenessuccinate-co-ε-caprolactone
PBL	Polybutylene succinate-co-L-lactate
PBS	Phosphate buffered solution
PCL	poly (ε-caprolactone)
PDLA	Poly-D, L-lactic acid
PEG	Poly (ethylene glycol)
PLDLLA	Poly-L- lactide- co-D, L – lactide
PLGA	Polylactide-co-glycolide
PHAs	Poly (hydroxyalkanoates)
POM	Polarizing Optical Microscopy
SEM	Scanning Electron Microscopy

SMCs	Smooth muscle cells
TGA	Thermogravimetric Analysis
WAXD	Wide-angle X-Ray Diffraction
XRD	X-Ray Diffraction
XRF	X-Ray Fluorescence

SYMBOLS AND NOTATIONS

A_{1650}	Absorbance of amide I vibration (%)
A_{3450}	Absorbance of OH vibration (%)
Crl	Crystallinity index (%)
D	Diffusion coefficient (m^2/s)
DA	Acetylation degree (%)
D_{hkl}	Crystalline size (A)
E_a	Activation energy (kJ/mol)
E_H	Hydrogen bond energy (kcal)
Ia	Intensity of amorphous region (au)
I_c	Intensity of crystalline region (au)
T_D	Diffusion time (s)
T_H	Hydrolysis time (s)
T_{max}	Temperature at which material decomposition rate was rapid (^0C)
T_{onset}	Temperature for the onset of thermal decomposition (^0C)
X	Degree of material decomposition during TGA (no unit)
V_o	Frequency corresponding to free OH groups (3600 cm^{-1})
W_o	Initial weight of specimen (g)
W_f	Final weight of specimen (g)
V	Frequency of the bonded OH group (cm^{-1})
β	Width of the crystalline peak at half height (rad)
θ	Diffraction angle corresponding to the crystalline peak (deg)

CHAPTER ONE

1.0 INTRODUCTION

1.1 Background of the Study

The advent of materials for bone fixation over the last two decades has significantly improved the efficiency of orthopaedic surgery. Materials used as potential medical devices must be biocompatible with body tissues, have good mechanical strength and corrosion resistance (Seal *et al.*, 2009). However, frequently used metallic implants such as stainless steels, cobalt, magnesium and titanium-base alloys are stiffer than the bone and weakening of the recuperating bone often occurs after implantation owing to this high implants moduli. The elastic moduli of titanium alloy (Ti6Al4V), stainless steel and chrome-cobalt alloys are 120 (Elias *et al.*, 2008), 200 and 230 GPa respectively (Seal *et al.*, 2009). The elastic moduli mismatch between the human bone, 10-30 GPa (Elias *et al.*, 2008) and metallic implants cause stress shielding and do not favour effective bone healing. Corrosion products of these metals are toxic to body tissues and often trigger inflammation (Hansen, 2008).Wear alongside corrosion is a surface degradation process that has limited the use of metals such as titanium as biomedical devices (Mitchell and Shrotriya, 2007). Contact between surfaces of artificial joints could lead to the formation of particulate and soluble metallic debris that can migrate locally or systemically and in process energize inflammatory events. There has also been an issue of metallic implants causing interference with imaging techniques such as X-rays hindering the fracture and bone healing to be easily observed (Figure 1).The desire to circumvent the disadva

ntages of metallic fixations usage has culminated in a paradigm shift to the use of biodegradable polymers that are light weight with low elastic moduli between 0.4-7 GPa (Farrar, 2005; Gunatillake and Adhikari, 2003). These biomaterials or devices break down over time into harmless by-products that can be eliminated from the body through natural pathways and ideally, leave no sign of the injury or repair. Unlike the metallic implants, biodegradable implants do not interfere with X-ray imaging which enables bone healing to be easily observed as shown in Figure 2.The most commonly investigated and widely used biodegradable polymer is polylactide/lactic acid (PLA), (Vieira *et al.,* 2011), which is a linear aliphatic thermoplastic polyester derived from 100% renewable sources such as corn (Xiao *et al.,* 2012). The polymer's biodegradability is utilized in biomedical applications such as sutures and drug delivery systems (Huertas *et al.,* 2010) due to their bioresorbable tendency (Pina and Ferreira, 2012), biocompatibility, availability and low cost of manufacture (Pinto *et al.,* 2013). Polylactide has been fabricated into scaffolds with controlled loading efficiency in tissue engineering (Jiang *et al.,* 2010). However, the use of conventional PLA has encountered challenges namely poor hydrophylicity and a much lower stiffness compared to the human bone (Bijarimi *et al.,* 2012). Improving the strength characteristics of PLA will require the use of biocompatible and biodegradable organic materials like chitin as fillers whose structural make up promotes mechanical strength of its host. Chitin is a naturally occurring structural polysaccharide that is biosynthesized by large number of organisms including crustaceans such as crab (Isa *et al*., 2012), lobster (Boßelmann *et al.,* 2007), shrimp (Abdou *et al.,* 2008; Andrade *et al.,* 2012), insects (Arakane *et al.,* 2008) and fungi (Malinovsky *et al.*,2014).

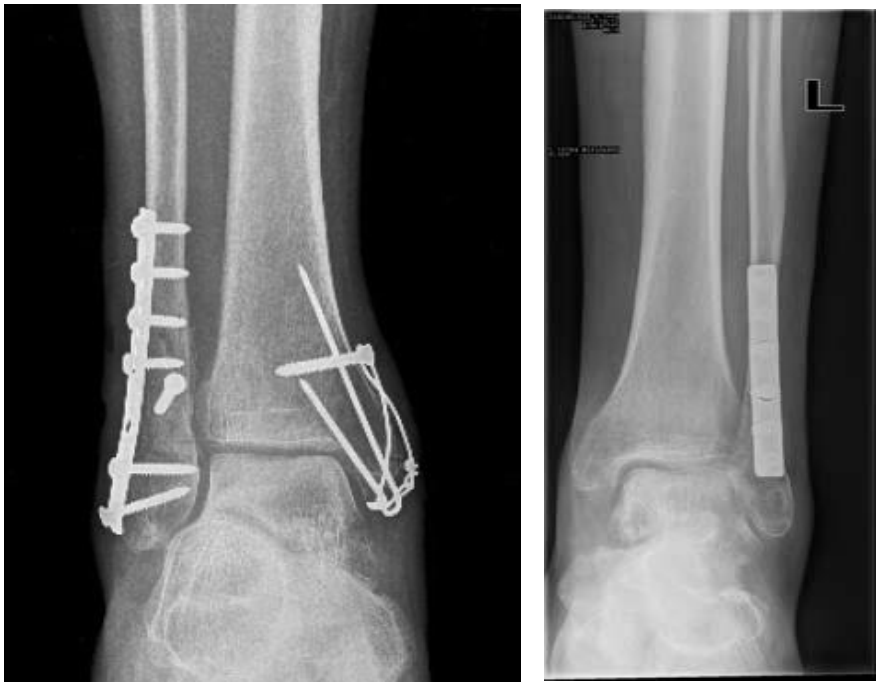

Figure 1: X-rays of ankle fractures fixed with metal where visualization of the fracture is obscured (Fuchs *et al.*, 2003)

Figure 2: X-rays of ankle fractures fixed using biodegradable implants with fully visible bone Version (Fuchs *et al.*, 2003)

The chitin-biopolymer has found applications as sponges and bandages for the treatment of wounds and suture threads owing to its appreciable biocompatibility, biodegradability and non-toxicity (Azuma *et al.,* 2015). In its α-form (obtained from crab and shrimp shells), chitin is confirmed to have best crystalline structure as its anti-parallel arrangement gives rise to extensive hydrogen bonding that culminates in its high structural flexibility (Nikolov *et al.,* 2011). These hydrogen bonds are known to play important roles in determining the conformational and mechanical properties of structural polysaccharides (Ciolacu *et al.,* 2010).

1.2 Statement of the Problem

Polylactide with its biocompatibility possesses much lower elastic modulus between 1.9 - 4.1 GPa (Shakoor *et al.,* 2013) compared to bone (10 – 30GPa). Thus, little or no load is transferred to the bone during healing. Therefore, there is need to enhance the stiffness of PLA through the use of biopolymer reinforcement to make the composite have comparable elastic modulus with that of bone. Polylactide is also noted to be strongly hydrophobic and can elicit an inflammatory response from the tissues of living hosts due to its low affinity with cells when used as tissue engineering material (Xiao *et al.,* 2012). Thus, there is need to reinforce PLA with a biopolymer that will improve its hydrolytic degradation potential at normal human body temperature in addition to its improved stiffness. On the other hand, it should be noted that application of chitin in the industry is limited due to its poor reactivity and solubility in aqueous media owing to its low content of amino groups (Khong, 2013). Hence, there is need to synthesize chitin with considerable amount of amino groups that will enhance its hydrophylicity without compromising its strengthening features.

1.3 Aim and Objectives of the Study

1.3.1 Aim

The study is aimed at developing PLA-chitin composite suitable as temporary supporting devices for orthopaedics.

1.3.2 Specific Objectives

The objectives are to:

1. extract α-chitin from crab and shrimp exoskeletons and evaluate the influence of acid and alkali concentrations on its acetylation degree (DA)
2. study the crystal structure, thermal stability and hydrogen bond energy of extracted α - chitin
3. investigate the influence of α - chitin addition on the stiffness of PLA
4. study the biodegradation of PLA-chitin composites and their suitability as temporary supporting devices in orthopaedics.

1.4 Significance of the Study

Natural polymers such as PLA and chitin can be obtained from agricultural products. The use of these materials in bone tissue engineering will reduce dependence on fossil fuels and check energy, environmental and global warming issues. Developing biodegradable PLA-chitin composites having comparable stiffness to that of human bone will limit complications during healing and the need for re-surgery will be avoided. This will enhance the economic situation of the country through investments not only in the production of the matrix and reinforcement sources, and materials but in the production of the scaffold for orthopaedics use. The health of othopaedic patients will improve and the citizens will be better for it.

1.5 Scope and Delimitation of the Study

This study covers extraction of chitin from crab and shrimp shells using varying concentrations of HCl and NaOH. Physicochemical characterizations to determine the DA, hydrogen bond energy, thermal stability, crystallinity and morphology are carried out to investigate the efficiency and efficacy of extracted samples. The chitin with the lowest DA is chosen as reinforcement material on corn starch PLA. Composites produced are subjected to In-vitro degradation in PBS under human physiological conditions where stiffness and biodegradation studies are carried out after immersion. However, this study does not cover In-vivo experimentation.

1.6 Definition of Operational Terms

Acetylation degree: Portion of N-acetyl-d-glucosamine units with respect to the total number of units. It is used to define chitin and chitosan. For chitosan, DA is considered to be below 50%.

Activation energy: A minimum amount of energy required to initiate a reaction. It is also used to determine the thermal stability of materials.

Biodegradable: A material that can break down into natural substances in the environment without causing harm.

Biopolymer: A polymer sourced from living organisms.

Bioresorbable: A material that can be broken down and absorbed by the body without the need for manual removal.

Crystallinity: The degree of structural order in a material.

Elastic modulus:	A material property that describes its stiffness and it is one of the most important properties of solid materials. It is also known as modulus of elasticity, Young's Modulus or tensile modulus.
Hydrolysis:	Cleavage of chemical bonds by the addition of water.
Hydrophilic:	Having a strong affinity for water and dissolving in it very easily.
In0vitro	A biological process performed with microorganisms, cells or biological molecules outside their normal biological context. It is often called "test tube experiments".
In-vivo	Entails experiment in which effects of various biological entities are tested on living organisms or cells usually animals, including humans and plants as opposed to a tissue extract or dead organism..
Morphology:	The size, shape, texture and phase distribution of internal objects of a material.
Orthopaedics	The medical specialty concerned with the correction of deformities or functional impairments of the skeletal system.
Polysaccharides:	Polymeric carbohydrate molecules composed of long chains of monosaccharide units.

Scaffold:	A structure which acts as template for tissue regeneration to guide the growth of new tissue.
Stress shielding:	Reduction in bone density as a result of stress removal from the bone by an implant.
Thermogram:	A curve describing the thermal behaviour of a material on application of heat.

CHAPTER TWO

2.0 LITERATURE REVIEW

2.1 Chemistry, Manufacture and Production of PLA

Polylactide is an aliphatic polyester (Figure 3) with outstanding advantages over other polymers in the areas of renewability, biocompatibility, processability and energy saving (Rasal *et al*., 2010).

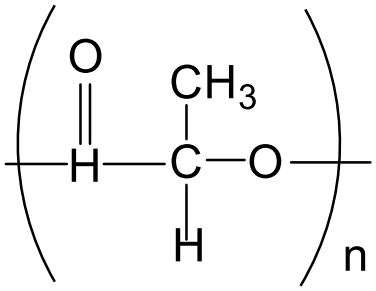

Figure 3: Molecular structure of PLA (Pluta *et al.*, 2007)

Polylactide can be prepared by different polymerization processes from lactic acid (lactide) including polycondensation, ring opening polymerization and by direct methods such as azeotopic dehydration and enzymatic polymerization (Garlotta, 2001). Currently, direct polymerization and ring opening polymerization are the most used production techniques (Lopes *et al*., 2014; Lopes *et al*., 2012; Liu *et al*., 2016).

2.1.1 Direct polymerization

The reaction in this process can take place directly by self-condensation owing to the fact that the lactide monomer has both –OH and –COOH groups which are necessary for polymerization as shown in Figure 4 (Drumright *et al*., 2000).

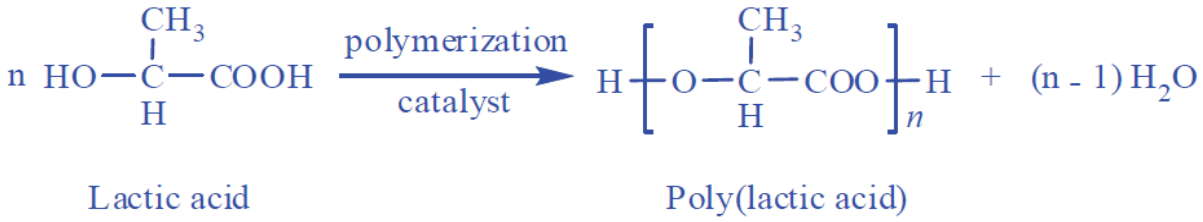

Figure 4: Direct polymerization of lactic acid (Drumright *et al*., 2000)

Direct polymerization entails solution and melt polycondensation, depending on whether a solvent is used in the reaction to dissolve the PLA or not. In the case of solution polycondensation, an organic solvent capable of dissolving the PLA without interfering with the reaction is added and the mixture is refluxed with removal of the water generated in the polycondensation process (Xiao et al., *2012*. This achieves PLA with a high molecular weight as many procedures have yielded a weight average molecular weight (M_w) of over 200,000 by this method (Ohta *et al*., 1995). Despite the smoothness of this reaction, solution polymerization suffers from certain disadvantages such as being susceptible to impurities from the solvent and various side reactions including racemization and trans-esterification. It also consumes large volumes of organic solvents which are potential pollutants to the environment.

In contrast to solution polycondensation, the melt polycondensation of monomers can proceed without an organic solvent but the temperature of the reaction must be maintained above the melting temperature of PLA (Gao *et al*., 2002). This method can lower the cost of the synthesis significantly due to the simplified procedure, but major problems still need to be solved before it can be applied industrially because of its sensitivity to reaction conditions **(**Maharana *et al*., 2009)**.** Moon *et al*., (2001) worked to develop a melt/solid polycondensation technique using a binary catalyst system (tin dichloride hydrate and *p*-toluenesulfonic acid). Thermal oligocondensates of LA were first subjected to melt polycondensation to obtain a melt

polycondensate, which was then subjected to solid state polycondensation at 105°C. This generated PLA with M_w as high as 600,000 after a short reaction time under optimized conditions. In summary, these one-step polymerization processes are relatively economical and easy to control but they are equilibrium reactions affected by numerous parameters such as the temperature, the reaction time, catalysts, pressure, etc. These factors can strongly influence the molecular weight of the products obtained. The water generated in this process can cause high molecular weight PLA to break down at high reaction temperatures. The polymer resulting from these reactions thus usually has an unsatisfactorily low molecular weight. Attention must be paid to three aspects of the reaction to obtain a high molecular weight namely, controlling the reaction kinetics, removing the water formed and preventing the degradation of the PLA chains.

2.1.2 Ring opening polymerization (ROP)

Considering the drawbacks of direct polymerization, PLA is typically synthesized by ROP which is an effective method to manufacture high molecular weight PLA as shown in Figure 5 (Lui *et al*., 2016).

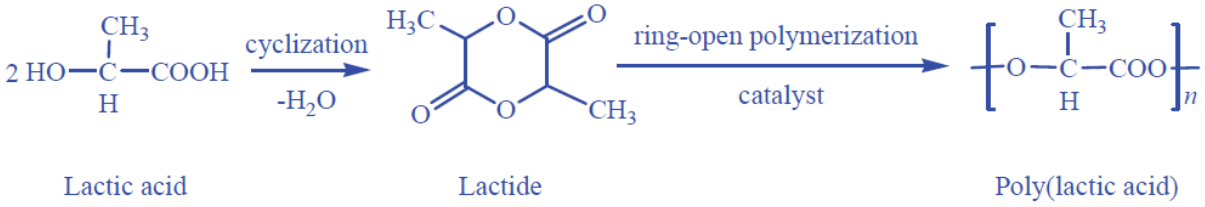

Figure 5: Ring opening polymerization of lactic acid (Drumright *et al*., 2000)

This reaction requires strict purity of the lactide monomer obtained by dimerization of the lactic acid monomer. Polylactide is obtained by using a catalyst with the monomer under vacuum or an inert atmosphere. The polymerization mechanism involved can be ionic, coordination or free-radical, depending on type of catalyst employed (Penczek *et al*., 2000). The ROP of lactide can be carried out in melt, bulk, or in solution and by cationic, anionic, and coordination-insertion

mechanisms depending on the catalyst. Various types of initiators have been successfully tested but among them, stannous octoate is usually preferred because it provides high reaction rate, high conversion rate and high molecular weights under mild polymerization conditions (Witzke *et al*., 1997). Ring-opening polymerization has been carried out most often by a stannous octoate catalyst but for laboratory demonstrations, tin (II) chloride is commonly employed. Stannous alkoxide, a reaction product between stannous octoate and alcohol, was proposed as the substance initiating the polymerization through coordinative insertion of lactide. Alcohol could affect the polymerization through reactions leading to initiator formation, chain transfer and trans esterification. Carboxylic acids affect the polymerization through a deactivation reaction. Experiments have shown that alcohol increases PLA production rate while carboxylic acid decreases it. The higher the alcohol concentration, the lower is the polymer molecular weight. However, the final molecular weight of PLA is not sensitive to the carboxylic acid concentration (Nampoothiri *et al*., 2010). Gupta *et al*., (2007) made an effort to present an updated review on the various aspects of PLA synthesis. The ROP of L-lactic acid O-carboxyanhydrides was initiated by triisopropoxyneodymium in toluene-THF mixtures. High yields and relatively high molecular weight PLAs were obtained within 4hrs at 25 °C. The reaction was highly controllable and easy to conduct while the molecular weight distribution of the PLAs was rather narrow (M_w/M_n = 1.10–1.36).

2.2 Environmental Sustainability of PLA

Environmental sustainability entails making products that serve useful market and social functions with lower detrimental environmental impact than the currently available alternatives. Conventional synthetic polymers rely on reserves of oil and gas for their monomer source and energy to manufacture. These reserves of fossil fuel take millions of years to regenerate and are

on a declining state. In contrast, the monomer used to manufacture PLA is obtained from renewable and degradable resources such as corn, rice, sugarcane, wheat and sweet potatoes (Vink *et al.*, 2004). The polymer can be renewed without degradation in quality or performance and such a product is made using only substances known to be safe for both humans and the environment. The production of PLA from these sources will help reduce the dependence on fossil fuels and at the same time check energy, environmental and global warming issues. Energy from the sun promotes photosynthesis within the plant cells (Figure 6) while carbon dioxide (CO_2) and water from the atmosphere are converted into starch. This starch is readily extracted from plant matter and converted to a fermentable sugar (e.g. glucose) by enzymatic hydrolysis. The carbon and other elements in these natural sugars are then converted to lactic acid through fermentation.

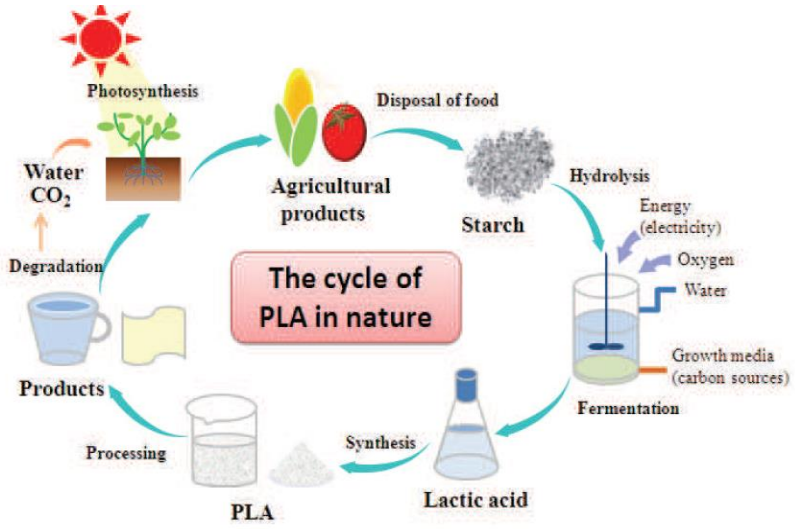

Figure 6: The cycle of PLA in nature (Xiao *et al.*, 2012)

Ideally, the life cycle of the sustainable product is in balance with the surrounding ecosystem. Fossil energy use, greenhouse gas emissions and water use have been classified as the three issues that are generally considered to have an increasing global importance (Vink *et al.*, 2004).

Figure 7 shows plots of fossil energy requirement for petrochemical – based plastics and PLA. A key finding of the analysis is that the first generation PLA production system (PLA1) uses 25 to 55% less fossil energy than the petroleum-based polymers (Vink *et al*., 2004; Xiao *et al*., 2012). It is thus envisaged that if efforts are geared towards minimizing fossil energy consumption to < 10% as compared to any of the petroleum based polymers for the near future, there will be significant reductions in air and water pollutions. Process improvements are targeted by NatureWorks LLC for the near future involving the use of biomass (B) and wind power (WP) as energy sources in the PLA production process (PLA B/WP). With these improvements, the use of fossil energy can be reduced by more than 90% compared to any of the petroleum-based polymers being replaced. This also will give a significant reduction in fossil energy related air and water emissions. This comparison represents the outstanding potential for environmental benefits for polymers such as PLA made from renewable resources.

Global climate change has been identified as perhaps the most important environmental issue of this century (Vink *et al*., 2004). Analysis has demonstrated that the PLA1 production process enjoys a substantial advantage over most polymers and it is comparable to several others. Even more exciting are the greenhouse benefits that derive from the transition to biomass feed stocks and reliance on wind energy for the balance of plant energy requirements. The utilization of the lignin fraction of lignocellulosic feedstocks for process heat generation 'closes the loop' on carbon related energy generation and in combination with other factors yields a negative greenhouse gas impact for PLA pellets. A most appealing result of the use of agricultural feed stocks for the PLA polymer production and most of the process energy requirement means that customers using PLA cannot only use PLA as a product, but as a component of their greenhouse gas reduction strategies. Life cycle assessment reveals that no petroleum-derived polymer can

rival the greenhouse gas sink effect of the improved PLA process. Although disposal of PLA products (whether by combustion, composting or other conventional means) results in a return of CO_2 to the atmosphere, which is an advantage.

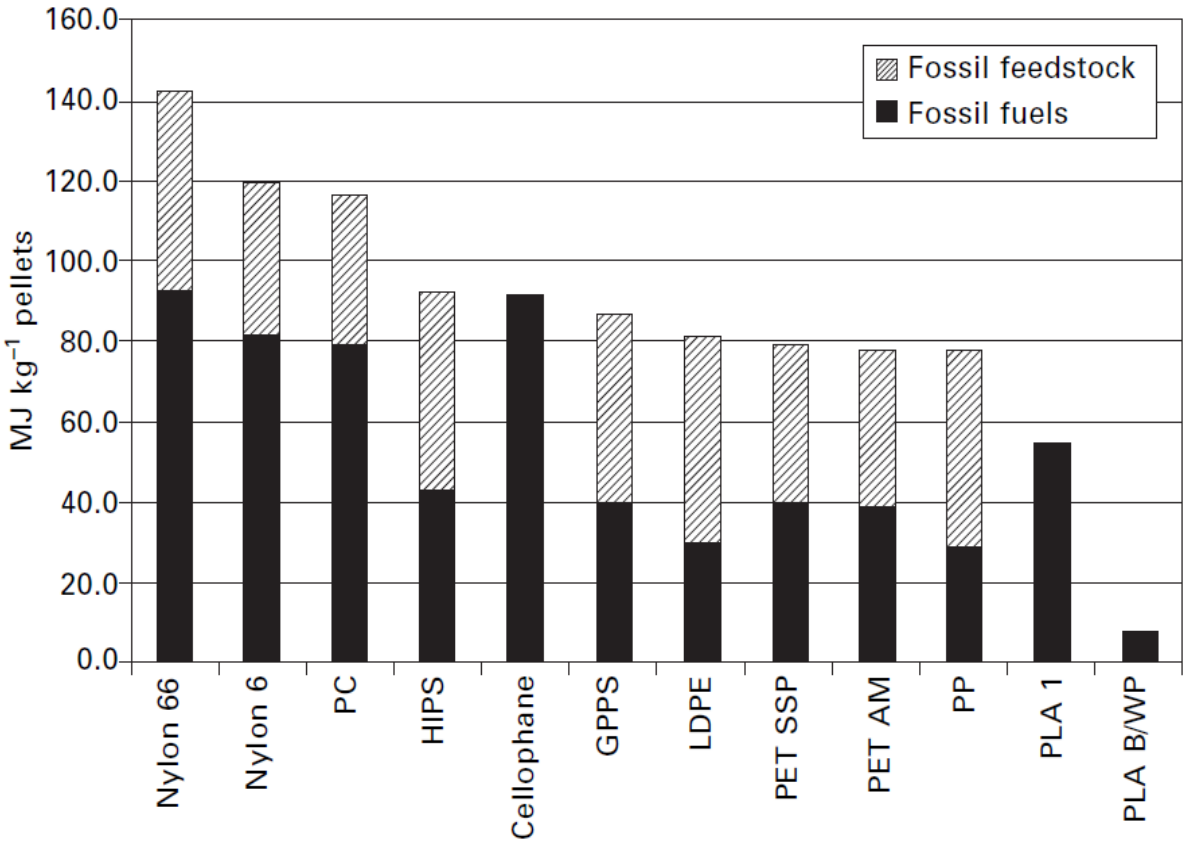

Figure 7: Fossil energy requirement for some petroleum-based polymers and PLA. The cross-hashed part of the bars represent the fossil energy used as chemical feedstock (the fossil resource to build the polymer chain). The solid part of each bar represents the gross fossil energy use for the fuels and operations supplies used to drive the production processes. PC = Polycarbonate; HIPS = High impact polystyrene; GPPS = General purpose polystyrene; LDPE = Low density polyethylene; PET SSP = Polyethylene terepthalate solid state polymerization (bottle grade); PET AM = Polyethylene terephthalate Amorphous (fibers and film grade); PP = Polypropylene; PLA1 = Polylactide (first generation); PLA B/WP (Polylactide, biomass/ windpower scenario).(Vink *et al*., 2004)

2.3 Degradation of PLA

Degradation designates the essence of polymer chain cleavage. All degradable polymers share the property of erosion upon degradation. Degradation behaviour of polymers can be optimized for different interesting applications. To classify degradable polymers, a distinction is made between surface (or heterogeneous) and bulk (or homogeneous) eroding materials (Gopferich and Tessmar, 2000), which is illustrated in Figure 8.

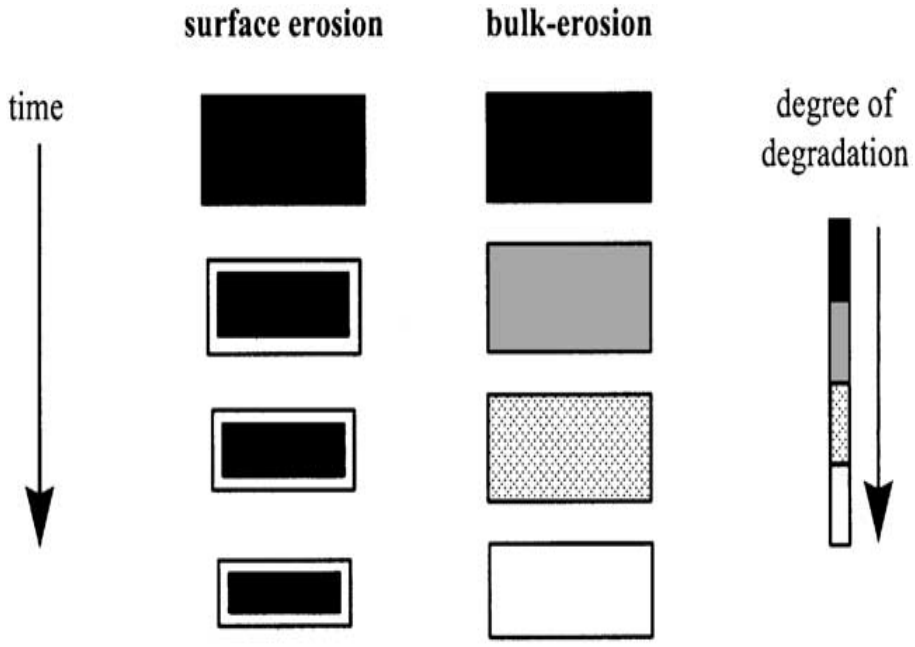

Figure 8: Schematic illustration of surface and bulk erosion (Burkersrod *et al*., 2002)

During an application, surface eroding polymers lose material from the surface only because the rate of which water diffuses into the polymer is slow compared to the polymer-water reaction rate. They get smaller but keep their original geometric shape. As the surface is eroded and removed, the hydrolysis front moves through the material core In the case of polymers that undergo bulk degradation, the rate of water penetration into the matrix is faster than the rate of polymer degradation. The bulk degradation process is considered as homogeneous, in which degradation occurs at a uniform rate throughout the polymer matrix (Mobedi *et al*., 2006).

Decrease in molecular weight, the reduction in mechanical properties and the loss of mass also occur simultaneously throughout the entire specimen (Vieira *et al.*, 2011). The advantage of surface eroding polymers is the predictability of the erosion process. This is desirable when using such polymers for drug delivery (Nair and Laurencin, 2007), where the release of drugs can be related directly to the rate of polymer erosion. The biodegradation process of PLA in an aqueous medium takes place through hydrolytic scission of the ester groups (Mobedi *et al*., 2011). Polylactide has been confirmed to undergo bulk degradation (Mobedi *et al*., 2011) hence, they are suitable as structures and templates for tissue regeneration as their degradation behaviour could vary based on application, for instance, 3 months (Bose *et al*., 2012). This will create more room for tissue to grow. The knowledge of the erosion mechanism is therefore, important for the successful application of a degradable polymer.

2.4 Applications of PLA in Tissue Engineering

Tissue engineering is a technique invented to reconstruct living tissues by associating the cells with biomaterials that will serve as a scaffold on which cell can proliferate in three-dimensional (3D) way. Under physiological conditions, scaffolds have emerged as potential alternative to tissue or organ transplantation and have thus attracted great attention in science, engineering, and medicine. Products made of PLA have been approved by the US Food and Drug Administration (FDA) for direct contact with biological fluids since 1970 (Xiao *et al.*, 2012). The degradation of PLA occurs in two phases – hydrolysis and metabolization (Figure 9). Hydrolysis occurs as body fluids (example, water) enter the implant and chemically reacting with the polymer by breaking its chains. Metabolization occurs as the single lactic acid molecules are metabolized in the liver into CO_2 and H_2O (water). For this reason, PLA has been recommended as an excellent material for biomedical applications in such use as sutures, clips, and drug delivery systems (DDS) owing

to its non-toxic and non-carcinogenic degradation products (H_2O and CO_2) with no adverse effect on the human (Bropp, 2012; Alsaheb *et al.,* 2015) . The processing of PLA has been carried out through several techniques including film casting (Rathi *et al.,* 2014), blow moulding (Li *et al.,* 2014), extrusion (Rathi *et al.,* 2014), injection moulding (Haris and Lee, 2006) and fiber spinning (Adeosun *et al.,* 2016). These processing techniques are enabled due to its greater thermal processability in comparison to other biomaterials such as PEG, PHAs and PCL (Rhim *et al*., 2006). These thermal properties contribute to its application in textiles and food packaging (Bropp, 2012)**.**

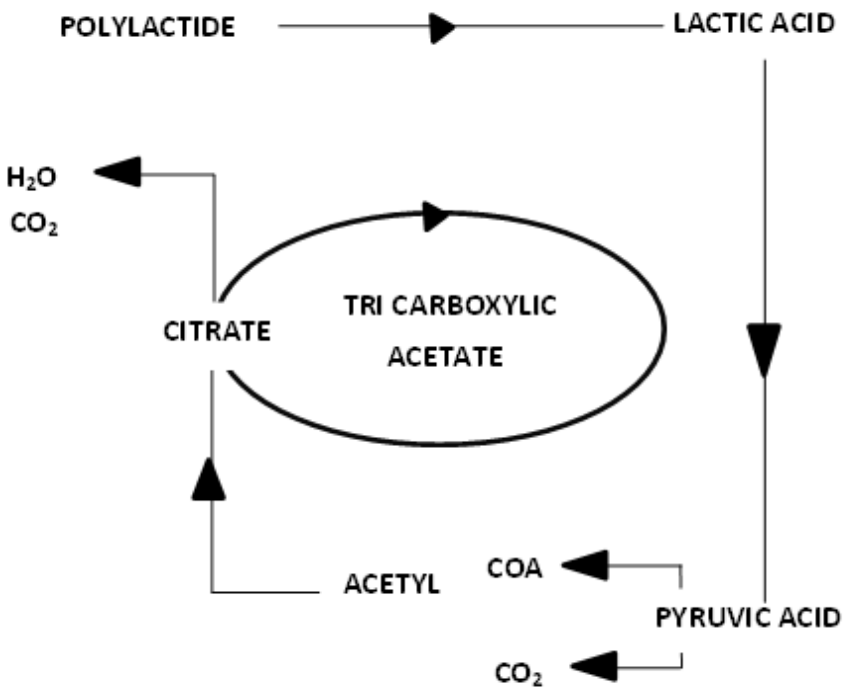

Figure 9: Schematic illustrating the in vivo degradation of PLA (MAST Bio surgery, 2006)

PLA has been a source material for the manufacture of tissue engineering scaffolds, bioabsorbable medical implants, covering membrane, dermatology and cosmetics (see some examples in Figure 10).

a

b

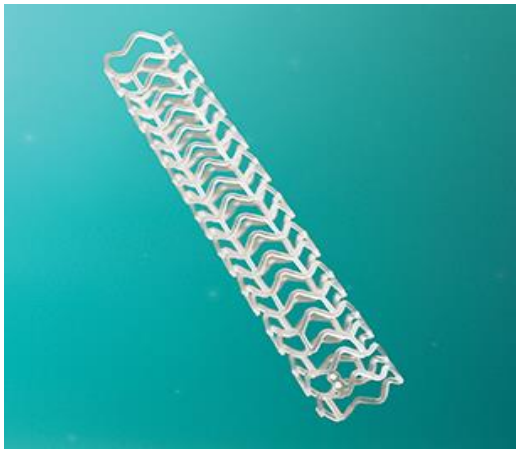

c

Figure 10: Materials from PLA (a) implant screws and plates (b) body scrub (c) scaffolds (http://www.medscape.com/viewarticle/472962)

Certain metals and alloys (Mg, Stainless steel and Ti6Al4V) may be good choices for medical implants due to their superior mechanical properties, however ,their ineptitude to degrade in biological environment makes them inappropriate for scaffold applications (Liu ana Ma, 2004). Polymers have great design flexibility as their composition and structure can be tailored to meet specific needs (Huang *et al.*, 2007). Thus, linear aliphatic polyesters such as PLA are frequently used in the fabrication of scaffolds.

The potential of 70:30 poly-L- lactide- co-D, L – lactide (PLDLLA) membranes as temporary implant under hydrolytic degradation in PBS of pH 7.4 at 37 ^{0}C for 20 weeks has been studied (Barauna *et al.,* 2013). The characterization of membranes before and after degradation was achieved using Differential Scanning Calorimetry (DSC), Gel Penetration Chromatography (GPC), Thermogravimetry Analysis (TGA), Scanning Electron Microscopy (SEM) and mechanical traction tests. Stability of membranes was observed for 16 weeks until noticeable decrease in glass transition temperature T_g occurred in the 18th and 20th weeks. This was attributed to the polymeric chain cleavage that surfaced during degradation. With the GPC, decrease in molecular weight M_w was observed after 2 weeks and the results showed that M_w loss takes place between the 18th and 20th weeks as a result of gradual breakage of polymer chains during hydrolysis. Analysis with TGA showed that the temperature at which mass loss began decreased with degradation time. Microscopic observation indicated that no pore was present before degradation but after degradation while pores and fissures on broken surface were evident. Membranes' resistance to traction and modulus of elasticity were found to be maintained till the 8th week. At the end of 16th week, there was a sharp reduction of these properties as a result of PLDLA degradation. Given these degradation characteristics, PLDLA membranes were found to be suitable for use as temporary implantations.

In-vitro degradation of 70:30 PLDLLA in PBS for 24 weeks and medical incision in dorsal subcutaneous tissue rats for 90 days were studied by Ciambelli *et al.,* (2013). The implants showed no effect on health and behaviour of the rats as no significant adherence between tissue and implants occurred within the first 7 days. In contrast, 15-day implants showed greater polymer-tissue attachment. This finding suggested that the polymer-tissue process tend to increase gradually through organization of the conjunctive tissue fibers into a conjunctive

capsule. Mechanical tension test showed that PLDLLA behaves like a ductile material under constant tension. The Young´s modulus, elongation at break and the maximal tension decreased as degradation time elapsed. Polymers retained their dense morphology within the first 4 weeks of incubation until after 12th week where pores and cracks were seen at the center of samples. Biocompatibility and mechanical stability of PLDLLA displayed in the experiments have made them attractive material in biomedical fields. Jiang *et al.,* (2006) evaluated chitosan/ polylactide-co-glycolide, PLGA scaffolds for bone regeneration through In vivo study. In the rabbit, ulnar critical-sized-defect model was created and this successfully bridged the critical-sized defect on sides both adjacent to and away from the radius using the scaffolds. However, the addition of chitosan to PLGA led to higher inflammation and lower mineralization than for the PLGA counterpart. Based on this result, Jiang *et al.,* (2010) functionalized chitosan/PLGA by heparin immobilization with controlled loading efficiency. Chitosan was introduced into PLGA microspheres to impart functionality (due to its reactive amino groups) for easy attachment of the biomolecule. The compressive strength and modulus were found to remain in the range of human trabecular bone after the heparinization process. More importantly, heparinized chitosan/PLGA scaffolds with a low heparin loading (1.71 g/scaffold) showed a stimulatory effect on cell differentiation, as indicated by enhanced osteocalcin expression when compared with a non-heparinized chitosan/PLGA scaffold. Todo *et al.,* (2007) blended four different kinds of ductile biodegradable polymers with PLLA to study its effects on the bending modulus, strength, impact fracture energy and mode I fracture property. The polymers include PCL, polybutylenessuccinate (PB), polybutylene succinate-co-L-lactate (PBL) and polybutylenessuccinate-co-ε-caprolactone (PBC). A field emission scanning electron microscope (FE-SEM) investigated mode I fracture while Polarizing Optical Microscopy (POM) measured the crack growth behaviour. Though

ductility of PB was thought to be lower than the other three ductile polymers, however, blending it with PLLA improved its modulus, strength and toughness. Thus, polymer with the least ductility was an effective blending partner to improve the mixing properties of PLLA. PLLA/PBC exhibited the best fracture properties such as mode I fracture energy and impact perforation energy. Ductility of PBC was highest and therefore, localized ductile deformation in crack-tip region was significantly enhanced.

Mechanical behaviour of poly-D,L-lactic acid/poly-ε-caprolactone (PDLA – PCL, with a 90:10 ratio of PLA and PCL) fibers during degradation in 37 ^{0}C PBS was examined by Vieira *et al.*, (2011). At the end of the 28 weeks incubation period, fibers' dimensions and degradation medium showed no significant change. Force – extension relationship revealed that plasticity and strength decreased progressively at the end of the 16th week. Constitutive models used with validated experimental results were found to be reasonable for other biodegradable materials. This model was considered as a fundamental tool in the design of regenerative medical devices where strain energy is an important requirement. Three-dimensional printing technology has rapidly expanded in tissue engineering field since it was first developed at the Massachusetts Institute of Technology. Ge *et al*. (2009) developed 3D-printed PLGA scaffolds, which could support the proliferation and osteogenic differentiation of osteoblasts. Based on the In-vitro study, they also evaluated PLGA scaffolds for bone regeneration within a rabbit model. In both the intra-periosteum and the iliac bone defect models, the implanted scaffolds facilitated new bone tissue formation and maturation over a period of 24 weeks. Comparison between In-vitro degradation of porous scaffolds (75% porosity) and non- porous thin films made of PLLA biopolymers in PBS of pH 7.4 were studied by Sultana and Abdul- Kadir (2011). Water uptake of PLLA porous scaffolds was observed to be higher than in thin films. Fragmentation and

scission of chains caused by porosity activated accelerated weight loss of scaffolds after 6 weeks. This was proven to dominate the degradation during the incubation period. Poly (lactide-co-glycolide) (PLGA 50/50) has been blended with hydrophilic chitin to form chitin/PLGA blend ratios of 1:3, 1:2, 1:1, 2:1 and 3:1, respectively (Mi *et al.*, 2002). Information from SEM revealed that PLGA particulates were homogeneously dispersed in chitin matrix and this suggested the occurrence of obvious phase separation from the blended chitin and PLGA 50/50 phase that occurred as a result of their thermodynamic incompatibility. Degradation study achieved by determining water uptake capacity in deionized water at room temperature showed that weight loss of the chitin/PLGA 50/50 microspheres increased with increase in hydrophilic chitin content. This implied that the hydrolysis of PLGA can be hastened after blending with hydrophilic chitin. Nugroho and Mitomo (2008) investigated the enzymatic degradation and thermal stability of PLA using proteinase-K and the combination treatment of irradiation and annealing respectively. PLA was irradiated with γ-rays in air and in vacuum at 25 ^{0}C and electron beam with different dose rates ranging between 50 – 200 kGy. Results showed that at low dose, degradation of PLA occurred by a chain scission at both atmospheres while at higher irradiation dose, the decrease in molecular weight was drastic. This suggested that recombination reaction of free radicals became almost equal to chain scission reaction. Enzymatic degradation of PLA revealed that weight loss decreased with molecular weight by irradiation, which introduced cross linking. High crystallinity of PLA could be achieved through annealing PLA at temperature as high as 90 ^{0}C. Combination of annealing and irradiation was more effective to improve the heat stability of PLA, as rearrangement of some scissions during irradiation occurs and this result in increased crystallinity.

Two kinds of biodegradable polymer blends of PLA/PCL and polylactic acid/polycaprolactide/lysine triisocyanate (PLA/PCL/LTI) have been prepared and subjected to annealing to study its influence on their mechanical properties (Takayama *et al.,* 2011). Fixed mixing ratio of PLA and PCL at 85:15 in weight fraction was used, with the inclusion of 1 wt. % LTI content. The observed results revealed that crystallization of the PLA phase by annealing at 100 ^{0}C for 3hrs strengthened the structure of the PLA/PCL blend, resulting in enhanced bending modulus and strength. The significant decrease observed in mode I fracture energy of PLA/PCL by annealing was attributed to the embrittlement of the PLA phase. In the case of PLA/PCL/LTI, the structural transformation due to polymerization by LTI addition and crystallization through annealing strengthened the microstructure and this resulted in dramatic improvement of the mode I fracture energy. Self-reinforced PGA (SR-PGA) and PLLA (SR-PLLA) pins have been fixed into the right and left femurs of rats for their shear load carrying capacity after 1, 3, 6, 12,2 4, 36,48 and 52 weeks of implantation (Nordstrom *et al.,* 2001). Shear load carrying capacity of femur devoid of implants (control sample) and those fixed with SR-PGA and SR-PLLA implants were observed to possess maximum values on the 36th week beyond which the property gradually deteriorated. On the 52nd week, the load bearing influence of pin on SR-PLLA implants ceased as SR-PGA implants and control specimens had higher magnitudes of load bearing capacities. Periods other than this revealed higher load bearing capacity values in the SR-PLLA implants where pins were the load carrier. Glarner and Gogolewski (2004) studied In-vitro degradation of 80/10/10 PLLA/PDLA/PGA pins in PBS (pH 7.4 at 37 ^{0}C) for 36 weeks. Results showed a progressive drop in molecular weight and mechanical properties of pins until the 24th week where fragmentation occurred. Crystallinity of pins increased during the first few weeks of incubation but decline on the 24th week. The high susceptibility of the pins to In-vitro

degradation was associated with the chemical composition and the molecular weights of samples used in the study.Elastic 50:50 PLA: PCL scaffolds have been seeded with smooth muscle cells (SMCs) and implanted in nude mice for biocompatibility and In-vivo degradation behavior studies (Jeong *et al.*, 2004). From the study, PLA-PCL scaffolds of this blend exhibited excellent tissue biocompatibility to SMCs, which suggested its suitability for vascular tissue engineering. It was also observed that the scaffolds displayed slow degradation time, while caprolactone units degraded faster than lactide. This was attributed to the amorphous regions containing caprolactone moieties, which degraded earlier than hard domains (crystalline) where most of lactide units were located**.** Scaffolds' perfect tissue compatibility to SMCs permits them for vascular tissue engineering. Two materials namely PDLA pins and composite pins of 10% β-tricalcium phosphate (β-TCP) (90/10) have been used to perform osteotomy on the medial femoral condyle of (Prokop *et al.,* 2004). At the end of 3, 18 and 36 months, a histological examination performed on the synovial membrane and lymph nodes revealed that minor reactions of the synovial membrane took place in the composite pins at the end of the 18th month. Owing to the slow degradation process of biodegradable PDLA, there was no clinically relevant inflammation of either joint or lymph nodes and the addition of 10% b-TCP did not result in any significant enhancement. Effects of crystallization and loading rate on the mode I fracture toughness and mechanism of PLA studied by Park *et al.,* (2006) concentrated more on thermal (with DSC) and dynamic mechanical analysis (DMA) properties of the PLA. Results showed that static values of G_{IC} decreased with increase in crystallinity due to disappearance of multiple craze formation that corresponded to decrease of amorphous region. Observations for the amorphous PLA showed that at impact loading rate, G_{IC} increased due to increase of fibril

structure. The study also recorded that the impact toughness for the crystallized PLA is superior to the static one and attributed it to the formation of fibril structure at the impact rate.

These reviewed works have shown the suitability of PLA usage in tissue engineering for its biodegradability and biocompatibility potentials in a human physiological environment. Several studies have been geared towards reinforcing PLA with synthetic and organic materials to improve its stiffness and also, control degradation rate. Shakoor *et al.*, (2010) reinforced PLA with hemp fibers using stir casting method at 170 ^{0}C and produced composite samples with modulus from 4.8-9.2GPa with the highest value at 30 wt. % hemp. Reinforcing PLA with 10 wt. % polypropylene yielded 1.17GPa modulus (Ali *et al.*, 2014) while PLA reinforced with 20 wt. % micro crystalline cellulose with silver microspheres showed modulus from 2.3 – 2.9GPa (Bijarimi *et al*., 2012). Characterizations have shown that PLA and its blends will be suitable for soft tissues such as ligaments, tendons, muscles and nerves. However, the reinforced PLA so far developed have failed to meet the stiffness and the biodegradation requirements of hard tissues like the femur (10-30GPa). These short comings are the focus of this study in extending the use of PLA in hard tissues (bone) by reinforcing it with chitin to improve its stiffness to that within the range of human bone. Biodegradation studies and its suitability as a temporary supporting device are also investigated.

2.5 Bone and its Healing

Bones are rigid organs that consist of osseous tissue, bone marrow, endosteum, periosteum, cartilage, nerves, and vascular channels constituting the skeleton of vertebrate animals. Osseous tissue, which fulfills mechanical functions, is formed by connective tissue cells such as osteocytes, osteoblasts and osteoclasts (Abdul Razak *et al*., 2012) in an extracellular matrix composed mainly of minerals, proteins, and water. The bone composition and configuration will

vary according to factors such as the anatomical location, supported load, age and gender of the individual and the possible diseases that the patient could suffer (Frickle *et al*., 2008). In regard to bone composition, mineral phase is between 60 - 70wt. % and water is between 5 - 10wt. %, while the remaining portion is an organic matrix of collagen with other proteins. Bones have mechanical, synthetic and metabolic functions. The mechanical functions entails protection of internal organs, body support and interaction with muscles and tendons to generate body movement (Weinier and Wagner, 2008). The synthetic function is conducted by the bone marrow where both bone and blood cells are synthesized in a process called hematopoiesis (Morrison and Scadden, 2004). Metabolic functions are related to act as a reservoir of calcium, phosphorus, growth factors and fat (Raposo *et al*., 2002). In addition, bone tissue helps to regulate pH level of blood releasing alkaline salts (Barriere *et al*., 2008). Referring to mechanical function, bones are the structural elements of the human body. Skeletal system supports loads due to the different activities of an individual as holding things, walking, pushing, etc. These loads induce tensile, compressive or shear stresses on the bone tissue. More complex stresses such as those caused by bending or twisting of bone can be decomposed into the three basic aforementioned stresses. To study these stresses, bone mechanical properties such as elasticity modulus, compressive and tensile strength are important. These properties are highly dependent on the position of the bone and the condition of the individual. Besides, mechanical properties of bone vary depending on the load orientation with respect to the orientation of the tissue (anisotropy) and the speed to which the load is applied (viscoelasticity) (Pawlikowski *et al*., 2008). Bone may suffer various diseases that can be caused by excessive load or hormonal deficiencies, among other reasons (Piper and Valentine, 2012). As an engineering material, bone can fail because mechanical loads originate stresses over the limits a healthy bone can bear or

because the mechanical properties of bone are decreased by various pathologies that make the bone weak and prone to be damaged.. All broken bones go through the same healing process (Shih, 2008). This is true whether a bone has been cut as part of a surgical procedure or fractured through an injury. The bone healing process has three overlapping stages: inflammation, bone production, and bone remodeling. Inflammation (Figure 11a) starts immediately after the bone is fractured and could span within 24hrs and 7 days of fracture (Marsell and Einhorn, 2011). When the bone is fractured, there is bleeding into the area leading to inflammation and clotting of blood at the fracture site (Kaleas and FACS, 2001). This provides the initial structural stability and framework for producing new bone. The energy requirements of fracture healing increase rapidly during inflammation and reach a peak during repair, when the cells in the fracture callus are proliferating and synthesizing large volumes of new matrix. These energy requirements remain high until cell density and cell activity begin to decline as remodeling starts (Abdul Razak *et al*., 2012).

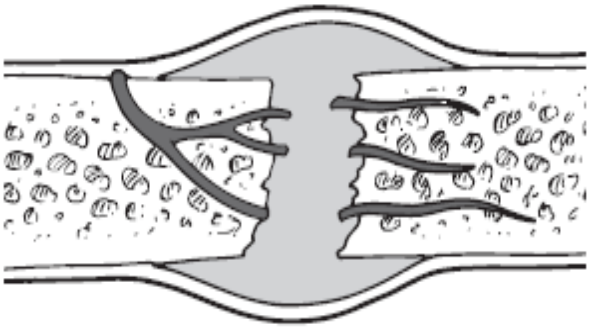

a

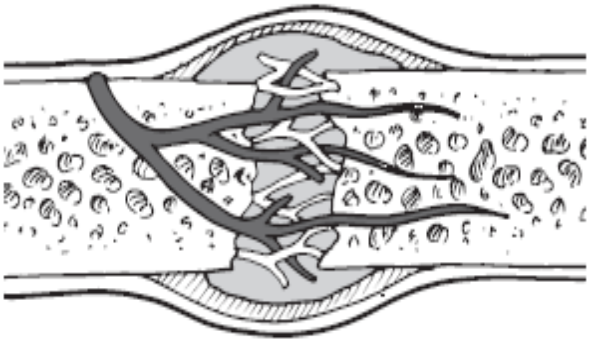

b

c

Figure 11: Stages of fracture healing (a) inflammation (b) bone production (c) bone remodeling (Shih, 2008)

Bone production (Figure 11b) begins when the clotted blood formed by inflammation is replaced with fibrous tissue and cartilage, known as soft callus (Rahn, 2002). The peak of soft callus formation occurs within 7–9 days post trauma (Marsell and Einhorn, 2011). As healing progresses, the soft callus is replaced with hard bone (hard callus) which is visible on x-rays for several weeks after the fracture. It is the final bridging of this central hard callus that ultimately provides the fracture with a semi-rigid structure which allows weight bearing (Gerstenfeld *et al*., 2006). Bone remodeling (Figure 11c) is the final phase of bone healing, and it goes on for several months. In remodeling, bone continues to form and becomes compact, returning to its original shape. In addition, blood circulation in the area improves. Gradual increase in bone mechanical stability is crucial during this stage and hence weight bearing (such as standing or walking) is encouraged (Marsell and Einhorn, 2011; Rahn, 2002).

Bone healing is a complex process as speed and success differ among individuals. The time required for bone healing can be affected by many factors, including the type of fracture and the patient's age, underlying medical conditions, and nutritional status. Bone generally takes 6 to 8 weeks to heal to a significant degree (Shih, 2008). In general, children's bones heal faster than those of adults. The foot and ankle surgeon for instance, will determine when the patient is ready to bear weight on the area. This will depend on the location and severity of the fracture, the type of surgical procedure performed and other considerations. For all patients with fractured bones, immobilization is a critical part of treatment because any movement of bone fragments slows down the initial healing process. Depending on the type of fracture or surgical procedure, the surgeon may use some form of fixation (such as screws, plates, or wires) on the fractured bone and or a cast to keep the bone from moving. During the immobilization period, weight bearing is restricted as instructed by the surgeon. Once the bone is adequately healed, Physical therapy

often plays a key role in rehabilitation. An exercise designed for the patient can help in regaining strength and balance that will assist rehabilitee bone in returning to normal activities.

2.6 Chitin and its Extraction from its Sources

Chitin is a linear polymer built up by units of amino sugars - β-(1→4) - linked 2-acetamido-2-deoxy-β-D-glucopyranose (GlcNAc) and or partly of β-(1→4)-linked 2-amino-2-deoxy-β-D-glucopyranose (GlcN) (Zhao *et al*., 2011). Kim (2011) stated that chitin is a copolymer of *N*-acetyl-D-glucosamine and D-glucosamine units linked with β-(1-4) glycosidic bond, where *N*-acetyl-D-glucosamine units are predominant in the polymeric chain (Figure 12). Chitin, the second most abundant natural polymer after cellulose, has its biological functions and chemical structure similar to cellulose as a structural polysaccharide. But the difference is that it has an acetamide group instead of a hydroxyl group at the C-2 position within the glucose unit (Figure 13) and may thus be regarded as a cellulose derivative with an acetamido group (Sharp, 2013). Cellulose strengthens the cell wall of plant cells (Kittle, 2012) while chitin promotes mechanical strength of fungal cell walls (Malinovsky *et al*., 2014; Anith and Rabeeth, 2010) and exoskeletons of arthropods (Liman *et al*., 2011). Thus, they both serve as structural components supporting cell and body surfaces.

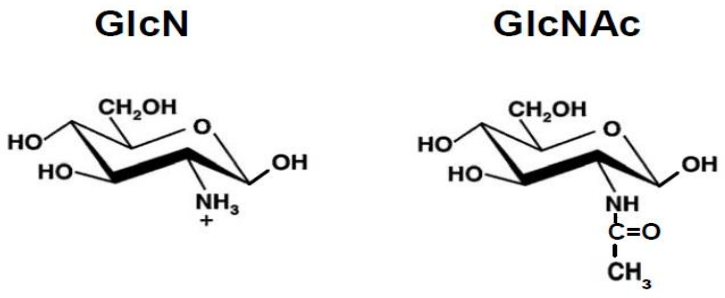

Figure 12: Chemical structure of glucosamine (GlcN) and *N*-acetylglucosamine (GlcNAc) (Einbu, 2007)

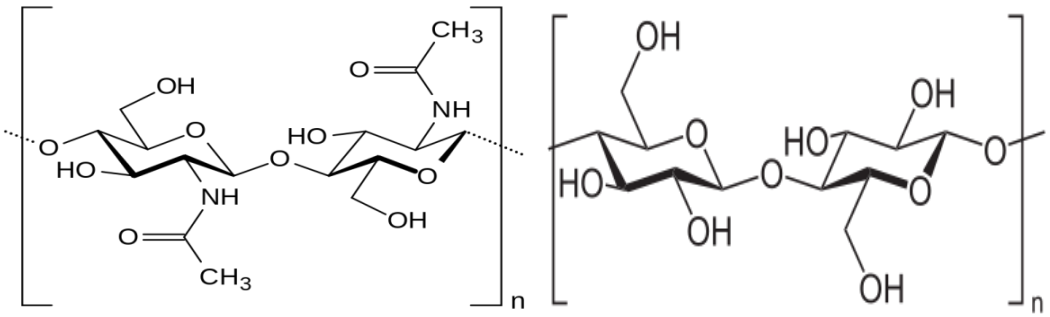

a b

Figure 13: Molecular structure of (a) chitin and (b) cellulose (Younes and Rinaudo, 2015; Wang and Uchiyama, 2013)

Chitin is present in insect's body wall (cuticle), gut lining (peritrophic matrix, PM), salivary gland, trachea, eggshells and muscle attachment points. It provides rigidity and chemical stability on both hard and soft extracellular structures such as the exoskeleton (cuticle) and the PM, both of which enable insects to be protected from the environment while allowing for growth, mobility, respiration and communication. These structures are primarily composites of chitin fibers and proteins (some of the chitins are covalently linked to protein) with varying degrees of hydration and trace materials distributed along the structures (Arakane *et al*., 2008). The composition and structure of their organic matrices are different from one another. The organic matrices of dry bees are composed of 10–12 % chitin, 50–80 % proteins, 20–30 % melanin and 2-3 % mineral compounds while dead bees after CO_2 extraction contains 20-22 % chitin, 25-30 % protein, 20-30 % melanin and 2-3 % mineral compounds (Nemtsev *et al*., 2004). The yield of chitin from adult *H. parallela* (moth) was discovered to be approximately 15%. The yields of chitin from other insects vary with species and their development stages**.** Zhong *et al*., (2000) reported that organic matrices of *Bombyx mori* larva cuticle and silkworm pupa exuviae contain

15–20 % chitin while a higher chitin yield of 36 % was reported for cicada sloughs (Sajomsang and Goni, 2010). Crustacean shells also consist of proteins (30–40 %), calcium carbonate (30–50 %), chitin (20–30 %) and pigments (astaxanthin, canthaxanthin, lutein or β-carotene). These proportions vary according to species and season (Aranaz *et al*., 2009). The structure of the cuticle of crustaceans is the same as insect cuticle, but its composition is different. In the skeletal tissue, protein and chitin combine to form a protein-chitin matrix, which is then extensively calcified to yield hard shells (Younes and Rinaudo, 2015). The waste may also contain lipids from the muscle residues and carotenoids, mainly astaxanthin and its esters (Ambati *et al*., 2014). These components all have to be quantitatively removed to achieve the high purity biopolymer necessary for biological applications. There are two broadly defined ways to do this either using chemical or biological based processes. Works on biological extraction have reported that the most common method is the use of proteolytic enzymes for protein digestion or a fermentation process using microorganism that allows a digestion of both proteins and minerals (Arbia *et al*., 2013; Gortari *et al*., 2013). Chemical treatment on the other hand, entails the use of acid and alkali solutions for the removal of mineral and proteins respectively. Regardless of the chosen treatment, the isolation of chitin begins with the shell selection. This selection has an important influence on the quality of the final isolated material. Ideally, shells of the same size and species are usually chosen. The selected shells are then cleaned, dried and ground into small particles. In the case of chemical treatment extraction process (which is used in this work), the following consecutive steps are taken after raw material conditioning: protein extraction (deproteinization), removal of inorganic components (demineralization) and decolouration. This sequence is preferred if the isolated protein is to be used as food additive for livestock feeding. Otherwise, demineralization can be carried out first (Isa *et al*., 2012). Demineralization is generally

performed by using acids such as HCl, HNO3, H_2SO_3, CH_3COOH, and HCOOH. However HCl has proven to be the preferred reagent owing to its demineralization efficiency and it is applied at a concentration between 0.2 and 2 M for 0.5-48hrs at temperatures varying from 0 to 100 ^{0}C (Zaku *et al*., 2011; Liu *et al*., 2012). The ash content (31-36%) of the demineralized shell is an indication of the effectiveness of the process. During the demineralization process, excessive undesirable foams are produced due to the CO_2 generated in the Equation (1) reaction (Younes and Rinaudo, 2015):

$$CaCO_3 + 2HCl \rightarrow CaCl_2 + CO_2 + H_2O \quad (1)$$

It is evident that if the amount of acid employed is below the stoichiometric ratio, the demineralization reaction will not be completed. The acid concentration and the reaction time depend on the source, extraction time, temperature, particle size, acid concentration and solute/solvent ratio (Abdulkarim *et al*., 2013; Yen *et al*., 2009). Deproteinization of chitin is usually performed by alkaline treatments, though other effective reagents have been reported. Typically, raw chitin is treated with approximately 1 M aqueous solutions of sodium hydroxide, (NaOH) between 1-72hrs at temperatures ranging from 65 to 100 ^{0}C to dissolve the proteins present (Isa *et al*., 2012; Kaya *et al*, 2014). With regards to chemical structure, protein is bound by covalent bonds to the chitin through aspartyl or histidyl residues, or both, thus forming stable complexes such as glycoproteins (Zhao, *et al*., 2010).

Acid and alkali treatments alone, however, produce a coloured chitin product. For commercial acceptability, the chitin produced from crustacean sources needs to be decolorized or bleached to yield cream white chitin powder (Yen *et al*., 2009). The pigment (carotenoids) bound to the crustacean shells forms complexes with chitin and the degree of association of chitin and

pigments varies from one species to another among crustaceans. Reagents such as hydrogen peroxides (H_2O_2) and potassium permanganate ($KMnO_4$) to eliminate pigments from crustacean exoskeletons have been used in previous studies (Liu *et al*., 2012). The stronger the shell-carotenoids bond, the more harsh treatment is required to prepare a white coloured chitin. During the process of decolouration, researchers have stated that the chemical used should not affect the physicochemical or functional properties of chitin. Yen *et al*., (2009) characterized chitin obtained from crab shell. Crude chitin from crab shells were ground, sieved to 65μm particle sizes and was treated with 1N HCl at room temperature for 6hrs to remove the mineral content. This was followed with aqueous NaOH solution treatment in the ratio1:10 (w/v) at 100 ^{0}C for 3hrs to remove protein. The mixture was filtered and washed with deionized water until neutral (pH=7.0). Potassium permanganate solution (1 %) was further used in treating the precipitate for 1hr for the purpose of decolourization, and followed by 1hr reaction with 1% oxalic acid for the same purpose. Decolourized precipitate was washed to neutral and freeze dried to obtain a purified chitin. Nitrogen, carbon and hydrogen contents as well as nitrogen/carbon ratio in purified chitin were observed to increase significantly after purification. Wide-angle X-ray diffraction (WAXD) of crude chitin exhibited its characteristic crystalline peaks at 2θ = 9.1-9.2^0 and 19.1-19.2^0 while after chemical treatments, purified chitin showed denser crystalline structure as evidenced by its sharper peaks. Scanning electron microscopic examination revealed that the distinctly arranged micro fibrillar crystalline structure in purified chitin was more noticeable than crude chitin. It was concluded that acid and alkaline treatments followed by decolourization were effective methods in improving the purity of purified chitin.

Chitin extracted from mussel shell has been characterized by Abdulkarim *et al*. (2013). Thoroughly washed 100 g shells were oven-dried to constant weight at a temperature of 35 ^{0}C

and demineralized for 6hrs at ambient temperature (30 ^{0}C) after being soaked in 0.68 M HCl (1:10 w/v). The shells were washed in the acid until evolution of bubbles ceased and no colour change observed. The demineralized shell was washed in distilled water to neutral and dried. Protein removal took place by soaking in 0.62 M NaOH solution (1:10 w/v) at the same temperature of demineralization for 16hrs. The mussel shell was discovered to contain 51.62 % $CaCO_3$ and 21.32 % chitin. In a bid to devise an unconventional method for demineralization, Mahmoud *et al*. (2007) suggested the use of organic acids such as lactic and acetic acids produced by cheese during fermentation to demineralize microbially deproteinized shrimp shells, where effects of acid type, demineralization temperature, retention time and shell to acid ratio were investigated. The study showed that the effectiveness of the used organic acids for the demineralization of shrimp shells had comparable results with that of conventionally used HCl. It was reported that using shells to acid ratio of 1:20, temperature of 24 ^{0}C (room temperature) and retention time of 2hrs yielded satisfactory results such that the total mineral removal efficiencies were 97.4 and 99.11% and 86.36 and 85.33% for lactic and acetic acids, respectively. The study concluded that using organic acids for the demineralization of shrimp shells would result in effective removal of minerals, reduction in the purification cost, preservation of natural chitin characteristics and production of value added products such as food preservatives and/or an environmentally friendly de-icing/ anti-icing agents.

2.7 Characterizations Determining the Physicochemical Properties of Chitin

2.7.1 X-Ray Diffraction

Chitin, as disclosed by X-Ray diffraction studies, is a highly ordered crystalline structure with three polymorphic forms, α, β, and γ - chitin (Aranaz *et al*., 2009), which differ in the arrangement of the chains within the crystalline regions as shown in Figure 14.

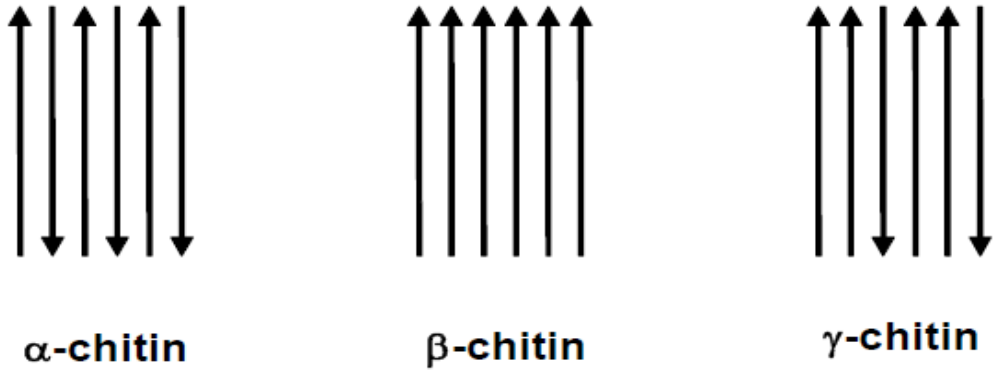

Figure 14: Arrangement of the polymer chains in the three forms of chitin (Einbu, 2007)

The three chitin variants differ in their degree of hydration, unit cell size and number of chitin chains per unit cell. The α- chitin is the most crystalline and compact form, where the chains are arranged in an antiparallel fashion (Nam *et al*., 2010). Chitin in its β - form consists of parallel chains, while in γ - chitin, two out of three chains are parallel with the third oriented in the opposite direction. The distribution of the polymorphic forms is not related to taxonomy, as different forms may occur in one organism, providing different functional properties: The most abundant of these forms is α- chitin and it is usually found where extreme hardness is required (Nam *et al*., 2010). Both β and γ - chitins seem to provide toughness, flexibility and motility and may have physiological functions other than support (Al Sagheer *et a*l., 2009). Alvarez, 2014 however reports that this parallel arrangement processed by β – chitin yields weak intermolecular forces. The poor solubility of chitin is a result of the close packing of chains and its strong inter and intra molecular bonds among the hydroxyl (OH) and acetamide ($RCONH_2$) groups (Einbu, 2007). The inability of α- chitin to swell upon soaking in water is explained by the extensive intermolecular hydrogen bonding (Nikolov *et al*., 2011). On the other hand, β -chitin lacks these interchain hydrogen bonds and therefore swells readily in water (Einbu, 2007).

Numerous X-ray spectroscopic studies of chitin have yielded the diffractive patterns of chitin. However, different sources have characterized these patterns with differently indexed crystalline peaks. They can be labeled either using *d*, the centre-to-centre spacing of the crystallites or Miller indices. It is also very common to describe the diffraction pattern using the values of angles .Typical spectrum of a chitin fiber shown in Figure 15 (Muzzarelli *et al*., 2004) exhibits broad peaks at d = 0.34, 0.45, 0.50 and 1.09 nm with a shoulder at 0.71 nm. The XRD patterns of α and β -chitins are shown in Figure 16. The XRD pattern of β -chitin exhibits a broad diffuse scattering and less intense peaks compared with the profile for α -chitin. The clear difference in the spectra of the two polymorphs is due to differences in the crystallographic arrangements of these two polymorphs (Daraghmeh *et al*., 2011). Typical chitin diffraction pattern, given in angle form has shown strong reflections at 2θ = 9–10° and 2θ = 20–21° with minor reflections at higher 2θ values, for example, at 26.4° and beyond (Shervani *et al.*, 2012) as shown in Figure 17.

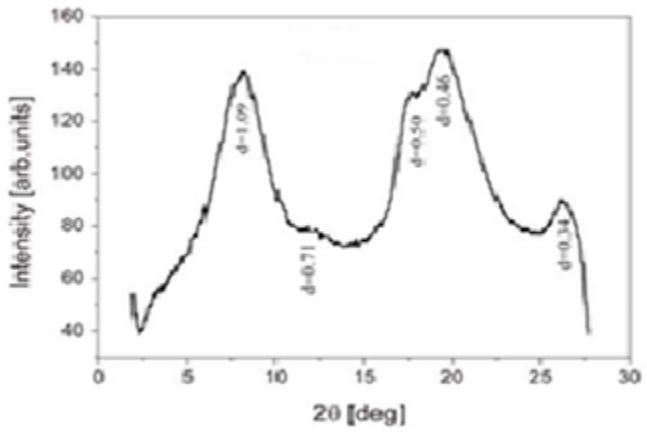

Figure 15: Labeling of chitin XRD peaks using d –spacing (Muzzarelli *et al*., 2004)

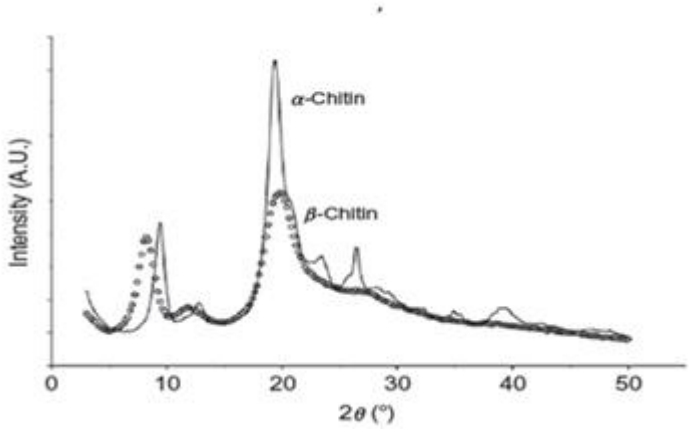

Figure 16: XRD patterns of α and β –chitins (Daraghmeh *et al*., 2011)

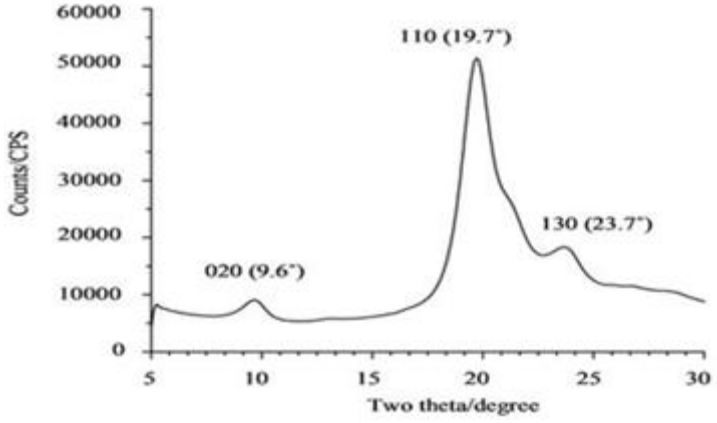

Figure 17: Labeling of chitin XRD peaks using Miller indices (Shervani *et al.*, 2012)

2.7.2 Infrared Spectroscopy (IR)

Infrared (IR) spectroscopy is one of the most important and widely used analytical techniques available to scientists working on chitin. It is based on the vibrations of the atoms of a molecule. The spectrum is commonly obtained by passing IR electromagnetic radiation through a sample that possesses a permanent or induced dipole moment and determining what fraction of the incident radiation is absorbed at a particular energy (Stuart, 2004). The energy of each peak in an absorption spectrum corresponds to the frequency of the vibration of a molecule part which allows qualitative identification of certain bond types in the sample. In recent times, the total spectrum is analyzed by an interference process and converted into the frequency or wavenumber range by means of a mathematical process known as the Fourier transform. Fourier transform infrared (FTIR) spectroscopy has dramatically improved the quality of infrared spectra and minimized the time required to obtain data (Lima *et al*., 2015). The FTIR spectra of α and β -chitin are shown in Figure 18 (Daraghmeh *et al*., 2011). For α -chitin, the amide I band is split at about 1650 and 1620 cm^{-1} (Figure 18a), whereas it is a single sharp band at about 1657 cm^{-1} for β -chitin (Figure 18b). The amide II band appears at about 1555 and 1559 cm^{-1} for α and β -chitin, respectively. Both polymorphs show strong absorption bands in the 3100–3285 cm^{-1} region which corresponds to the N–H group. The bands in the 2840–2960 cm^{-1} region are due to CH, CH_2, and CH_3 in both chitin polymorphs.

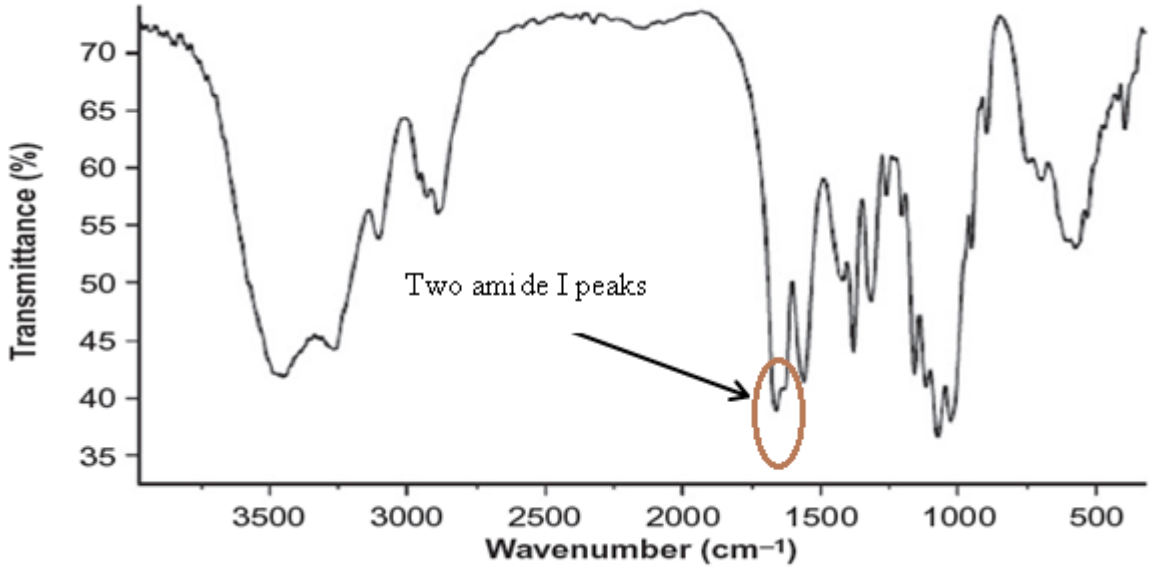

a

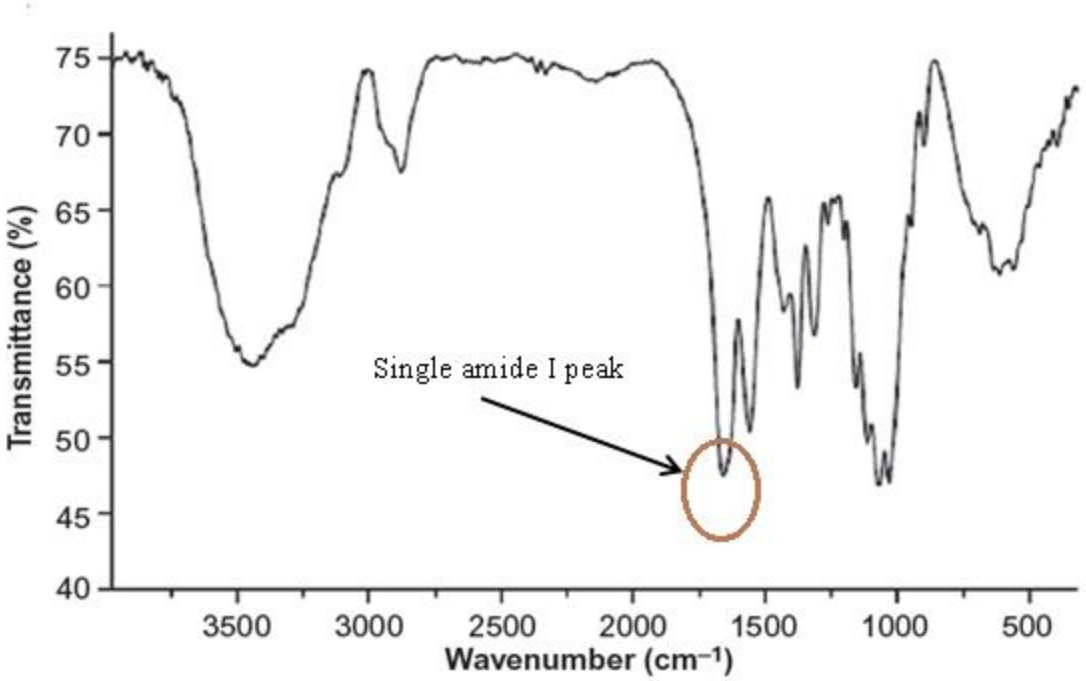

b

Figure 18: FTIR of (a) α – chitin (b) β – chitin (Daraghmeh *et al*., 2011)

2.7.3 Mophorlogy

The morphology of chitin has been determined using a Quanta-200 3D SEM operated at an accelerating voltage of 1200 V by Daraghmeh *et al*., 2011. The sample (0.5 mg) was mounted onto a 5 x 5 mm silicon wafer affixed via graphite tape to an aluminum stub. The powder was then sputter-coated for 105sec at a beam current of $20mA/dm^3$ with a 100 Å layer of gold/palladium alloy. The SEM image (Figure 19) showed a highly porous structure of α-chitin in addition to the high particulate surface area. Under SEM examination, Yen *et al*., 2009 observed the morphology of purified chitin sourced from crab shell to possess distinctly arranged microfibrillar crystalline structure (Figure 20). Wang *et al*., 2013 reported that the structure of Antarctic krill chitin is tightly arranged (Figure 21). This structural arrangement was similar to that observed in the raw Antarctic krill shell which explains that chitin is a major component of the shell reticular skeleton. In addition, protein macromolecules are irregularly attached to the chitin backbone while inorganic components such as calcite are strongly embedded in chitin gaps. The spaces between the chitin chains were considerably reduced after protein and mineral removal while the pattern observed before treatment was preserved, suggesting that the native structure of chitin was also preserved. The surface morphology of chitin varies according to the organisms they are sourced from (Kaya *et al*., 2014). According to them, chitin may be classified into three surface morphologies: (1) with porosity and microfibrillar structure, (2) without porosity or microfibrillar structure, and (3) with only microfibrillar structure. Extracting chitin from water louse, beetle, dragon fly, backswimmer (aquatic insect) and bug, Kaya *et al*., (2014) concluded morphologies showed only microfibril and no porous structure (Figure 22).

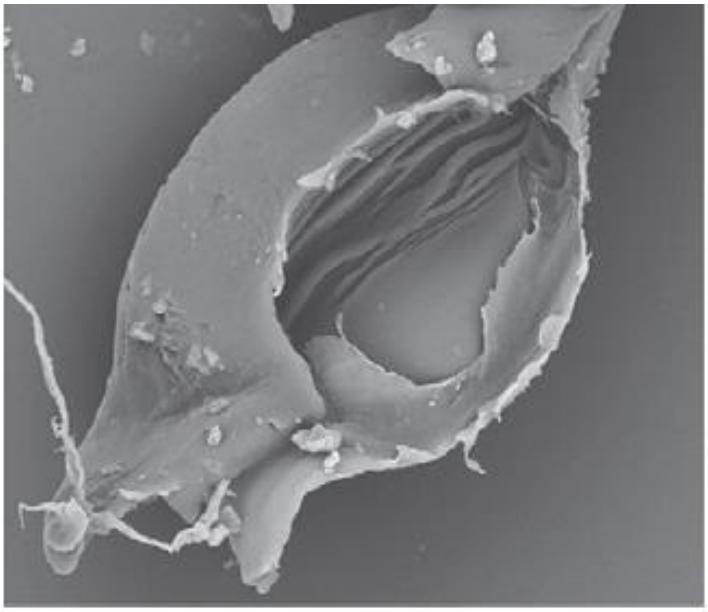

Figure 19: SEM of α-chitin showing a porous structure (Daraghmeh *et al*., 2011)

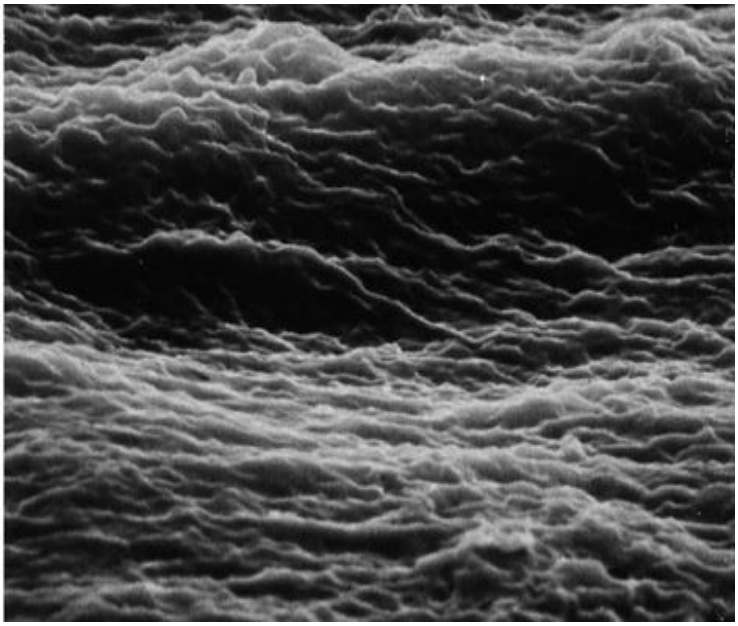

Figure 20: SEM of crab chitin showing distinctly arranged microfibrillar crystalline structure (Yen *et al*., 2009)

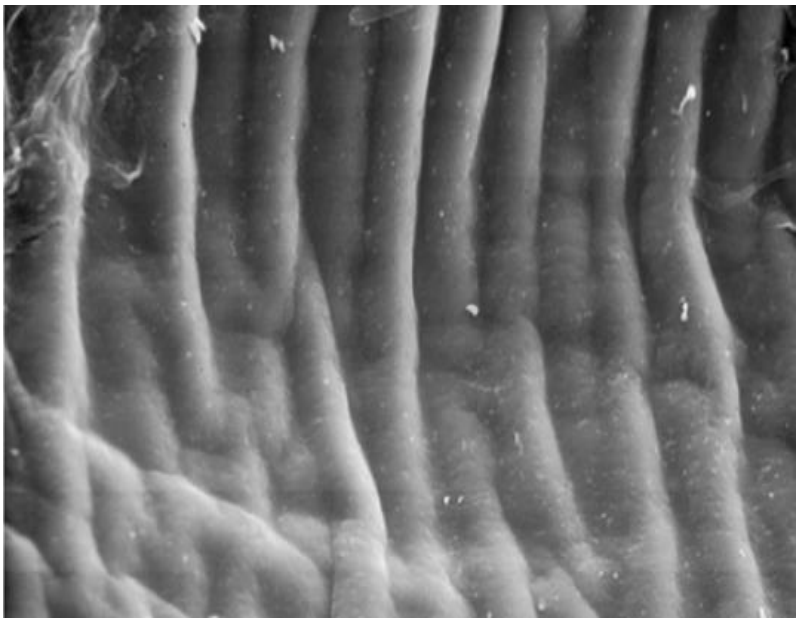

Figure 21: SEM of Antarctic krill chitin shown a tightly arranged structure (Wang *et al*., 2013)

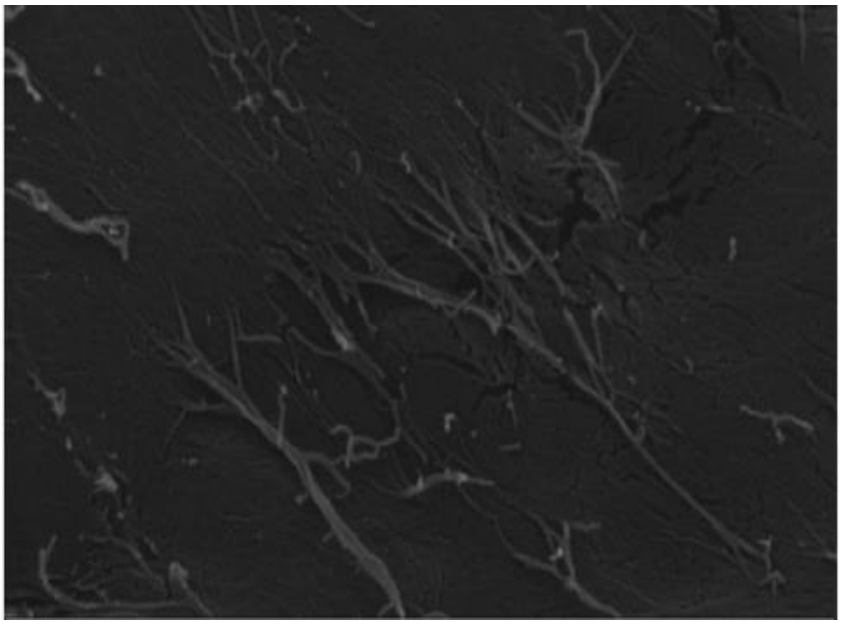

Figure 22: SEM of water louse chitin showing microfibrils with no porous structure (Kaya *et al*., 2014)

2.8 Review of Related Works on Chitin

Andrade *et al*. (2012) characterized chitin extracted from exoskeletons of shrimp and crabs. Both shells were washed, cleaned and ground to 0.297 mm particle size. HCl concentrations of 2.5 % v/v and 7.0 % v/v were used in the demineralization process for the ground shrimp and crab shells respectively to reduce the ash content as well as the elimination of carbonates and phosphates from the samples. Deproteinization step involved the use of 5 % w/v NaOH to reduce the nitrogen content of protein. Samples were subsequently washed, dried and finally depigmentized by mixing deproteinized samples with 0.36 % v/v solution of sodium hypochlorite (NaOCl) under stirring to produce chitin. The yield of chitin obtained from shrimp exoskeleton was observed to be 41% while that from crab shell was 56%. Thermogravimetric analysis of both samples showed degradation of saccharide structure of the molecules occurring in the range 400-500 ^{0}C. The topography of chitin samples inspected under SEM showed that both chitin samples possessed similar structures with loosely attached geometrically irregular fine particles. Ameh *et al*. (2013) studied the kinetics of demineralization of shrimp exoskeleton in chitin by commencing with deproteinization in 3 % NaOH at variable times between 5 and 30 minutes by boiling at 95 ^{0}C, where the yield of deproteinized material was determined with time. At the optimum deproteinization time, the shell was demineralized in 1.25 N solution of HCl at room temperature for times ranging between 20-100 minutes with stirring. Treated samples were characterized for compositional analysis using XRF. The result was that the composition of calcium decreased with increasing time. Cadmium was found to be present in the demineralized samples and this was attributed to the accumulation of metallothionein proteins within aquatic invertebrates of this kind that strongly bind to the metals. Based on the reducing trend in the calcium content of the demineralized shell with time, a tool that modelled fluid-

particle reactions (shrinking code model) was employed, where calcium content was used as a reference. This model provided three expressions, which were represented on a graph of fractional conversion of calcium against time namely, chemical reaction controlled mechanism (CRC), diffusion through ash layer controlled mechanism (ALDF) and fluid film diffusion controlled mechanism (FFDC). Fitting experimental kinetic data to the shrinking core model for fluid-particle reactions, the CRC gave the best predictive model, as depicted by the fit (R^2 = 0.92), with a 3hr time of complete reaction. Liman *et al*., (2010) deproteinized shrimp and squilla shell wastes by boiling in 3 % aqueous NaOH for 15 minutes. This process was repeated after draining the initial alkali for the removal of residual protein from the shell. Demineralization was done with the use of 1.25N HCl at room temperature for 1 hr after which the acid was drained off and washed thoroughly with tap water followed with distilled water. The chitin obtained was dried at ambient temperature (30 ± 2 ^{0}C) and pulverised into powder using a dry grinder for antioxidant, antibacterial and antifungal activity characterizations. Chitin extracts from the crustacean shells exhibited excellent protective features in antioxidant activity tests. Thus, it could serve as a natural source to replace synthetic antioxidants in the food industry. The study showed that various products of chitin with high antibacterial and fungicidal activities can be generated from crustacean by-products. Crab, crayfish, periwinkle and shrimp shells were ground to 250 μm particle sizes after being washed and dried (Isa *et al*., 2012). Demineralization was carried out at room temperature using 1 M HCl and this process was repeated several times until no gas evolved. The resulting solids from different samples were washed with distilled water until neutral pH and dried in an oven at 60 ^{0}C to constant weights. Deproteinization was carried out on each sample by heating samples in 1 M NaOH solution in a beaker at 100 ^{0}C. This treatment was repeated several times until no evidence of protein was noticed as the medium

show no colour at the end of the last treatment. Samples were washed with distilled water up to neutral and dried. The number of baths and duration for complete demineralization were noticed to be dependent on shell type as the crab shell took longer time and number of bath. Investigation showed that the shrimp had the highest yield of chitin of 8.15 % while crab, crayfish and periwinkle yielded 7.8, 2.88 and 0.44 % respectively. Mineral content ($CaCO_3$) of 76.8, 78.7, 66.8 and 97.5 % was contained in shrimp, crab, crayfish and periwinkle shells respectively. Proximate analysis showed that chitin from shrimp had highest moisture and protein content of 8.7 % and 4.1 6% respectively. Crayfish had the highest ash and fiber contents of 7.20 % and 6.98 % respectively while crab shell had the highest lipid content of 1.70 %. X-ray patterns of shrimp, crab and crayfish chitins showed five sharp peaks at 2θ =20, 24, 26, 34 and 39^0 but with different intensities, while the peaks of the shrimp showed the highest intensity at 2θ angle of 20^0. The XRD profile of the chitin of shrimp exhibited well resolved and intense peaks unlike crab and crayfish chitins that displayed broad diffuse scattering and less intense peaks, indicating that shrimp chitin was the most crystalline.

Isolation of chitin from *Gammarus* was done by Kaya *et al*. (2014) for physicochemical investigations. *Gammarus* was ground to fine powder and was refluxed in 1100 ml 1M HCl solution for 2hrs at 60 ^{0}C. Sample was filtered off and the residue was rinsed thoroughly with deionized water. To achieve deproteinization step, the filtrate was treated with 100 ml of 1M NaOH solution for 23hrs at 77.5 ^{0}C. After washing repeatedly with deionized water, the sample was placed in a vacuum oven at 70 ^{0}C. Following the drying process, it was incubated in an organic solution mixture containing chloroform, methanol, and water (in the ratio of 1:2:4) for 1 hr for elimination of lipids, decolourisation and bleaching. The chitin content was investigated and established to contain 11-12 % of dry weight. Two strong (9.24 and 19.44^0) and three weak

(12.8, 23.4 and 26.58^0) peaks were observed in the X-ray diffraction pattern of extracted chitin, revealing that the crystalline structure of α - chitin polymer was found in *Gammarus*. Fibrous structure with sizes ranging between 15 and 55 nm with porous structure of about 150 nm sizes were revealed in the SEM analysis. The characterization studies of α-chitin isolated from *Gammarus* provides an insight into possible applications of chitin-derived products in textile, wound dressing and drug delivery system, serving as an alternative chitin source.

Insect chitin was isolated from adult beetle by Liu *et al*., (2012). The beetles were starved for 48 hrs to eliminate gut contents, washed with water and killed by freezing. They were allowed to thaw at room temperature (32^{0}C) and air-dried at 50 ^{0}C for 2 days. The dried beetles were milled to powder to pass through a 20-mesh screen and stored at 4^{0}C in airtight containers. Demineralization was carried out using 250 ml of 1 M HCl solution at 100 ^{0}C for 30 minutes to remove minerals and catechols. This step was followed by rinsing with distilled water until neutrality was reached. Deproteinization was performed using 250 ml of 1 M NaOH solution at 80 ^{0}C for 24hrs and the product was washed with distilled water until the pH became neutral. Potassium permanganate solution (100 mL) was used on the washed precipitate for 1hr for the purpose of decolorization. Finally, lightly brown chitin was washed with distilled water and dried at 50 ^{0}C in a dry heat sterilizer. Elemental analysis showed that the total nitrogen content after extraction dropped to 6.45 % from 11 % observed before treatment and this indicate protein removal. Strong reflections at 9.2 and 19.1° with minor reflections at 12.6, 22.9 and 26.2°were shown in the XRD. The crystallinity degree of 89.05 % was calculated from the data and the chitin DA was found to be 93.1 %.

Characterization of chitin from irradiated and non-irradiated shrimp wastes (Nesr *et al*., 2013) has been done. These wastes were washed, dried and minced to powder with a food blender to

250μm size sieves. Powders were classified into three groups before chemical treatments: (1) no gamma ray irradiation (2) and (3) were packaged in polyethylene bags and irradiated at doses of 20 and 25 kGy, respectively. Demineralization was carried out at room temperature using 1 M HCl, which was washed with distilled water until neutrality. Dried demineralized samples were deproteinized using alkaline treatments with 1 M NaOH solutions at 100 ^{0}C. The treatment was repeated several times until a clear solution was formed and this indicated the absence of proteins. Finally, it was washed with hot ethanol and boiled in acetone to remove any impurities. It was found that the irradiation dose at 25 kGy, caused the reduction time of deproteination and demineralization processes by a factor of 3 and 5 folds respectively compared with non irradiated samples. Two methods of extraction have been used to compare the yield and purity of chitin extracted from silkworm (Paulino *et al*., 2006), which involved using a closed reactor and an open system (beaker). Dried chrysalides of silkworms were treated with 1.0M HCl for 20 minutes at 100 ^{0}C in a closed reactor for the elimination of catechols and also calcium, magnesium and potassium. Using the vacuum pump, it was filtered and the residue was repeatedly washed with deionized water to neutralize the excess of acid. In the sequence, the treatment with 1M NaOH at the same proportion used for the acid was performed for 24hrs at 80 ^{0}C for protein elimination. The hot solution was filtered and washed several times with deionized water to remove the excess of NaOH. The crystals of chitin finally extracted were washed several times with 0.4% sodium carbonate (Na_2CO_3), dried in an oven at 80 ^{0}C for spectroscopic characterization. Both methods produced chitin of high purity but the yield was found low when compared with those produced from crustacean shells. In searching for more ways of getting chitin from waste biomass, Zaku *et al*. (2011) attempted to extract chitin from the scales of common carp fish. The fish scale was washed and sun dried for three days and later ground in a

milling machine to fine powder. The ground scale was cleaned of mineral remains with 1M HCl (1:5 w/v) for 24hrs at room temperature (30 ^{0}C). Afterwards, it was severally rinsed with deionized water and deproteinized in 0.5 % NaOH (1:1 m/v) for 30 minutes at a temperature of 95 ^{0}C. Extracted chitin was rinsed several times with deionized water and dried for 4hrs at temperature of 80 ^{0}C. The percentage chitin yield calculated from the weight of chitin produced as a percentage of starting dry raw materials was 20.49 %. Morphological examination of the chitin by SEM showed that the biopolymer had porous and fibril structures while both crystalline and amorphous regions were observed in the structure using the XRD.

The above works have reported extraction and purification of chitin from various sources via chemical treatments. Physicochemical characterizations with XRD, XRF, SEM, TGA and FTIR were conducted to investigate chitin properties with respect to its origin where parameters such as treatment time, temperature, sample' size and reagent type were considered. However, studies on the effects of acid and alkali concentrations on the yield of α-chitin, DA, crystalline structure and thermal stability need to be carried out.

CHAPTER THREE

3.0. MATERIALS AND METHODS

3.1. Conceptual Framework

All broken bones go through the same healing process whether it is being cut as part of a surgical procedure or fractured through an injury (Shih, 2008). The healing potential of a bone is influenced by a variety of biochemical, biomechanical, cellular, hormonal and pathological mechanisms. A continuously occurring state of bone deposition, resorption and remodeling facilitates the healing process. Fracture healing is completed during the remodeling stage where the healing bone is restored to its original shape, structure and mechanical strength. This stage is facilitated by mechanical stress placed on the bone such that as the fracture site is exposed to an axial loading force, the bone is generally laid down where it is needed and resorbed from where it is not needed (Kaleas and FACS, 2001). Process of remodeling can lead to the phenomenon of stress shielding when an implant with much higher elastic moduli compared to the human bone is present (Seal *et al*., 2009). On the other hand using implants of much lower elastic moduli compared to the human bone can lead to an instance where there will be a rapid imposition of load (by the body mass) on the healing bone that could result to its further weakening. Bioresorbable and biodegradable polymeric materials such as PLA and chitin are chosen for this study because they can be broken down via degradation and absorbed by the body without the need for manual removal. Cui *et al.*, (2016) reported that the acetyl groups (CH_3CO) in chitin increases hydrogen bond occupancy, which eventually stabilizes its crystalline structure and enhances ultimate stress, stiffness and fracture strength. Despite these characteristics, its application in the industry is limited due to its poor reactivity and solubility in aqueous media (Guo *et al.,* 2002; Khong, 2013). Einbu (2007) reported that the acetyl groups in chitin contribute

to the formation of extensive hydrogen bonds that makes it behave in such manner. To curb this, its derivative with much lower mechanical strength, chitosan has been developed by removing the acetyl groups on C2 (de acetylation) to produce water soluble amino groups, NH_2 (Zhao *et al.,* 2011). Thus, chitin with the lowest DA is chosen as reinforcement for this study. Degradation of polymers can be categorized into two groups on the basis of their mechanisms: surface and bulk degradation. The rate of fluid (example, water) flow into the matrix is slower than the rate of polymer degradation in the case of surface or heterogenous erosion. As the surface is eroded and removed, the degradation front moves through the material core (Mobedi, *et al*., 2011). Surface eroding polymers have a greater ability to achieve zero-order release kinetic, and are therefore ideal candidates for developing drug delivery devices (Nair and Laurencin, 2007). In the case of polymers that undergo bulk degradation, the rate of fluid penetration into the matrix is faster than the rate of polymer degradation. The bulk degradation process is considered as homogeneous in which degradation occurs at a uniform rate throughout the polymer matrix (Vieira *et al*., 2011). Materials such as these can be used as temporary supporting devices as there will be no instance where one portion will degrade faster than the other. The fluid considered for this In vitro study is PBS, which is a physiological salt solution that works in the internal fluid of all cells. It consists of di-hydrogen phosphate ions ($H_2PO_4^-$) as a weak acid and hydrogen phosphate ions (HPO_4^{2-}) as a conjugate base of weak acid. These two ions are in equilibrium with each other. In the absence of phosphate buffer from cell fluid, there will be sharp changes in pH of cell fluids, which may cause cell death or improper working of different proteins and cell organelles present within the cell (Li *et al.,* 2016). The internal pH of most living cells has been reported to be close to 7.0 (Morimoto *et al.,* 2016). The pH of human blood for instance is 7.4 and, hence, a blood of pH < 7 or > 7.8 can cause death within minutes

(Casiday and Fray, 2012). Buffering of blood pH maintained at 7.4 is very important in most biological processes as small change in pH (deceased or high) can cause metabolic implications in human body like acidosis and alkalosis. Several In-vitro experiments in tissue engineering have been conducted using the PBS (Tsuji *et al.*, 2011; Chen, 2010).

3.2 Materials

3.2.1 List of Materials and Equipment

The materials and equipment used for this study are listed below:

- 500ml conical flasks with stoppers, 1litre beaker, 100ml and 2litre measuring cylinders, purchased at UCHE chemicals Bariga, Lagos – Nigeria
- Dibasic sodium phosphate (Na_2HPO_4)
- Dichloromethane (DCM), purchased at UCHE chemicals Bariga, Lagos – Nigeria
- Distilled water, obtained from the laboratory, Department of Chemistry, University of Lagos – Nigeria
- FTIR spectrometer (Nicolet 6700 M), located at the Materials Chemistry Laboratory, Redeemers University, Ede, Osun state-Nigeria
- Hydrochloric acid (HCl), purchased at UCHE chemicals Bariga, Lagos – Nigeria
- Hydrogen peroxide (H_2O_2), purchased at UCHE chemicals Bariga, Lagos – Nigeria
- Laboratory dry oven (DHG – 9030), situated at The Central Research Laboratory, University of Lagos - Nigeria
- MEXTECH TM 2 digital thermometer and hydrometer, purchased at UCHE chemicals Bariga, Lagos – Nigeria
- Mono basic potassium hydrogen phosphate, (KH_2PO_4)

- Polylactide (PLA), purchased from NATUREWORKS China
- PHS -25 pH meter, purchased at UCHE chemicals Bariga, Lagos - Nigeria
- SM 801A water bath, positioned at The Central Research Laboratory, University of Lagos-Nigeria
- Sodium hydroxide (NaOH), purchased at UCHE chemicals Bariga, Lagos – Nigeria
- Steel ball mill (A 50 43, Mashine, France), situated at The Federal Institute of Industrial Research, Oshodi (FIIRO) Lagos – Nigeria
- Stirring rods
- Standard sieve (60 BSS)
- Thermogravimetric Analyzer (TGA Q500), situated at the Materials Science Department, Soochow University, Suzhou-China
- PANanalytical X' Pert PRO MPD X-ray diffraction system PW3040/60 machine, installed at the Materials Science Department, Soochow University, Suzhou-China
- Tensometer (Instron 3369M), located at The Centre for Energy, Research and Development (CERD) Obafemi Awolowo University, Ile-Ife, Nigeria
- Variable pressure SEM (ASPEX 3020 model) operated with an electron intensity beam 15kV, equipped with Noran-Voyager energy dispersive spectroscope. Machine is located at the Department of Mechanical Engineering, Covenant University, Ota, Ogun state – Nigeria

3.2.2 Flow Chart of Research Methodology

A chart showing the stages involved in the experimental procedure for this study is shown in Figure 23.

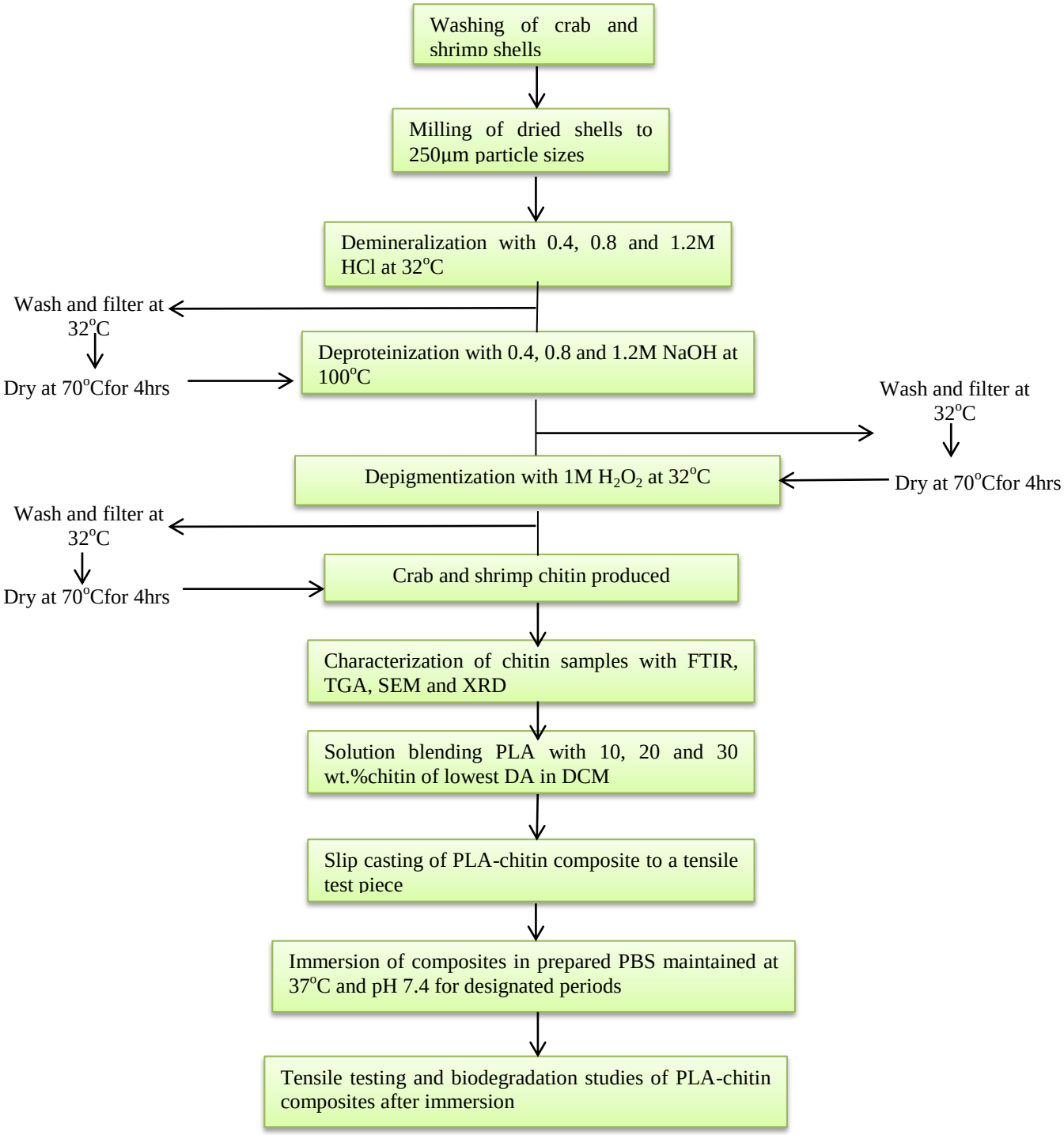

Figure 23: Flow chart of research methodology

3.3 Methods

3.3.1 Chitin Extraction

Shells of crab and shrimps were scraped free of loose tissues, washed, dried and ground with the use of a steel ball mill. The ground particles were sieved to size *2*50 μm using a standardized sieve of 60BSS as done by Isa *et al*., (2012). These crustacean shells were chosen for their relative abundance and ease of chitin isolation (Abdou *et al*., 2008; Isa *et al*., 2012). Demineralization was carried out at room temperature (32 ^{0}C) by soaking 100 g of ground samples in 0.4, 0.8 and 1.2MHCl. Using an acid of 37% purity and 1.18g/ml density, 0.4, 0.8 and 1.2M were prepared by dissolving 66.88, 133.76 and 200.64ml HCl for each concentration respectively in distilled water to fill a 2litre standard flask, which was shaken to achieve a homogenous mix. For each concentration, the process was repeated several times until evolution of gas ceased and the number of baths (in terms of acid volume) used was noted. The demineralized samples were washed with distilled water to neutral (pH7.0), filtered and dried in the oven at 70 ^{0}C for 4hrs to constant weights. Alkali solutions were prepared by dissolving 32, 64 and 96 g of NaOH pellets of 98% purity in distilled water to produce 0.4, 0.8 and 1.2M concentrations. Deproteinization was carried out on each sample by heating mineral - devoid samples in the different concentrations of NaOH solutions in a beaker at 100 ^{0}C for 1hr. At the end of this period, samples were filtered and soaked in fresh sets of alkali solutions (0.4, 0.8 and 1.2M) for 18 hrs at room temperature (32 ^{0}C) for effective protein removal. The samples were washed with distilled water to pH 7.0, filtered and oven dried at 70 ^{0}C. Depigmentization and bleaching was carried out by soaking extracted chitin in 1M H_2O_2 for 24hrs at 32 ^{0}C. The chitin was washed in distilled water and dried for 4hrs in an oven at 70 ^{0}C before characterizations.

3.3.2 Fourier Transform Infrared Spectroscopy (FTIR)

The FTIR is an essential and crucial characterization technique used by scientists to elucidate the structure of matter at the molecular scale. The chemical composition and the bond arrangement of constituents in a homopolymer, copolymer and polymer composite materials in general can be obtained via this spectroscopy (Bhargava *et al*., 2003). A Nicolet 6700 M spectrometer in transmission mode was used in carrying out FTIR spectra of samples. Ten milligram of fine samples were dispersed in a matrix of KBr (500 mg), followed by compression at 22 - 30MPa to form pellets. The transmittance measurements were carried out in the range of 500 - 4000 cm^{-1} and 4 cm^{-1} resolution. This was carried out at the Materials Chemistry Laboratory, Redeemers University, Ede, Osun state-Nigeria.

3.3.3 Degree of *N*- Acetylation (DA)

The DA of chitin determines many properties of the biopolymer including reactivity, processing and biodegradability. Of all the various analytical techniques developed for DA determination (Kasaai, 2010), FTIR has attracted the most attention as its method is convenient and relatively quick. It allows the DA values of chitin to be determined on the basis of absorption ratios in the solid state (Biskup *et al*., 2012). Several procedures using different absorption ratios have already been proposed for determining DA for chitin (Brugnerotto *et al.*, 2001; Duarte *et al*., 2002). Because amide I band is associated with acetyl groups of the molecule, DA use is justified for stating the acetylation degree of a chitin sample (Negrea *et al*., 2015). Thus, the ratio of absorbance of the characteristic acetyl band to the reference absorbance (O-H band) was chosen. The DA was calculated using the formula in Equation (2) as adopted by Kaya *et al*., (2014):

$$DA = \frac{A_{1650}}{A_{3450}} \times \frac{100}{1.33} \qquad (2)$$

where: A_{1650} is the absorbance of amide I vibration; A_{3450} , absorbance of OH vibration; 1.33 is a factor that represents the ratio of A_{1650}/A_{3450} for fully *N*-acetylated chitin.

3.3.4 Hydrogen bond

It is known and accepted that hydrogen bonds play an important role in determining the conformational and mechanical properties of structural polysaccharides (Ciolacu, *et al*., 2010). To study the hydrogen bonding of crab and shrimp chitins, broad and overlapped FTIR absorption spectra existing between 3600 and 3000 cm^{-1} were resolved and improved by their deconvolution from a background scattering using a Gaussian function curve-fitting analysis with an $r^2 > 0.99$.

The energy of the hydrogen bond, E_H (kcal) was calculated using Equation (3) (Ciolacu *et al*., 2010):

$$E_H = \frac{1}{k} x \left(\frac{V_o - V}{V_o}\right) \quad (3)$$

where: V_o is the standard frequency corresponding to free OH groups (3600 cm^{-1}); V is the frequency of the bonded OH groups and $k = 1.68 \times 10^{-2}$ $kcal^{-1}$

3.3.5 Thermogravimetric Analysis (TGA)

In TGA, the change in mass of a sample is usually measured as a function of temperature or time under an inert (nitrogen) or oxidative (air) atmosphere. TGA was used to quantitatively determine the constituent of minerals and organic compound (including the biopolymer) in the samples. Analysis of samples was carried out on TGA Q500 instrument situated at the Materials Science Department, Soochow University, Suzhou-China where 2 mg of samples was heated to 750 ^0C at 10^0C/minute heating rate. In this test, the temperature for the onset of thermal

decomposition (T_{onset}), the temperature at which decomposition rate was rapid (T_{max}) and chitin content were deduced from the thermograms.

3.3.6 Activation Energy (E_a)

The E_a for the thermal degradation has been used to explain the thermal stability of chitin (Wang *et al*., 2013). It was calculated from the TGA curves using the Broido method (Broido, 1969) as adopted by Abdel Hai *et al*. (2014) using Equation (4):

$$\text{Ln}\left(- \text{Ln}\,(1- X)\right) = - \frac{E_a}{RT} + \text{Const.} \qquad (4)$$

E_a is the activation energy of the degradation reaction (kJ/mol), R is the universal gas constant (8.314 J/mol·K) and T is the absolute temperature (K). The degree of decomposition X is given by Equation (5):

$$X = \frac{W_o - W_i}{W_o - W_f} \qquad (5)$$

where W_o is the initial weight of the sample, W_i is the instantaneous weight of the sample at time t and W_f the final weight of the sample. The plot of Ln (- Ln (1- X)) against 1/T gives a straight line whose slope is –E/R.

3.3.7 X-Ray Diffraction (XRD)

The XRD of the samples was conducted using PANanalytical X' Pert PRO MPD X-ray diffraction system PW3040/60 machine at the Materials Science Department, Soochow University, Suzhou-China. Samples were exposed to a monochromatic Cu Kα radiation (k = 1.5406 Å), operating at 40 kV and 40 mA. The samples were registered in a zero background sample holder to avoid external background interferences. The diffractograms were registered in the range of 7^0 to 90^0 (2θ) in a step scan mode of 0.026261 at a counting time of 17.34 seconds

per step. In order to calculate the crystallinity index (CrI), a method which has been employed previously for chitin was used and the expression is given in Equation (6) (Juarez de-la Rosa *et al*., 2015):

$$CrI = \left(\frac{I_c}{I_c + I_a}\right) \times 100 \quad (6)$$

where I_c and I_a represent the intensities of the crystalline and amorphous regions respectively.

3.3.8 Crystalline Size

Crystalline size normal to the h k l plane (D_{hkl}) was calculated from the full width of peak at the half height of the source curve using Equation (7) as adopted by Al Sagheer *et al*. (2009) and Wang *et al*. (2013):

$$D_{hkl} = \frac{k\lambda}{\beta \cos \theta} \quad (7)$$

where K is a constant (indicative of crystallite perfection and is assumed to be 1; λ(Å) is the wave length of incident radiation (1.5406 Å); β (rad) is the width of the crystalline peak at half height, and θ (deg) is the diffraction angle corresponding to the crystalline peak.

3.3.9 Scanning Electron Microscopy (SEM) with Energy Dispersive X-ray Analysis (EDS)

An ASPEX 3020 model variable pressure SEM operated with an electron intensity beam 15kV and equipped with Noran-Voyager energy dispersive spectroscope was used to observe the morphological features of chin samples. The samples to be observed under the SEM were mounted on a conductive carbon imprint left by the adhesive tape prepared by placing the samples on the circular holder and coated for 5 minutes to enable it conduct electricity. For EDS analysis, samples were analyzed at an accelerating voltage of 15 kV. This was carried out in the Department of Mechanical Engineering, Covenant University, Ota, Ogun state –Nigeria.

3.3.10 Preparation of Phosphate Buffered Solution (PBS)

Two solutions were combined to make the PBS. The first solution was prepared by dissolving 9.47g dibasic sodium phosphate, Na_2HPO_4 in distilled water to make 1litre. Mono basic potassium hydrogen phosphate, KH_2PO_4, constituted the second solution and was prepared by dissolving 9.08g in distilled water until 1litre mixture was achieved. The solution mixture (161ml Na_2HPO_4 and 39 ml $KH_2PO_{4)}$ was maintained at pH7.4 and 37 ^{0}C.

3.3.11 Processing of PLA and PLA-Chitin Composites

Twenty grams of corn starch-sourced PLA pellets obtained from NATURE WORKS (Figure 24a) was added to 75 ml DCM, and sealed in a glass beaker for 3hrs at room temperature (32 ^{0}C). Within this period, the mixture was manually stirred for 3 minutes and resealed at the end of each hour. At the end of the soaking time, PLA melted fully in DCM leaving a clear solution (Figure 24b). The melt was poured into a flexible silicon mould (Figure 24c) for easy sample removal with a cavity of a tensile test piece shape. Fully solidified processed PLA sample (Figure 24d) was removed after 6hrs of pouring. Composites were produced by adding α-chitin particles from both sources (shrimp and crab) to PLA melt as 10, 20 and 30 wt. % reinforcements, respectively. Mixture of chitin and PLA pellet was stirred in DCM as done for unreinforced PLA to ensure a homogenous mix prior to pouring. Solidified composite samples were recovered after 4hrs (composites solidified faster).

a b

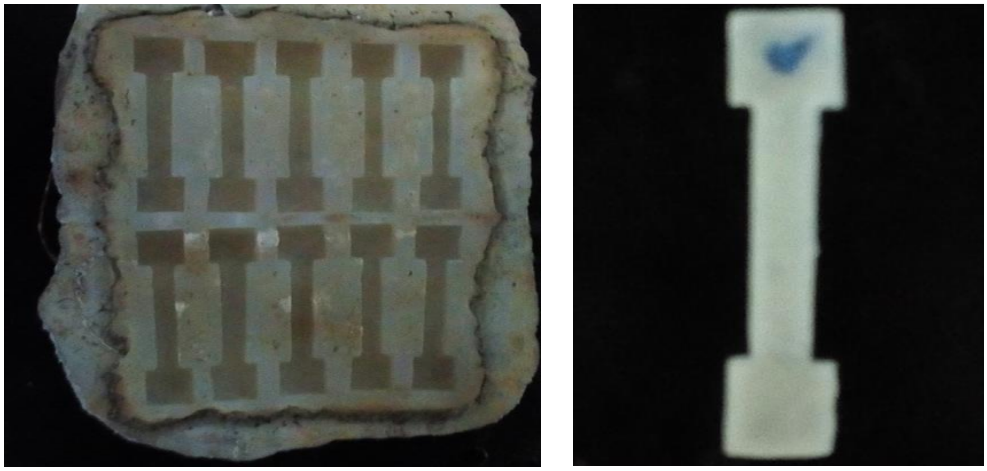

c d

Figure 24: (a) PLA pellets (b) PLA melt in DCM (c) flexible silica mold with cavities filled with molten PLA (d) cast PLA tensile test piece

3.3.12 In-vitro Degradation Studies

In this study, the In-vitro degradation characteristics of pure PLA and its composites were evaluated by immersing pre weighed samples in 500ml conical flasks containing PBS of pH 7.4 at 37 ^{0}C. Samples characterized for elastic modulus were immersed in PBS for 8 weeks to conform to the recommendation of Shih (2008) who reported that on the 8th week of implantation, bone would have healed to a remarkable level for gradual load bearing. Degradation time of 12 weeks was allowed for samples assigned for hydrolytic degradation study such that the maximum mass of fluid diffused into each sample could be adequately determined. At the end of each week, samples were removed and immediately weighed. Drying of samples was done using an oven operated at 70 ^{0}C for 5hrs and weighed before characterizations.

3.3.13 Degree of Erosion

The degree of erosion associated with the biodegradation process is usually estimated from measurements of mass loss (Vieira *et al.,* 2011). The percentage weight loss, W% was computed using Equation (8):

$$W\% = \frac{W_o - W_f}{W_o} \times 100 \qquad (8)$$

W_o and W_r, are the initial and the residual weight of the specimen, respectively.

3.3.14 Diffusion Time and Hydrolysis Time

Increase in weight of samples as a result of fluid absorption (PBS) was described in terms of diffusion coefficient, D and the mass of maximum fluid content, M_m as shown in Equation (9) (Ndazi and Karlsson1, 2011).

$$D = \pi \left(\frac{kh}{4M_m}\right)^2 \quad (9)$$

M_m is the maximum amount of fluid absorbed; h is the thickness of the specimen; t is the fluid time; k is the initial linear curve of M_t against $t^{1/2}$. M_t is the degree of fluid absorption at time t.

Diffusion time was calculated using Equation (10) (Vieira *et al.*, 2011).

$$T_D = \frac{h^2}{D} \quad (10)$$

Hydrolysis time was calculated using Equation (11).

$$T_H = \frac{t}{Mt} \quad (11)$$

3.3.15 Tensile Testing

The tensile test of pure PLA and PLA/chitin composites cast was determined using the Instron 3369M Tensometer located at CERD Obafemi Awolowo University, Ile-Ife, Nigeria. Each sample was fixed and held firmly at both ends by the gauge as load was applied at until the sample finally failed. Data of stress and strain values were generated by the equipment and the elastic modulus of samples was calculated from the linear portion of these values.

3.3.16 Strength Decrease Rate

Strength evolution has been found to follow the same trend as the molecular weight loss during polymer degradation (Vieira *et al.,* 2011). It is thus represented with a similar relationship obtained for the molecular weight using Equation (12):

$$\sigma = \sigma_0 e^{-u_s t} \quad (12)$$

where u_s is directly related to the kinetic constant of the material and explains the rate at which such material looses its strength during degradation; σ and σ_0 are fracture and yield strengths respectively calculated from tensile test results.

CHAPTER FOUR

4.0 RESULTS AND DISCUSSION

4.1 Crab Shell FTIR Analysis

Various absorption bands within the 4000-500 cm $^{-1}$ range were recorded in the FTIR spectrum of crab shell (Figure 25). The spectrum shows that there are different functional groups detected on the surface of the shell. Broad peaks detected between 3500 and 3300 cm-^{1}could be assigned to O-H stretching of the water molecule and N-H groups. The peak at 2895 cm^{-1} correspond to C–H stretching vibrations of aliphatic hydrocarbons (alkane groups) while the peak at 1655 cm^{-1} is caused by stretching vibrations of C=O (amide I). A small absorption band occurring at 2521cm^{-1} represents carboxylic acid (-COOH) and this is similar to the work of Islam *et al*. (2011) where this functional group was observed at 2520cm^{-1} in their bid to characterize calcium carbonate from cockle shell. Absorption peaks at 1794 cm^{-1} , 1476 cm^{-1} and 874 cm^{-1} represent stretching and bending vibrations of calcite, $CaCO_3$ (Rahman and Halfar, 2014; Sreedha*r et al*., 2012). Absorption band at 1419 cm^{-1} confirms the presence of CH_3 bending and CH_2 deformation (Daraghmeh *et al*., 2011). The obtained spectrum in this study compare favorably with that reported by Porpino *et al*. (2011), where the spectra of *Ucides cordatus* carb shells were observed.

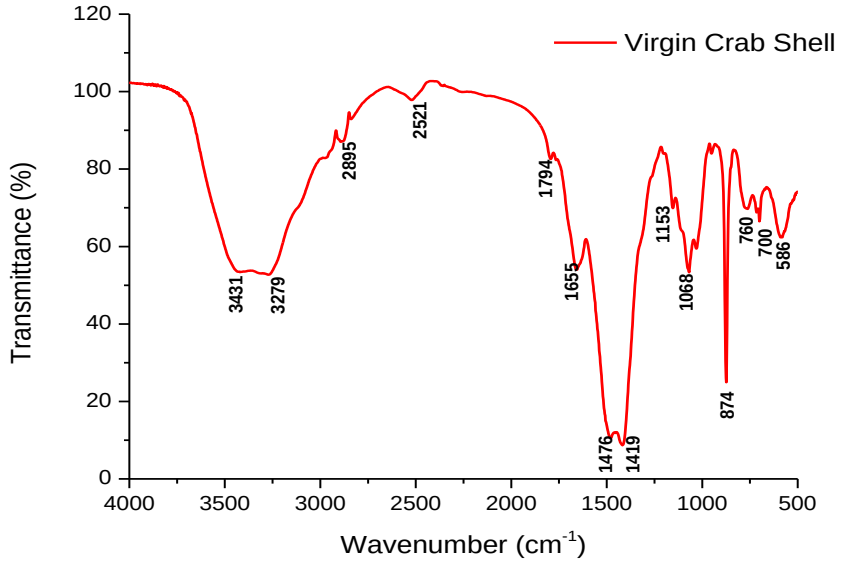

Figure 25: FTIR spectra of virgin crab shell

To verify the efficacy of reagents used, spectra of untreated, fully treated (acid with alkali) and acid treated crab shell particles are superimposed for comparison (Figure 26). The significant information from this comparison is the disappearance of the peaks at 1794, 1476 and 874 cm^{-1}. The elimination of these peaks in the FTIR spectra of acid treated and fully treated shells confirm that these peaks belong to the free carbonate ion, CO_3^{2-} (Veerasingam and Venkatachalapathy, 2014; Luquet *et al*., 2013). Thus, the current chemical extraction treatment removes the proteins and minerals through series of chemical processing steps. Examining the acid treated only and the fully treated spectra for the crab shell (Figure 26), the involvement of acid in the treatment leads to the disappearance of the $CaCO_3$, thereby generating a chitin spectrum but with significant prominence when NaOH is involved as observed in fully treated sample. The spectra position and shape were almost similar having little differences. In the region of the OH and NH groups (3000–3600 cm^{-1}), chitin shows a more detailed structure than the sample treated only with acid as two peaks at 3496 and 3446 cm^{-1} assigned to the intra molecular hydrogen bonds

O H(6)· · ·O C and O H(3)· ·O-5, respectively exist. In this region, acid treated only sample shows a single broad band centered at 3457 cm^{-1}; this slight structural difference in this region could be attributed to the presence of proteins existing in the partially treated sample causing different packing arrangements of macromolecules. The bands due to NH group at 3266 and 3107 cm^{-1} assigned to the vibrational modes involved in intermolecular hydrogen bonding CO·.·HN and the intra molecular bonds NH groups respectively are clearly seen in the chitin spectra but weak and not easily observed in the partially treated sample (acid treated only). In addition, there exists a band at 2400 cm^{-1} in the sample treated only with acid representing carboxylic acid (-COOH) that shifted from 2517 cm^{-1} in the virgin shell. After deproteinization with NaOH, transmittance of all chitin bands increase, thus showing higher prevalence of bonds. This implies that the accentuation of peaks in the fully treated sample (chitin) is activated by the alkali contact. Furthermore, the heterogeneity nature of virgin crab exoskeleton prevents the bending of N-H at 1559 cm^{-1}, stretching of C-N groups and CH_2 wagging at 1314 cm^{-1} while the formation of amide I band at 1655 cm^{-1} is noted to be weak.

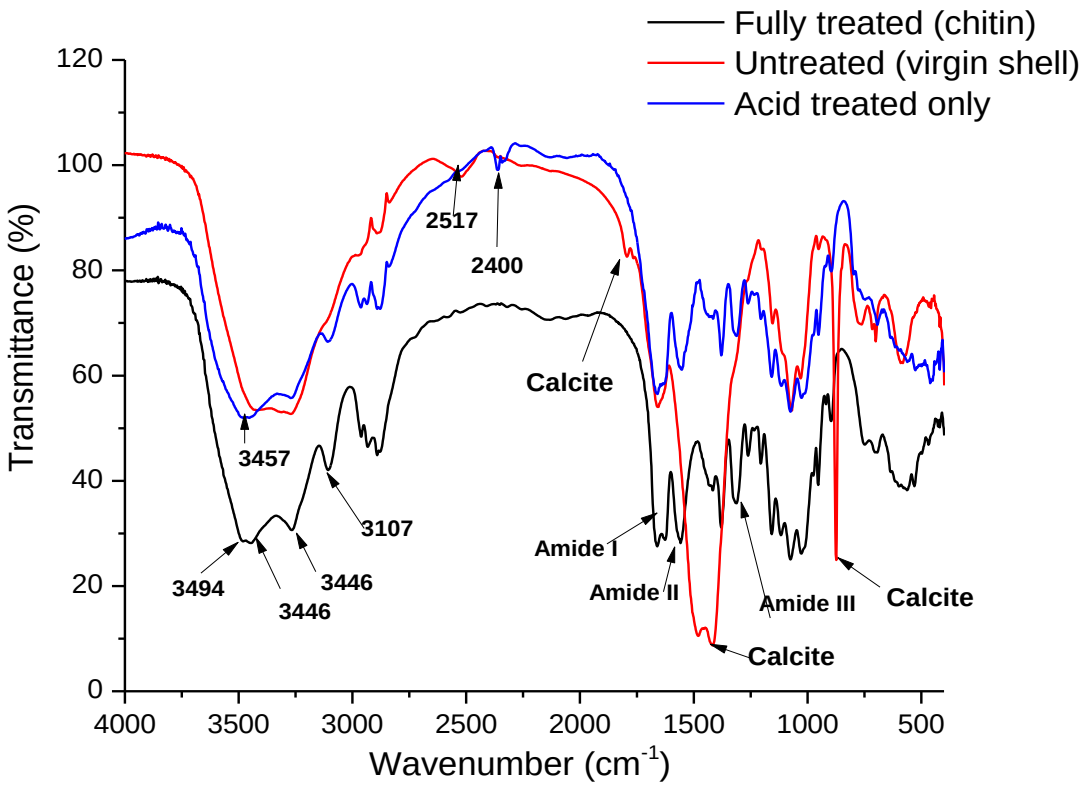

Figure 26: FTIR spectra of untreated, fully treated and acid treated crab shell

Spectra of chitin extracted from crab shell are shown in Figure 10 a-c and are similar to those obtained in literature (Daraghmeh *et al*., 2011) for commercial chitin. This attests to the potency of qualitative demineralization and deproteinization processes adopted. Bands at 3447 and 3279 cm^{-1}, indicate the stretching vibration of aliphatic O-H and NH, which is more evident in the chitin spectrum. Absorption peak at 2933 cm^{-1} represents C-H vibration of CH_3 while the stretching vibrations of the carbonyl group, C=O from acetamide ($-NHCOCH_3$) at 1663 and 1628 cm^{-1} confirms the presence of amide I. The FTIR spectrum has been one of the major techniques used in distinguishing between the two major polymorphs of chitin- α and β-chitin respectively (Kaya *et al.*, 2014). According to Cárdenas *et al*. (2004) the significant spectral difference is attributed to the frequency of the vibration modes of amide I, which is in the region 1660 – 1620

cm^{-1}, where two absorptions are observed at 1660 and 1627 cm^{-1} for α- chitin and only one band at 1630 cm^{-1} for β –chitin. Brunner *et al*. (2009) reported that for α-chitin, the amide I band is split into two components at 1660 and 1630 cm^{-1} respectively. This is attributed to the occurrence of the intermolecular hydrogen bond C=O· · .H N and the intra molecular hydrogen bond C=O· · ·$HOCH_2$ respectively, which exists in α- chitin. But for chitin in the β- form, only the intermolecular hydrogen bonds exists (Liu *et al*., 2012). Extensive hydrogen bonding in α-chitin was reported by Kurita (2001) to be a reason for its improved stability as it possesses poor solubility in water (Kumirska *et al*., 2010). It has been confirmed to contribute significantly to increase in crustacean shell strength (Ehrlich, 2010) as it is the substrate that binds other macro molecule, which later induces nucleation of the physical phase (Weiss *et al*., 2006). The existence of amide I bands at 1662 and 1628 cm^{-1} in this work implies that the chitin extracted is α- form and has not been altered by concentrations of reagents. Other characteristic absorptions for chitin were at 1558 and 1313 cm^{-1}, implying the bending vibration of –NH (amide II) and stretching vibration of –CN (amide III) from acetamide group respectively. The stretching vibration for –C-O-C- of the glucosamine ring occur at 1028 and 1074 cm^{-1} (Juarez de-la Rosa *et al*., 2012).The existence of peaks at 3447, 2891 and 951 cm^{-1} have been affirmed to be absent in β- form, which further confirms that α- allotropic form of chitin is extracted in this present study (Daraghmeh *et al*., 2011). Similar spectra pattern are observed for each chitin samples extracted from varying acid and alkali concentrations as no additional band is identified (Figures 27-29). The difference in peak intensities is attributed to the influence of reagent concentrations on chitin structure, which reduces with increasing reagent concentrations.

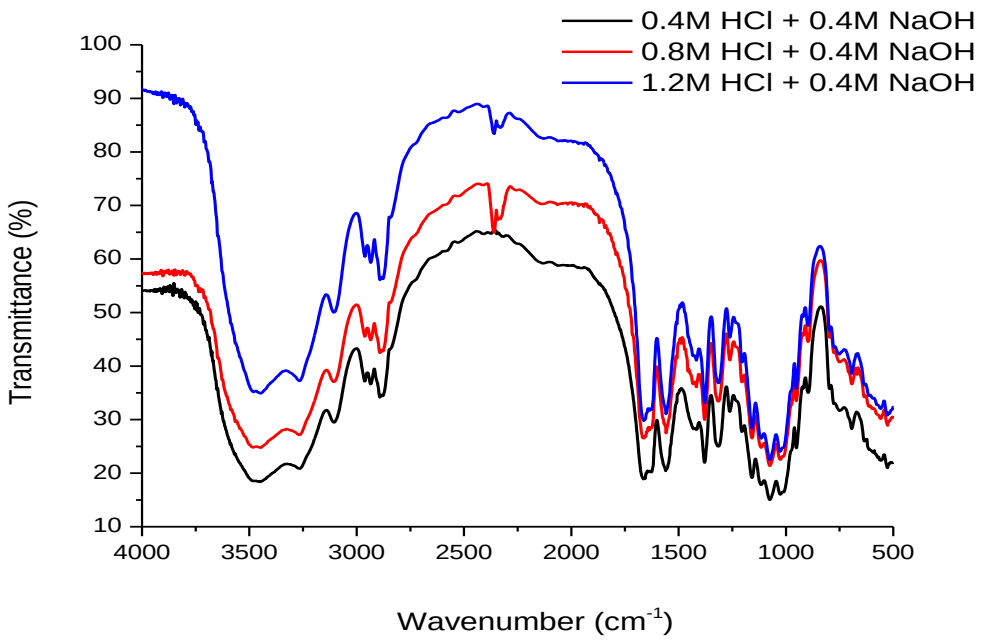

Figure 27: FTIR spectra of crab chitin extracted from different acid concentrations and 0.4M alkali

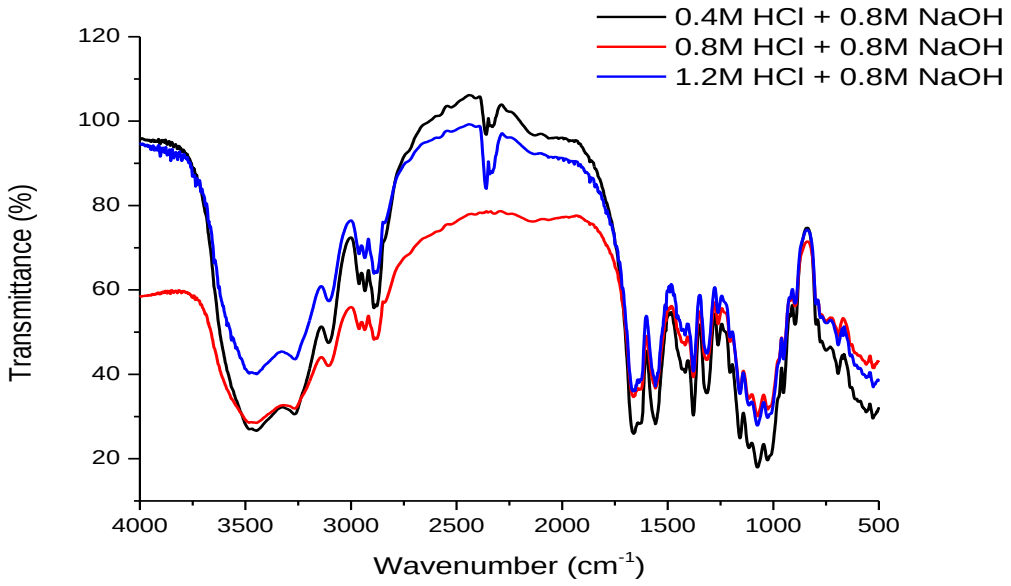

Figure 28: FTIR spectra of crab chitin extracted from different acid concentrations and 0.8M alkali

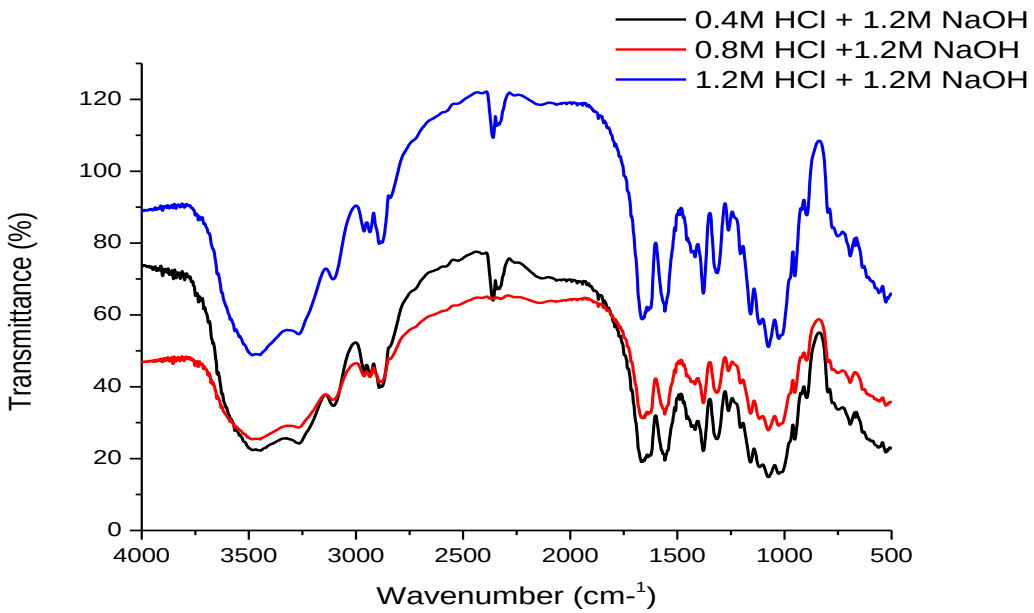

Figure 29: FTIR spectra of crab chitin extracted from different acid concentrations and 1.2M alkali

Maximum DA (98.5%) is obtained when treated with 0.4M HCl, and NaOH (Figure 30) and this shows that the number of glucopyranose units with the number of *N*-acetyl groups of this biopolymer is the highest for this sample. This is followed by 89.4 and 87.9% measured for crab shell fully treated with 0.8 and 1.2M HCl at 0.4M NaOH respectively. The DA of 88.6, 83.8 and 82.1% are calculated for 0.4, 0.8 and 1.2M HCl respectively at the same alkali concentration (0.8M). The lowest DA of 63.7% is recorded for crab shell treated at the highest acid and alkali concentrations (1.2M). Here, the resistance of acetamide groups imposed by the *trans* arrangement of the C2-C3 substituent in the sugar ring is lowered as in earlier study (Aranaz *et al*., 2009), hence, causing hydrolysis of such groups by the high alkali concentration as pointed out by Rojas *et al*., (2014). Other acetylation rates of 78.4 and 75.9% are obtained for 0.8 and 1.2M HCl treated shells respectively. Therefore, from this work, increasing concentrations of acid and alkali reduces chitin DA. Hajji *et al*. (2014) claimed that acetylated chitins with a rate of 70–90% and low in protein content are considered as good final products, while Kim (2011)

defined chitin to have DA>50%, otherwise its derivative, chitosan is formed. At DA < 20%, the polysaccharide is found to exhibit the highest structural charge density. Chitosan displays polyelectrolyte behaviour related to long-distance intra- and intermolecular electrostatic interactions, which are responsible for chain expansion, high solubility and ionic condensation. For values of DA between 20-50%, hydrophilic and hydrophobic interactions are progressively counterbalanced while for DA over 50% electrostatic interactions are essentially short-distance interactions. Thus, hydrophobic interactions due to increase in acetyl group content become predominant (Kumirska *et al*., 2011).

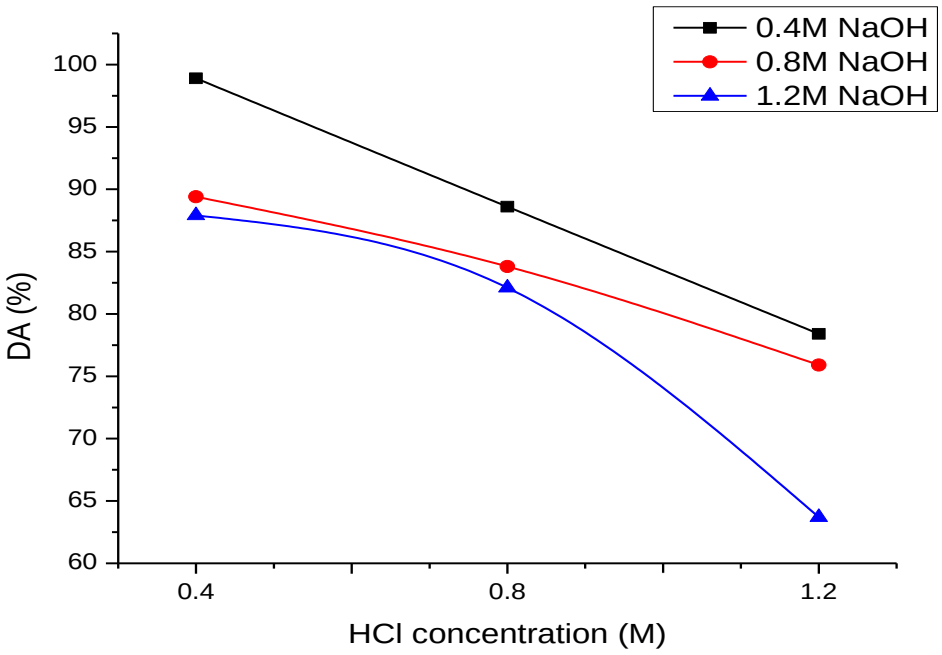

Figure 30: DA of crab chitin extracted with varying HCl and NaOH concentrations

4.1.1 Hydrogen Bond

Chitin chains are organized in sheets and tightly held by a network of hydrogen bonds. This tight network is linked by the strong C=O and H-N-groups. The broad band between 3600 and 3000

cm^{-1} is due to the OH and NH stretching vibration, which gives considerable information about the hydrogen bonds (Figure 31). The band due to the OH group has two intra molecular hydrogen bonds represented by peaks existing between 3497 and 3439 cm^{-1}.

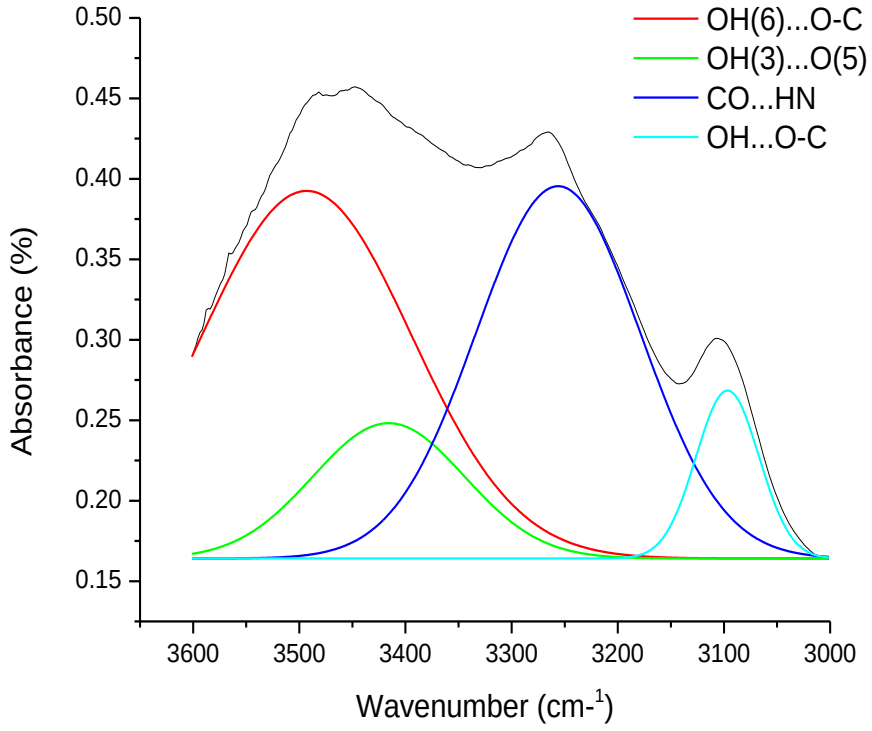

Figure 31: Spectra fitting of hydrogen region for crab chitin

The first intra molecular hydrogen bond occurs when a carbonyl group on C-2 bonds to the hydroxyl group on C-6 i.e. O H (6)…O=C (Figure 32a) while the second hydrogen bond exists between the OH group on C-3 and the ring oxygen (OH (3)….O-5) (Guo *et al*., 2002). The bands related to NH of the amide group lie between 3264 and 3110 $cm^{-.1}$ and are assigned to the vibration modes involved in strong intermolecular hydrogen bond networks C=O⋯.HN and OH⋯O=C respectively as shown in Figure 32b (Rojas *et al*.,2014; Liu *et al*., 2008). It is known

and accepted that these hydrogen bonds play an important role in determining the conformational and mechanical properties of structural polysaccharides (Ciolacu, *et al*., 2010).

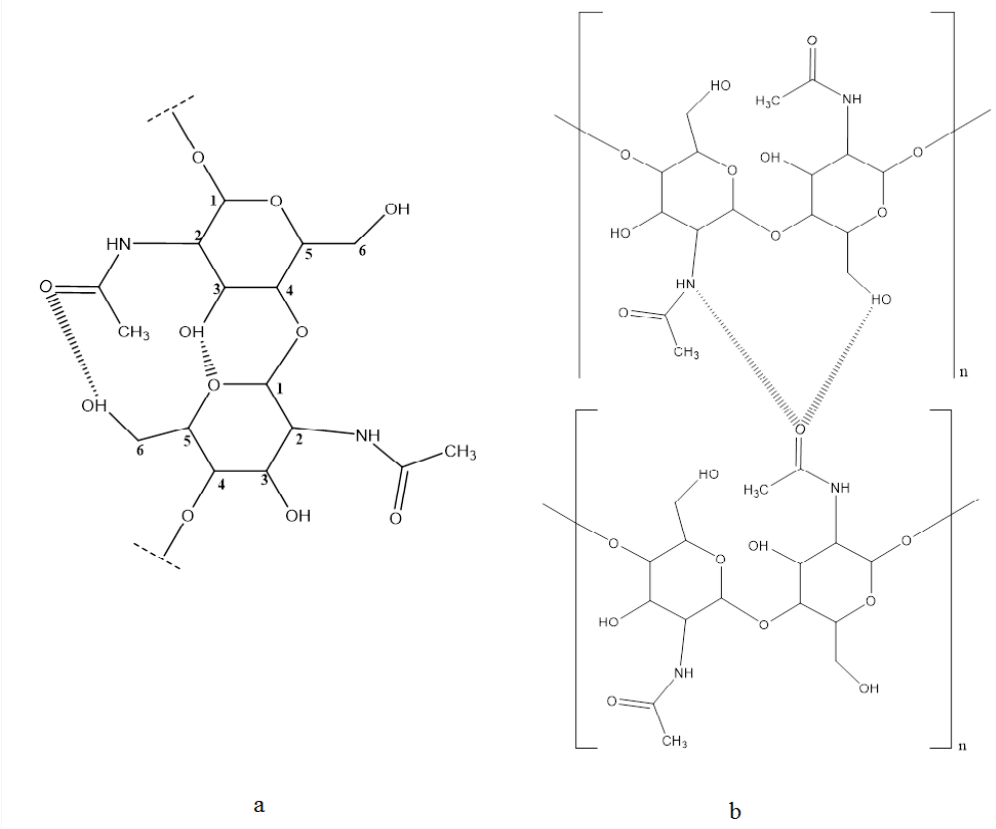

Figure 32: (a) Intra and (b) intermolecular hydrogen pattern in chitin monomers

It is evident that the chitin samples extracted from the crustacean shells contain these bonds in varying wavenumbers, amount and strength (Table 1). Chitin extracted from 0.4M HCl and 0.4M NaOH has its OH (6)…OC, OH(3)…O(5), CO…HN and OH…OC intra and intermolecular hydrogen bonds at 3493, 3416, 3256 and 3097cm^{-1} respectively. The intra molecular OH(6)…OC bond occupies the largest portion (45.38 %) of the hydrogen bonds within this broad band, followed by 35.96 % occupied by CO…HN, 12.07 % by OH(3)…O(5) and OH…OC occupying the least (6.59 %). The energy of the hydrogen bond, E_H is high for the inter molecular bonds compared to their intra molecular counterparts as the wavenumber approaches 3000 cm^{-1}.This is

so as the hydrogen bond length increases, the energy increases as well. The E_H for OH…OC measures 8.32kCal, while CO…HN in the sample is calculated to be 5.69kCal. There is a shift in its OH (6)…OC intra molecular hydrogen bond to lower wavelength when chitin is extracted from crab shell at the same NaOH concentration (0.4M) but a higher acid concentration of 0.8M (see Table 1).

This bond exists at 3495 cm^{-1} having E_H of 1.74kCal. The CO…HN and OH…OC lie at 3253 and 3096 cm-^{1} respectively and this shows a minimal shift resulting in a calculated E_H of 5.74 kCal and 8.33 kCal. These energies are almost similar to the chitin extracted using 0.4M HCl. Like the earlier sample (0.4M HCl and 0.4M NaOH), OH (6)…OC bond is the largest of the hydrogen bonds (in terms of proportion) as it is measured to be 38.63 %. Second to this is 32.13 % occupied by CO…HN bond and followed by 23.68 % occupied by OH (3)…O (5) bond. The OH…OC bond has the least amount of 5.5 6%. Increasing the acid concentration to 1.2M leaves the CO…HN and OH…OC inter molecular bonds vibrating at 3256 and 3097 cm^{-1} occupying 32.04 % and 5.93% of the overall bonds. Fitting results for hydrogen bonding band of chitin extracted from crab shell treated using 0.4 M HCl and 0.8M NaOH, show the bands OH(6)…OC, OH(3)…O(5), CO…HN and OH…OC appear at 3495, 3422, 3256 and 3096 cm^{-1} respectively. The dominant bond in this sample is the OH (6)…OC, with 43.11% of the total amount followed by CO…HN with 31.60 %, OH(3)…O(5) with 19.54 % and OH…OC with 5.75%. Increasing HCl concentrations to 0.8 and 1.2M, the amounts of OH (6)…OC reduce while that of OH (3)…O (5) increase. The average E_H for hydrogen bonding is highest in chitin extracted from 0.4M HCl (4.69kCal) followed by 4.66 and 4.51 kCal respectively for chitin extracted from 0.8 and 1.2M HCl at 0.8M NaOH. Using these acid and 1.2M alkali concentrations on crab shell, Table 1 shows varying bands of inter and intra molecular hydrogen

bonds with OH(6)…OC reducing, and OH(3)…O(5) increasing in amount as acid concentration increases. Amount of inter molecular CO…HN bond is ≈ 33% in each sample while OH…OC varies between 5.65- 6.08 %. In summary, average hydrogen bond reductions have been engendered by gradual removal of *N*-acetyl groups for each sample during acid and basic treatments (with increasing concentrations) as it prevents the formation of inter and intra molecular hydrogen bonding that is needed for the formation of hard compacts. Thus, deacetylated portions in the structure will be available to form hydrogen bonds with incoming water molecules resulting in increased hydrophylicity of the polymer.

Table 1: FTIR absorption band assignment to the OH band (3600-3000 cm^{-1}) for crab chitin

samples	OH(6)…OC			OH(3)---O(5)			CO…HN			OH…OC			
Reagent ratio (acid : alkali)	cm^{-1}	Amount (%)	E_H (kCal)	cm^{-1}	Amount (%)	E_H (kCal)	cm^{-1}	Amount (%)	E_H (kCal)	cm^{-1}	Amount (%)	E_H (kCal)	Average E_H (kCal)
0.4;0.4	3493	45.38	1.77	3416	12.07	3.04	3256	35.96	5.69	3097	6.59	8.32	4.71
0.4;0.8	3495	43.11	1.74	3422	19.54	2.94	3252	31.6	5.75	3096	5.75	8.33	4.69
0.4;1.2	3495	40.73	1.73	3424	20.03	2.91	3252	33.17	5.75	3096	6.08	8.33	4.68
0.8;0.4	3495	38.63	1.74	3430	23.68	2.81	3253	32.13	5.74	3096	5.56	8.33	4.66
0.8;0.8	3497	37.14	1.7	3430	26.55	2.81	3253	31.03	5.74	3096	5.36	8.33	4.64
0.8;1.2	3497	34.66	1.7	3431	26.64	2.79	3256	33.05	5.69	3097	5.65	8.33	4.63
1.2;0.4	3487	32.12	1.7	3435	29.91	2.73	3253	32.04	5.74	3096	5.93	8.33	4.63
1.2;0.8	3496	30.98	1.72	3466	30.1	2.22	3248	33.51	5.82	3097	5.41	8.32	4.52
1.2;1.2	3497	31.18	1.7	3465	30.01	2.23	3249	33.05	5.8	3097	5.76	8.32	3.93

4.2 Shrimp Shell FTIR Analysis

The FTIR spectrum of shrimp shell shows similar characteristic peaks as the virgin crab shell (Figure 33) and this confirms that the dominant compound contains the mineral calcite. The corresponding characteristic bands of stretching vibrations of the mineral are at 1796, 1456 and 874 cm^{-1}, (Felsen *et al*., 2012). Major peaks detected in spectra are identified between 3500 to 3200 cm^{-1} (O-H and N-H) as observed by Jaafarzadeh *et al*., (2016), 2853 cm^{-1} (-CH of the alkanes group), 1653 cm^{-1} (C = O of amide I group) and 1423 cm^{-1} ($-CH_3$). Broader OH and NH bands with more effective CH_2/CH_3 stretch (as indicated by greater absorptions between 3500-3000 cm^{-1}) are observed in the shrimp shell (Figure 34). In addition, the predominant calcite peaks intensities are more in the virgin crab shell than the shrimp. This is attributed to the use of more volume of acid baths in crab shell for complete demineralization (Table 2). The structure of shrimp exoskeleton has also shown the formation of an additional chitin band of NH band plane and CH stretch at 1327cm^{-1} (amide III). This confirms that the carbonate-polymer binding strength in the shrimp exoskeleton is less than that in the crab shell.

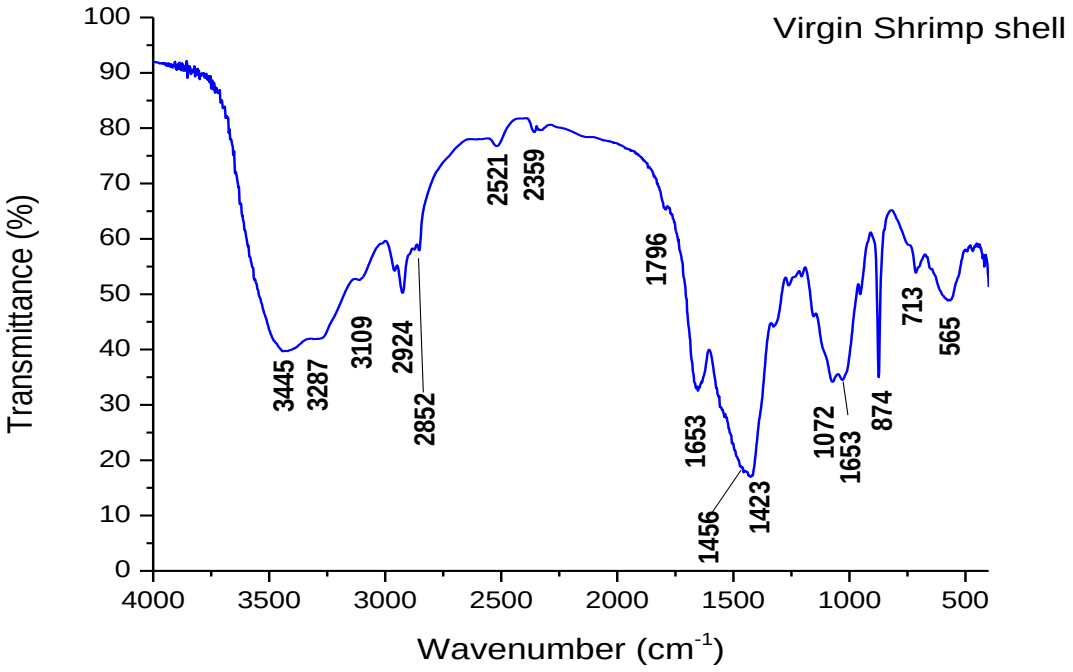

Figure 33: FTIR spectra of virgin shrimp shell

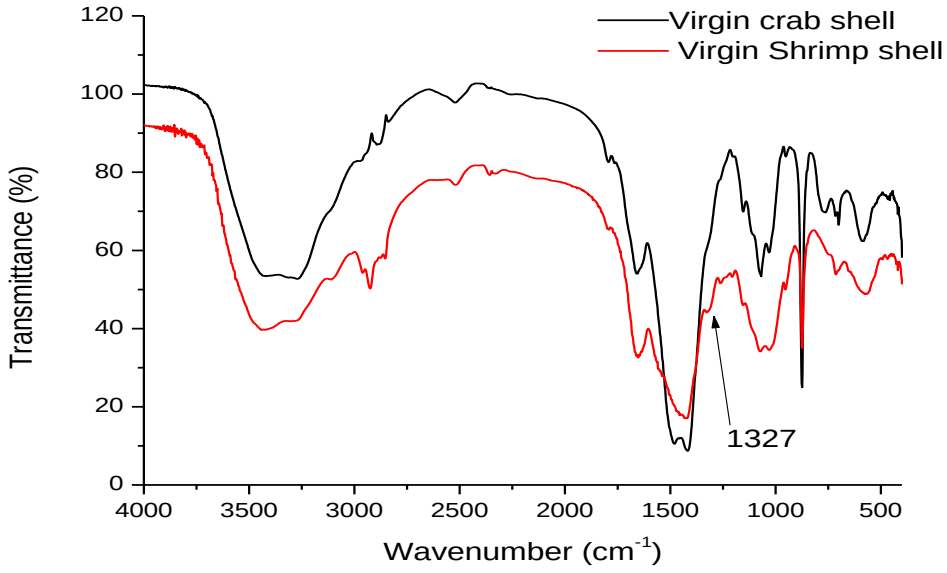

Figure 34: FTIR spectra of virgin crab and shrimp shells

Table 2: Volume of HCl used during demineralization

Acid volume (ml)		
HCl	Crab shell	Shrimp shell
0.4M	1900	1730
0.8M	1830	1630
1.2M	1780	1560

.

Analysis of the chitin FTIR spectra extracted chemically from shrimp shell (Figures 35-37) shows the presence of a band in the range 3445–3265 cm^{-1}, associated with stretching vibrations of O-H and N-H groups i.e., at 2933 cm^{-1} from stretching vibrations of C-H (CH_3 and CH_2). The most important signals in the spectrum of chitin are the peaks at 1660, 1559 and 1312 cm^{-1}, with characteristic stretching vibrations of amides I, II and III bonds. As observed in the crab chitin, two separate peaks occurred at 1660 and 1626 cm^{-1} showing that the chitin structure obtained from the shrimp shell is the α – form. The FTIR spectrum of the extracted polysaccharide also features peaks at 1157, 1074 and 1028 cm^{-1} relating to the presence of C-O-C bonds in the structure. Chitin extracted from shrimp shell following acid and alkali treatments at varying concentrations have similar spectra as no new band is formed (Figures 35-37). Although, majority of acetylated groups exist within the chitin, free amino groups are also present to some extent as a result of deacetylation during deproteinization process in the alkaline medium, which is different from that observed in the crab chitin. Thus, different DA of chitin samples will arise as a result of their sources of origin and mode of isolation.

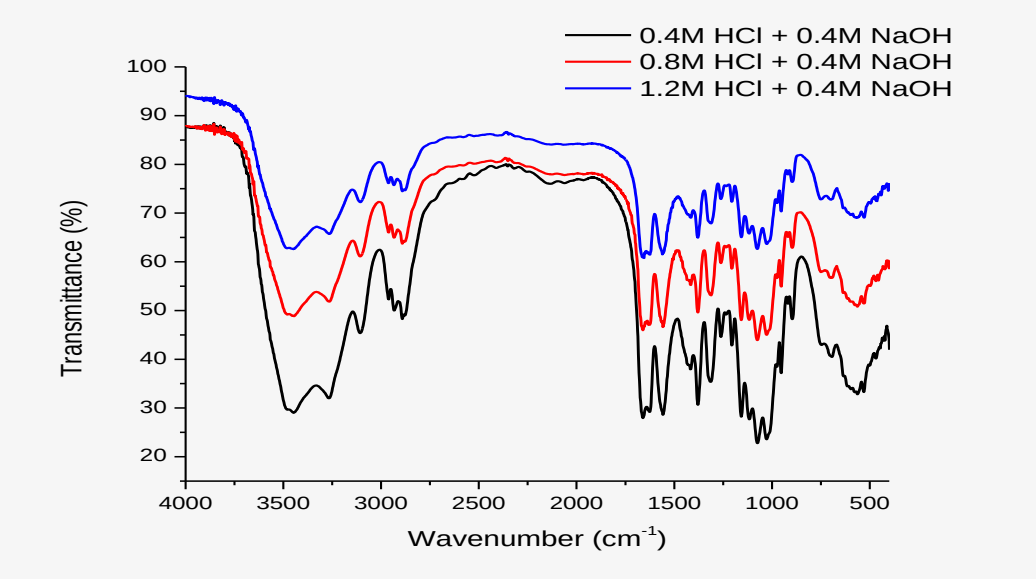

Figure 35: FTIR spectra of shrimp chitin extracted from different acid concentrations and 0.4 M alkali

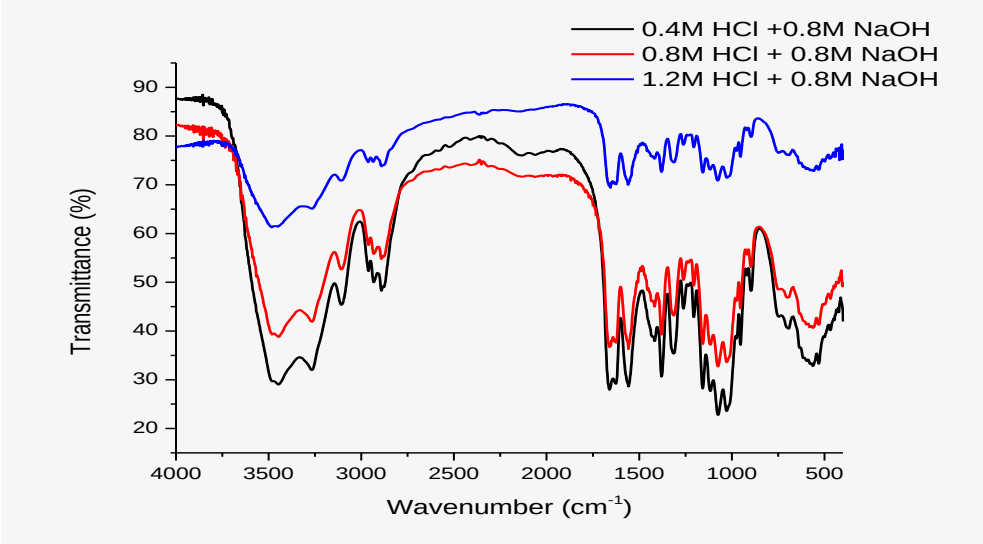

Figure 36: FTIR spectra of shrimp chitin extracted from different acid concentrations and 0.8 M alkali

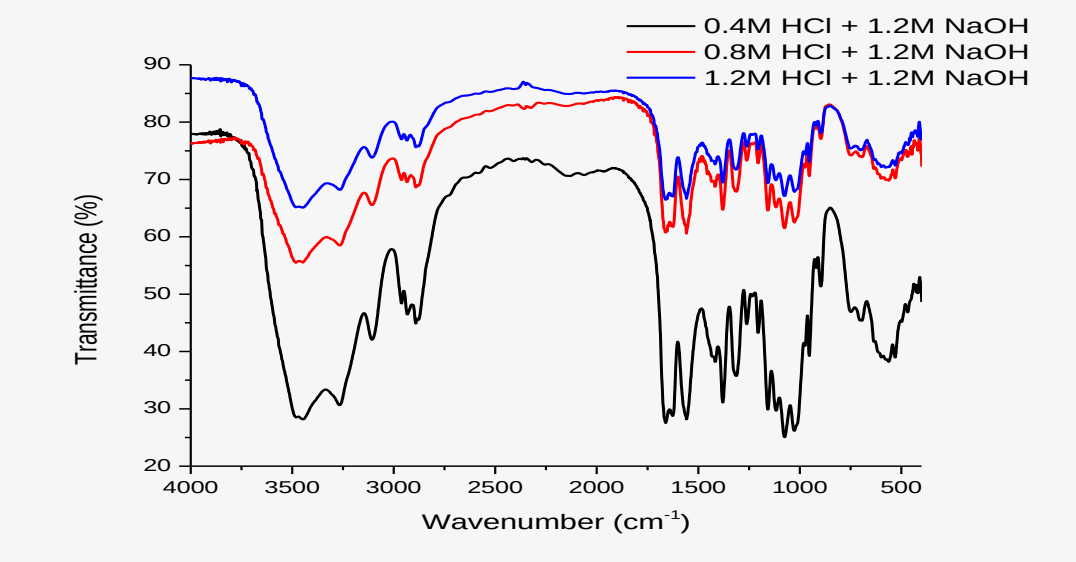

Figure 37: FTIR spectra of shrimp chitin extracted from different acid concentrations and 1.2 M alkali

Figure 38 shows the DA of shrimp chitin extracted using HCl and NaOH solutions. A maximum DA of 99.4% is measured for shrimp chitin extracted using 0.4M acid and alkali. This shows that there is an increase in the repeating unit of *N*-acetyl-D-glucosamine at low acid and alkali concentrations. The use of acid concentrations of 0.8 and 1.2M result in chitin samples with DA of 84.7 and 81.1% respectively under the same condition of alkali (0.4M NaOH) Chitin extracted from shrimp shell using 0.25M HCl and 1M NaOH had DA of 96% as obtained in the study by Al Sagheer *et al*., (2009). On the other hand, DA of 79.5, 79.1 and 77.4% are recorded for chitin extracted with 0.4, 0.8 and 1.2M HCl at 0.8M NaOH, showing that chitin contains a small but significant fraction of de-*N*-acetylated unit. The chitin extracted using 1.2M of both acid and alkali is found to be the most amenable to deacetylation (DA, 65.6%) than those obtained from 0.4 (DA, 74.3%) and 0.8M (DA, 73.8%) acid at the same alkali concentration of 1.2M NaOH. Rojas *et al*. (2014) reported that basic conditions impose amide hydrolysis of chitin samples as observed in this work. This study has also shown that HCl induces a partial removal of the *N*-acetyl groups, which leads to decrease in DA at increasing concentrations.

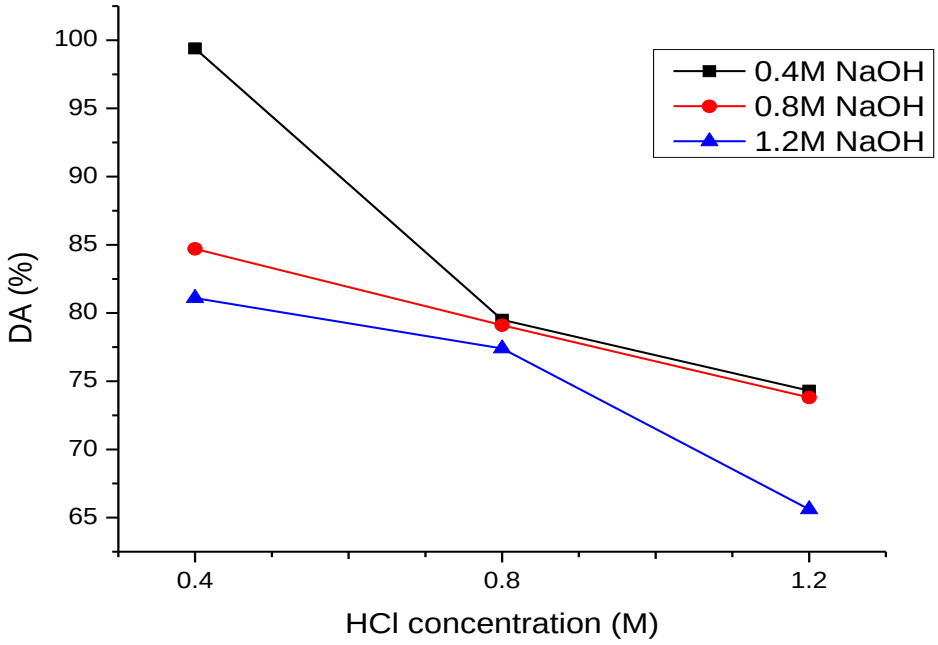

Figure 38: DA of shrimp chitin with varying HCl and NaOH concentrations

4.2.1 Hydrogen Bond

Figure 39 shows the fitting of hydrogen region between the broad band 3600 and 3000 cm^{-1}. Like the crab chitin, both intra and inter molecular hydrogen bonds are evident in chitin samples extracted from shrimp shells. The OH(6)…OC and OH(3)…O(5) intra molecular hydrogen bonds are formed between 3458-3463 cm^{-1} and 3371 – 3464 cm^{-1} respectively while CO…HN and OH…OC intermolecular hydrogen bonds are formed between 3249 – 3264 cm^{-1} and 3100 – 3102 cm^{-1}.The E_H for OH(6)…OC, OH(3)…O(5), CO…HN and OH…OC measure 3.31, 3.77, 5.65 and 8.27 kCal respectively for chitin extracted from 0.4M HCl and 0.4M NaOH (Table 3). Increasing the acid concentration to 0.8 and 1.2M lowers the values from 5.22 (at 0.4M HCl) to 4.98 and 4.64kCal, which confirms gradual cleavage of hydrogen bonds. Shrimp chitin extracted using 0.4M HCl and 0.8M NaOH has its OH(6)…OC, OH(3)…O(5), CO…HN and OH…OC

intra and intermolecular hydrogen bonds existing at 3460, 3371, 3264 and 3102 cm^{-1} respectively (Table 3). The intra molecular OH(6)…OC bond occupies the largest portion (55.65%) of the hydrogen bonds within this broad band, followed by 33.50 % occupied by CO…HN, 6.92 % by OH…OC and OH(3)…O(5) occupying the least (1.93%).

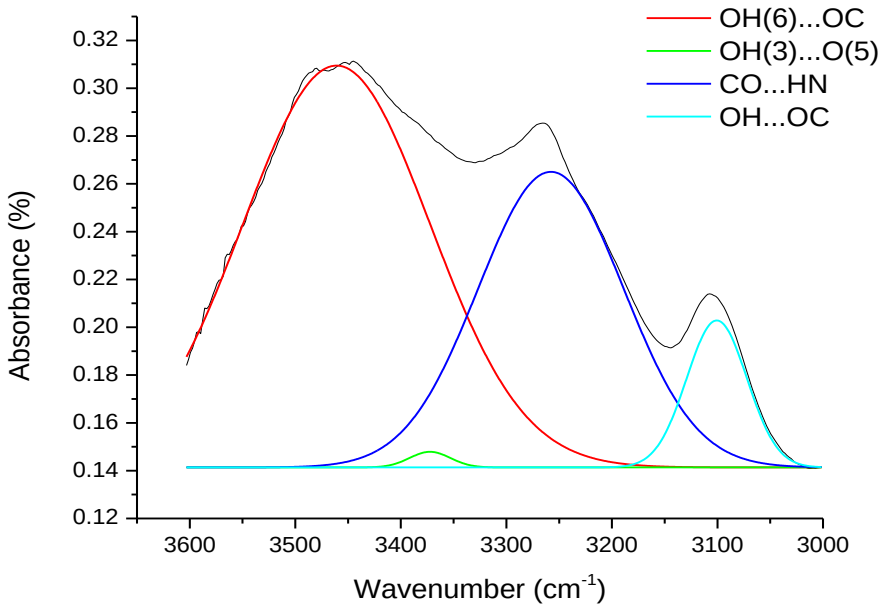

Figure 39: Spectra fitting of hydrogen region for shrimp chitin

The average E_H is high for this sample and calculated as 5.22kCal. With the same alkali concentration (0.8M), OH(6)…OC, OH(3)…O(5), CO…HN and OH…OC appear at 3462, 3372, 3264 and 3100 cm^{-1} respectively when demineralization is carried out at 0.8M HCl. The most prominent bond in this sample is the OH(6)…OC, which is 54.6% of the total amount followed by CO…HN with 38.0%, OH…OC with 5.4 % and OH(3)…O(5) with 2 .%. The amount of OH(6)…OC and CO…HN drop to 28.43 and 35.23% while the portion of OH(3)…O(5) and OH…OC rise to 28.50 and 7.84 % respectively when shrimp shell is treated with 1.2M HCl and 0.8M NaOH. The average E_H for this sample is 4.63kCal. At varying acid concentrations of 0.4,

0.8 and 1.2M HCl with1.2M alkali on shrimp shell, Table 3 shows varying bands of the inter and intra molecular bonds with average E_H reducing to 4.99, 4.64 and 4.22kCal as acid concentration increases Amount of inter molecular CO…HN bond is ≈ 33 % in each sample while OH…OC varies between 5.65- 6.08%. In summary, average hydrogen bond reductions are affected by gradual removal of *N*-acetyl groups for each sample during acid and basic treatments (with increasing concentrations) as it prevents the formation of inter and intra molecular hydrogen bonding needed for the formation of hard compacts.

Table 3: FTIR absorption band assignment to the OH band (3600-3000 cm^{-1}) for shrimp chitin

samples	OH(6)…OC			OH(3)---O(5)			CO…HN			OH…OC			
Reagent ratio (acid : alkali)	cm^{-1}	Amount (%)	E_H (kCal)	cm^{-1}	Amount (%)	E_H (kCal)	cm^{-1}	Amount (%)	E_H (kCal)	cm^{-1}	Amount (%)	E_H (kCal)	Average E_H (kCal)
0.4;0.4	3460	58.9	3.31	3372	2.32	3.77	3258	33.63	5.65	3100	5.15	8.27	5.25
0.4;0.8	3460	55.65	3.31	3371	1.93	3.79	3264	35.5	5.56	3102	6.92	8.23	5.22
0.4;1.2	3461	59.94	2.3	3374	2.28	3.74	32657	30.97	5.61	3102	6.81	8.23	4.99
0.8;0.4	3464	57.66	2.25	3374	1.76	3.74	3258	33.59	5.65	3100	6.99	8.27	4.98
0.8;0.8	3462	54.6	2.28	3372	2	3.77	3264	38	5.56	3100	5.4	8.27	4.97
0.8;1.2	3458	51.87	2.35	3458	7.76	2.35	3261	37.39	5.61	3101	2.98	8.25	4.64
1.2;0.4	3464	53.1	2.25	3464	22.3	2.25	3249	19.5	5.8	3100	5.1	8.27	4.64
1.2;0.8	3459	28.43	2.33	3459	28.5	2.33	3260	35.23	5.62	3101	7.84	8.25	4.63
1.2;1.2	3463	49.8	2.25	3464	19.7	2.25	3249	24.2	5.8	3100	6.3	8.27	4.62

4.3 TGA

4.3.1 Crab Shell TGA

Decomposition curve for crab shell in Figure 40 occurs in three stages. The first occurs between 60 – 100 ^{0}C with mass loss of 3.88 % and it is attributed to decomposition of water and other volatile components. The second decomposition of chitin as confirmed by Gallego *et al*. (2013) occurs in the range 316 – 397 ^{0}C with a 10.38 % in mass. This agrees with the work of Paulino *et al*. (2006) where chitin was confirmed to thermally decompose in the range 300-400 ^{0}C. The third weight loss of 30.93 % is observed within the range of 682 and 729 ^{0}C, which is evident by the decomposition of calcite, $CaCO_3$ to CaO and CO_2. This is comparable to Correia *et al*. (2014) where 30.93 % of $CaCO_3$ decomposed after 721 ^{0}C for crab shell.

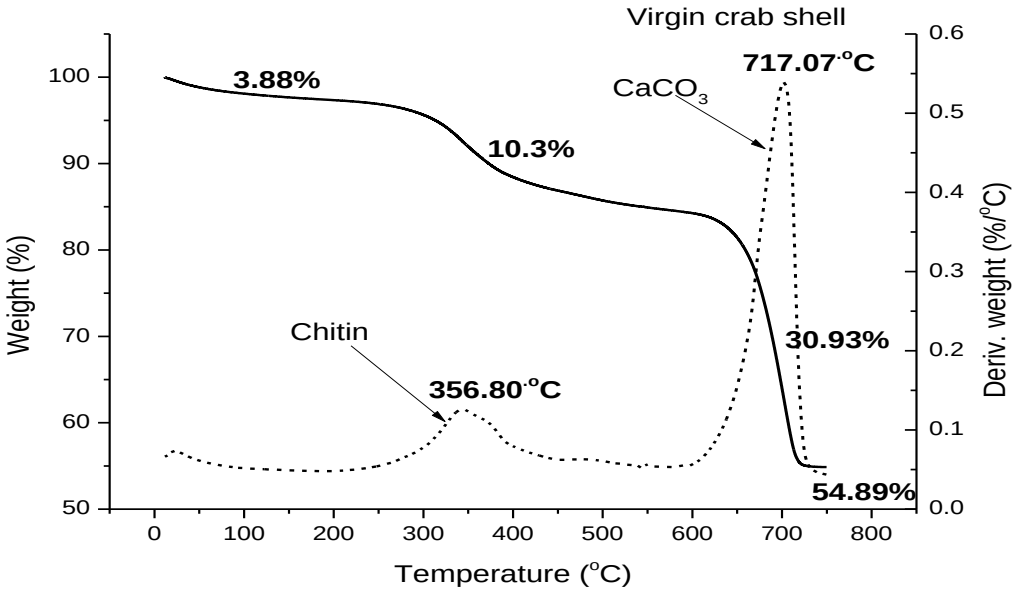

Figure 40: TGA-DTG curve for virgin crab shell

The maximum peaks observed on the derivative form of TGA (DTG) indicate the maximum temperature at which the decomposition was rapid at 356.8 ^{0} C and 717.07 ^{0}C for chitin and $CaCO_3$

respectively. The thermogram for the crab shell illustrates that 45.11% of the original weight loss throughout the heating process leaving the rest as residue (54.89%) containing SiO_2, Al_2O_3 and MgO. Complete demineralization and deproteinization show the elimination of calcite and greater chitin content as shown in Figures 41- 43. Two significant decomposition stages, which include moisture elimination and chitin decomposition, are observed for a complete mineral removal at 0.4, 0.8 and 1.2M HCl with 0.4M NaOH deproteinization (Figures 41- 43). Chitin decomposition of 62.3, 61.65 and 61.47 % by mass are observed using 0.4, 0.8 and 1.2M HCl respectively. For all the samples, this stage can be related to the beginning and progress of several processes such as degradation, depolymerization and denaturation (Juarez de la Rosa *et al*., 2015). In this thermal transformation, the aliphatic compounds (CH_2, CH_3 functional groups) are separated from the chitin structural ring, followed by the amides I and II groups (C=O, N–H) and the saccharide structure (C–O–C) (Juarez de la Rosa *et al*., 2012). Residue (SiO_2, Al_2O_3 and MgO) present in the bulk sample include 30.9, 28.2 and 31.55 % for treatments involving 0.4, 0.8 and 1,2M HCl respectively. Thus, chitin is still present in the 54.89 % residue obtained in the virgin crab shell (see Figure 40). The derivative curve, DTG illustrates maximum chitin peaks of 398.42, 395.33 and 393.16 ^{0}C for 0.4, 0.8 and 1.2M HCl treated samples respectively. This shows the existence of the most rapid decomposition events associated with the samples. Chitin extracted from grasshopper by Kaya *et al*. (2015) have its T_{max} measured as 387 ^{0}C. The smallest temperature at which this structural polysaccharide decomposition commences is at 343.70 ^{0}C and obtained at 1.2M HCl. Chitin of crab shell with highest stability in this category is one extracted at 0.4M HCl and followed by 0.8M HCl where decomposition starts at 351.99 and 346.30 ^{0}C respectively.

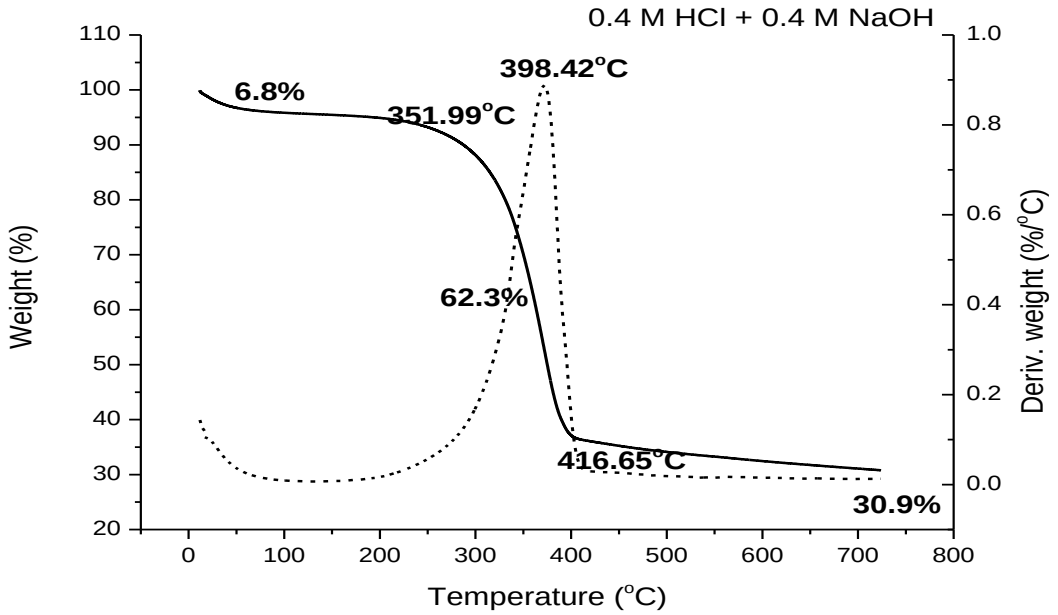

Figure 41: TGA-DTG curves for chitin extracted from crab shell at 0.4M HCl and 0.4M NaOH

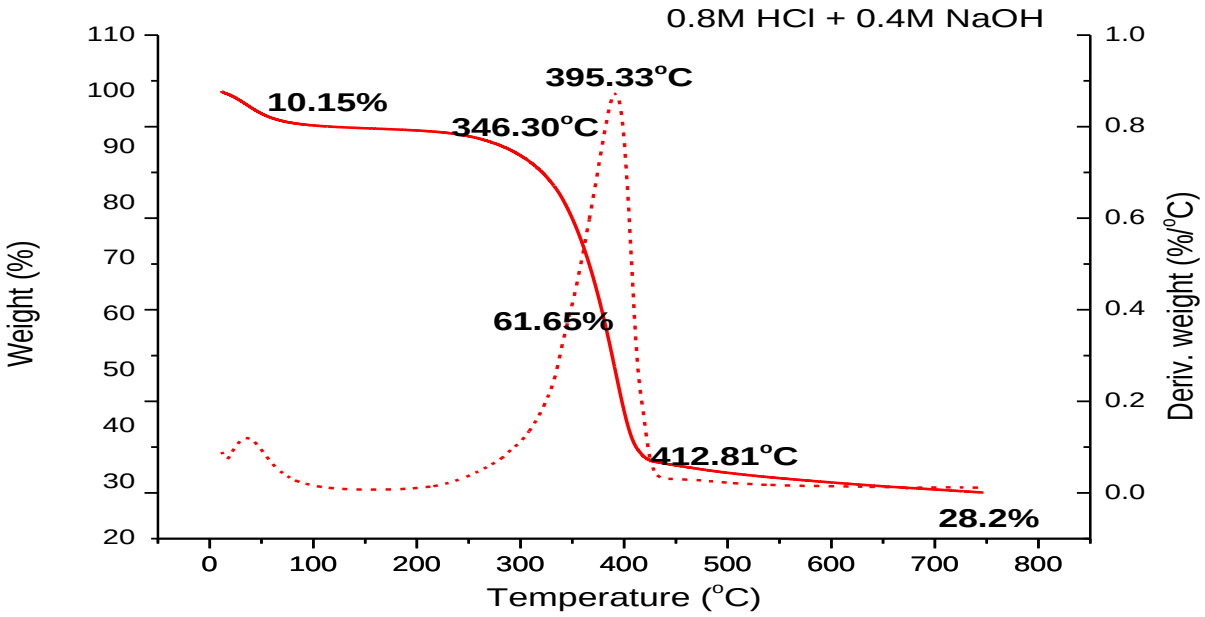

Figure 42: TGA-DTG curves for chitin extracted from crab shell at 0.8M HCl and 0.4M NaOH

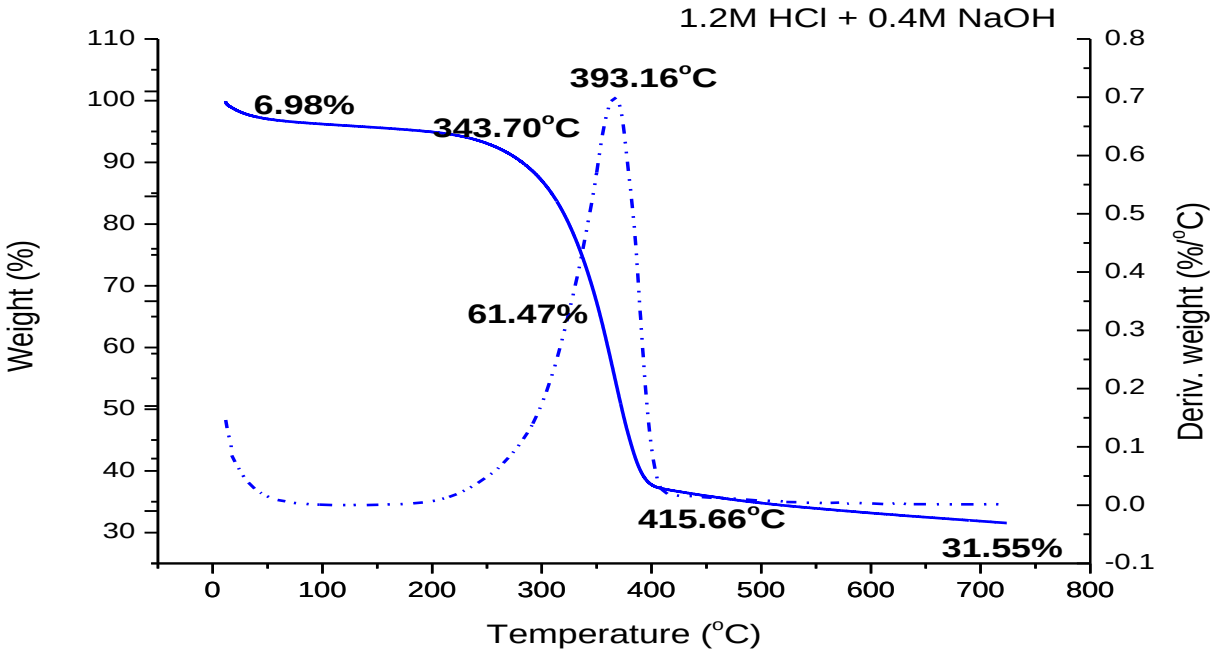

Figure 43: TGA-DTG curves for chitin extracted from crab shell at 1.2M HCl and 0.4M NaOH

Two- event decomposition curves are also obtained with the use of 0.8M NaOH (Figures 44 - 46). Maximum chitin content of 67.74 % is observed at the second decomposition event when 0.4M HCl is used to decalcinate crab shell (Figure 44). It is also observed that at this concentration, chitin extracted possesses the highest thermal stability as T_{onset} measures 350.12 ^{0}C. The quantity of chitin extracted from the shell using 0.8 and 1.2M HCl is obtained as decomposition of 64.48 and 65.19 % respectively by mass take place (Figures 45 and 46). Thermal degradation of chitin with the use of 0.8M HCl starts at 346.10 ^{0}C and ends at 416.19 ^{0}C while that extracted using 1.2M HCl degrades thermally in the range 342.16 – 413.61 ^{0}C. The residue left after thermal decomposition of whole sample is 23.97, 25.12 and 23.56 % for extractions at 0.4, 0.8 and 1.2M HCl.

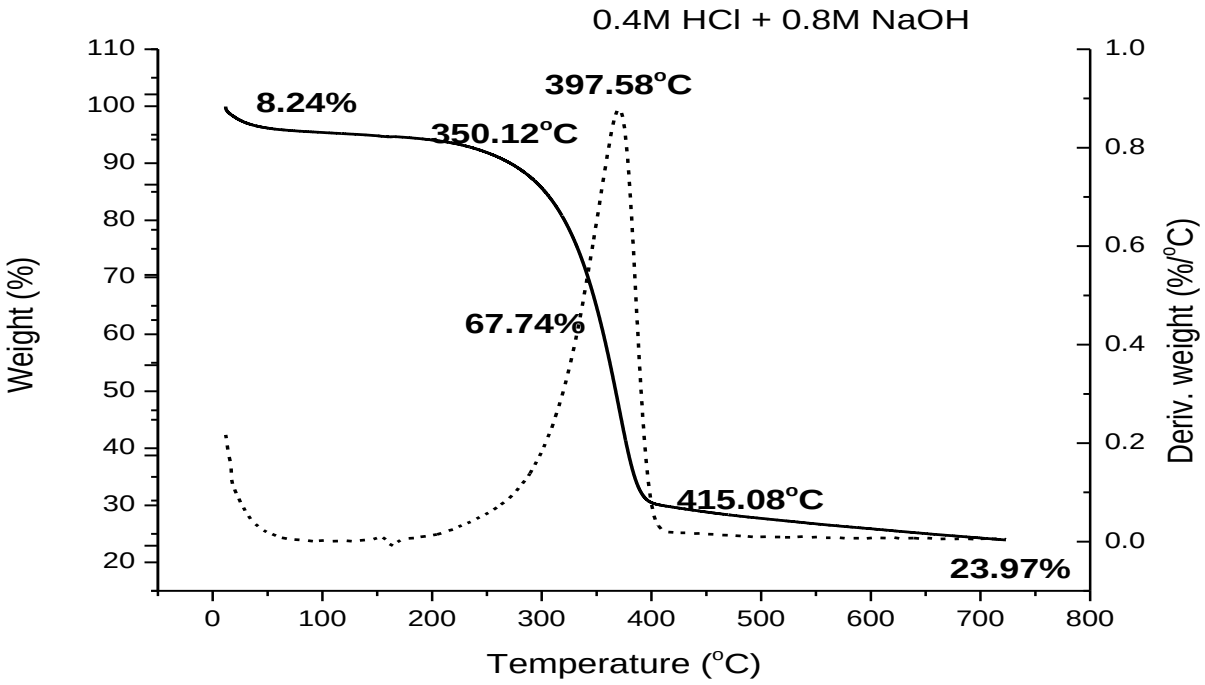

Figure 44: TGA-DTG curves for chitin extracted from crab shell at 0.4M HCl and 0.8M NaOH

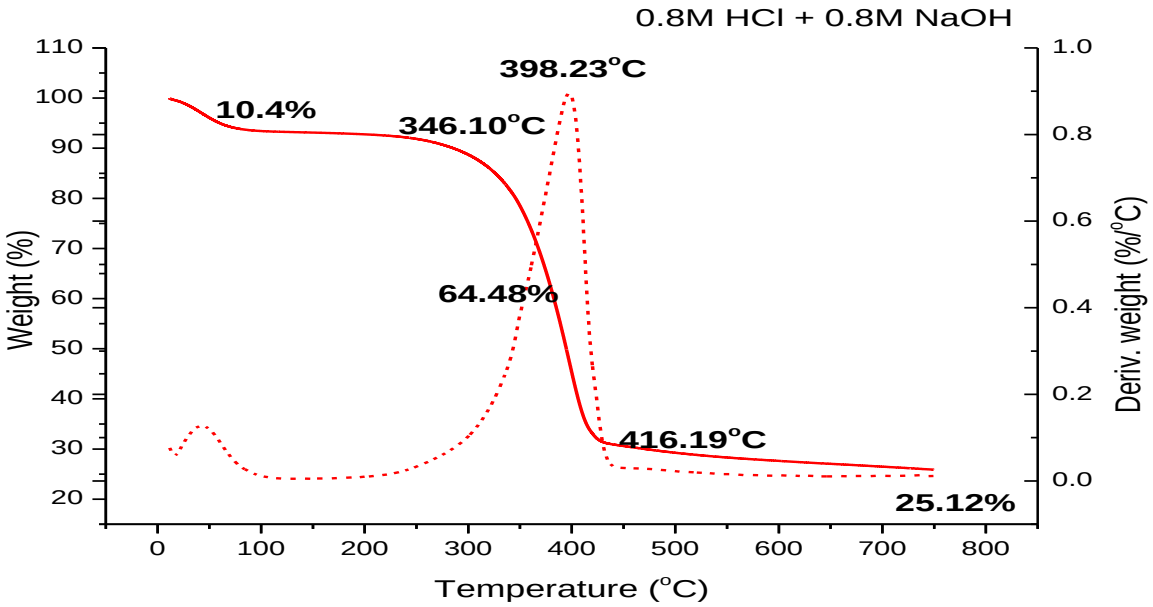

Figure 45: TGA-DTG curves for chitin extracted from crab shell at 0.8M HCl and 0.8M NaOH

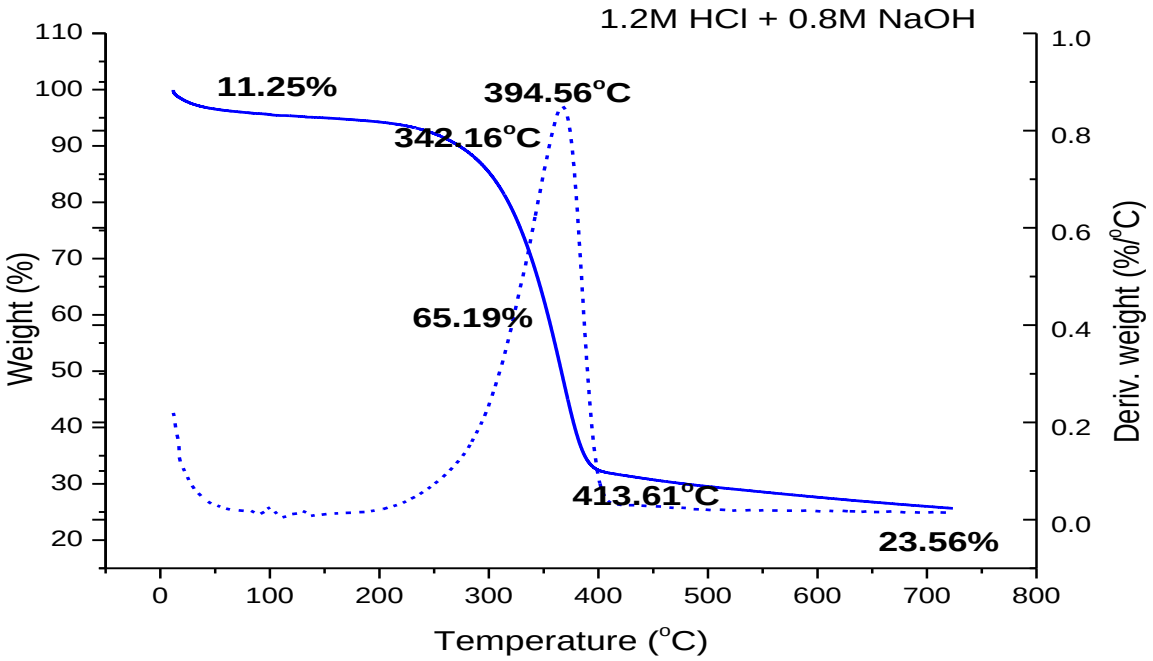

Figure 46: TGA-DTG curves for chitin extracted from crab shell at 1.2M HCl and 0.8M NaOH

It is clear from the thermograms of crab shell treated with same varying acid concentrations and 1.2M alkali (Figures 47 - 49) that the weight of the sample decreases rapidly with increasing temperature. Presence of chitin (67.5%) is observed with the application of 0.4M HCl between 348.3 – 413.62 ^{0}C (Figure 47). The point of highest rate of change on the weight loss as indicated by the peak of the first derivative occurs at 395.29, 394.52 and 367.44 ^{0}C, for 0.4, 0.8 and 1.2M HCl respectively (Figures 47 - 49). Sixty-nine percent commercial chitin was found to decomposed between 275-400 ^{0}C (Uzun and Celik, 2015) while 83 % chitin from Antarctic krill disintegrated between 250-400 ^{0}C (Wang *et al*., 2013). Thermogram of 0.8M HCl demineralized shell has its thermal degradation of chitin to occur in the range 345.36 – 413.69 ^{0}C, leaving 26.71 % as residue. Chitin content of 65.2 % is observed using 1.2M HCl and 1.2M NaOH. Degradation starts at 341.06 ^{0}C and stops at 409.91 ^{0}C while a residue of 22.3 % is observed.

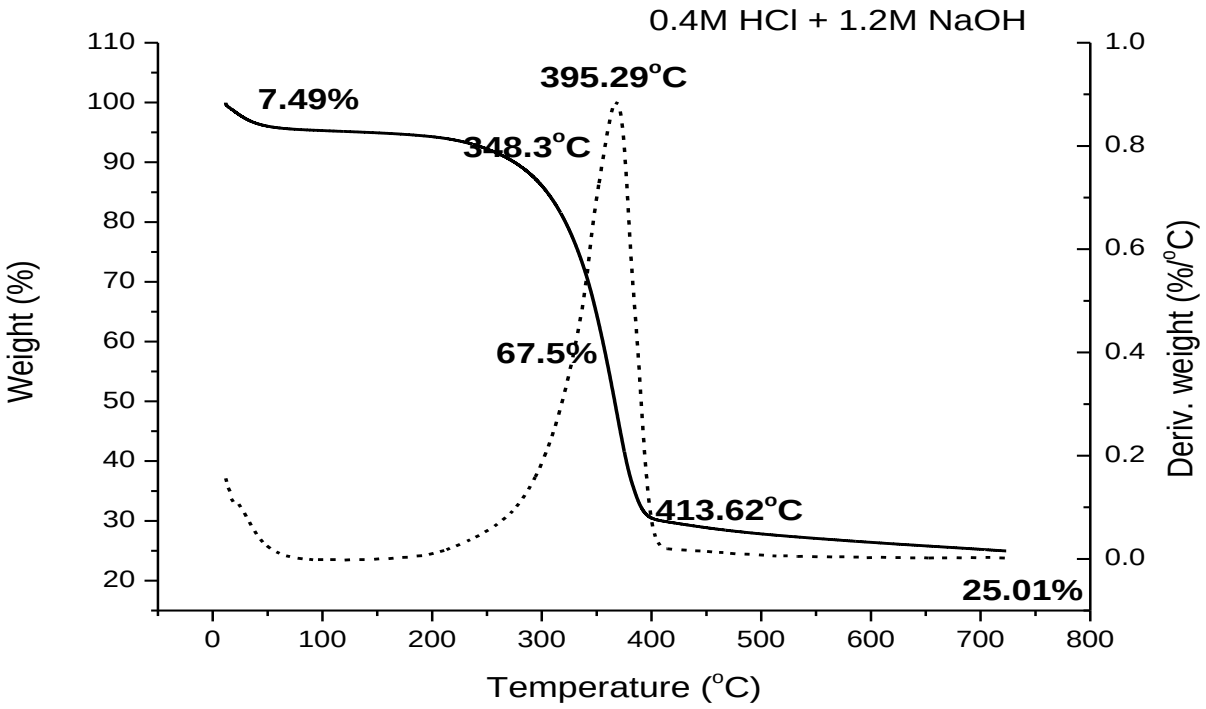

Figure 47: TGA-DTG curves for chitin extracted from crab shell at 0.4M HCl and 1.2M NaOH

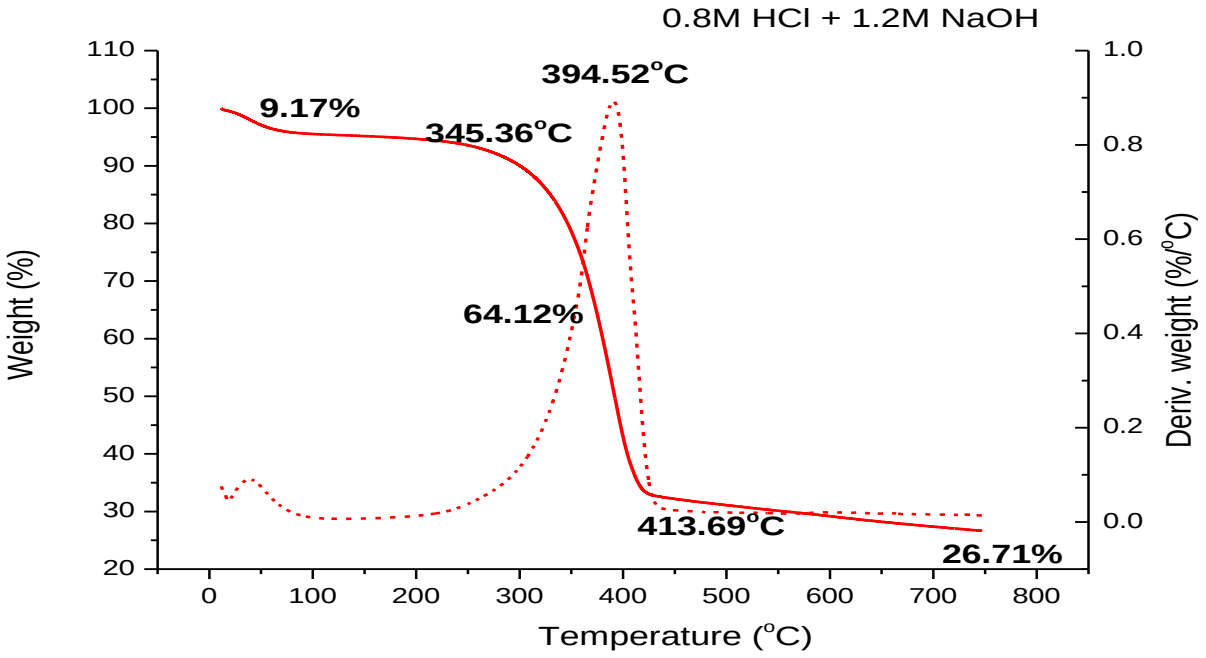

Figure 48: TGA-DTG curves for chitin extracted from crab shell at 0.8M HCl and 1.2M NaOH

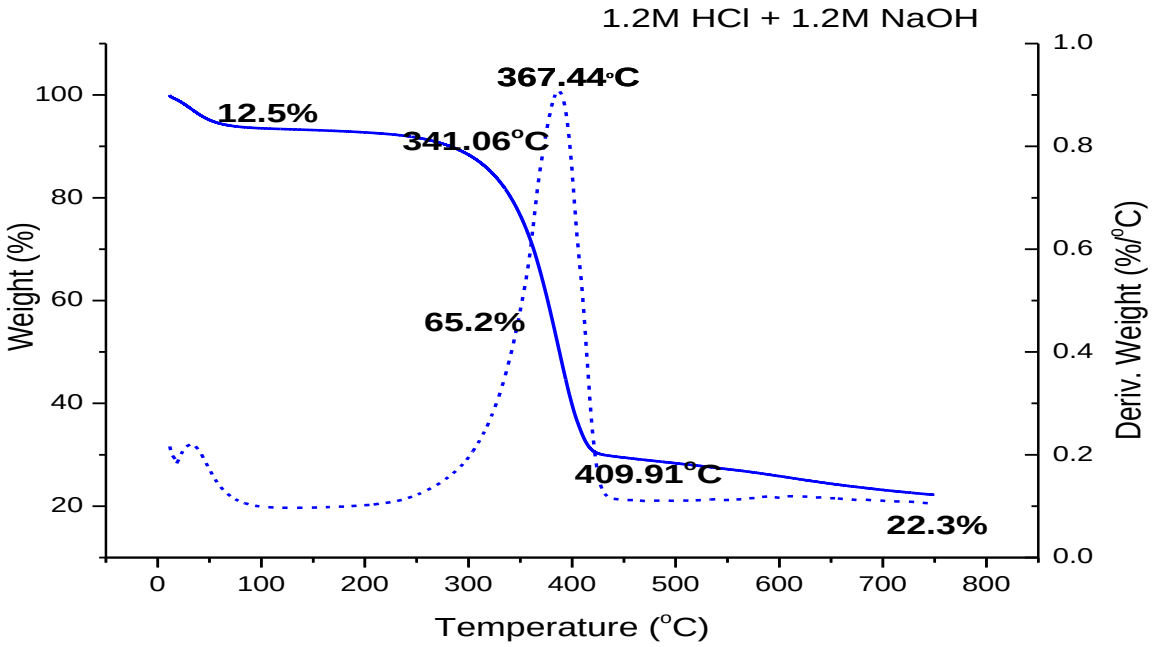

Figure 49: TGA-DTG curves for chitin extracted from crab shell at 1.2M HCl and 1.2M NaOH

4.3.2 Shrimp Shell TGA

The TGA curve for virgin shrimp shell shows thermal decomposition (Figure 50) with three stages of weight loss. The initial weight loss (8.77 %) observed between 80 and 110 ^{0}C is attributed to the vaporization of the water from the sample, while degradation of chitin sample starts at higher temperature, precisely after 321.01 ^{0}C. Above this temperature, the thermal stability of chitin gradually decreases and its degradation completes at 397.93 ^{0}C. This occurs at the second decomposition stage as 33.7 % chitin degrades. With temperature in the range 665- 713 ^{0}C, the 18.85 % $CaCO_3$ contained in shrimp shell is converted to CaO. However, the sample weight is constant until the temperature reaches 750 ^{0}C. Improved chitin content (38.2%) was also observed from lobsters by Boßelmann *et al*. (2007), with 16.1% $CaCO_3$ and a residue of 38.67 % after decomposition.

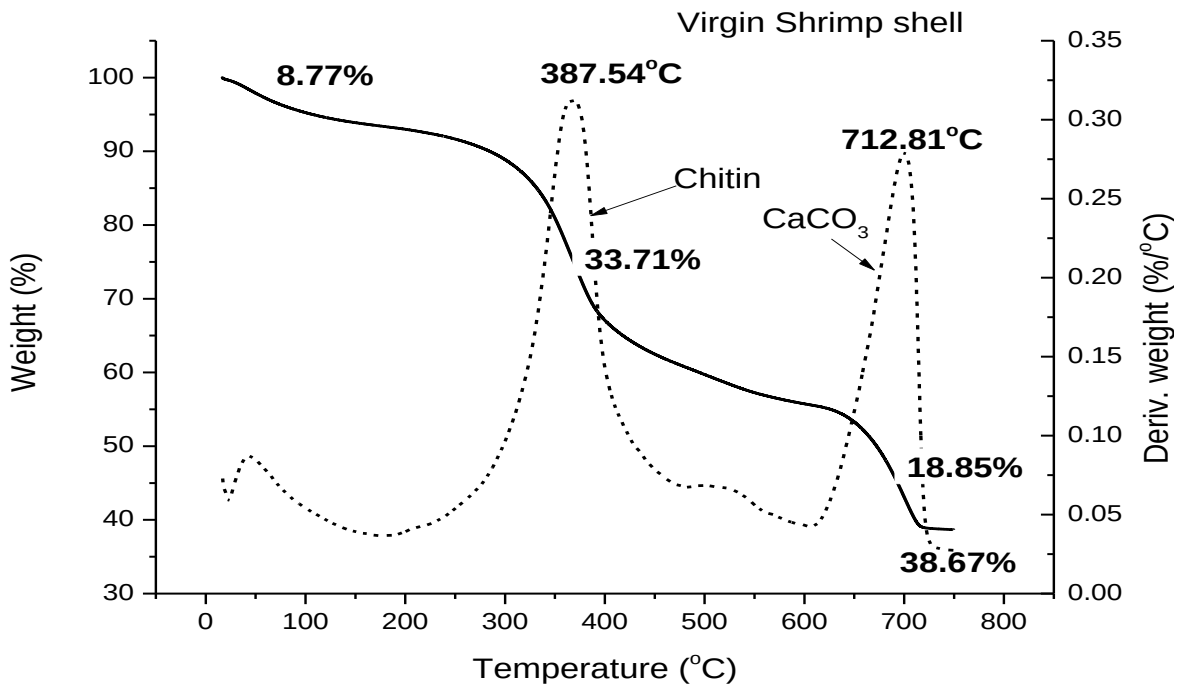

Figure 50: TGA-DTG curve for virgin shrimp shell

Figures 51- 53 show the TGA-DTG curves of shrimp shells fully treated using varying concentrations of acid at 0.4M NaOH. The degradation (7.02 %) starts between 50-100 ^{0}C and it is associated with evaporation of water molecules. The second stage of decomposition between 364.12 – 418.29 ^{0}C results in the degradation of saccharide structure of the molecules with the dehydration of saccharide rings and decomposition of the acetylated units of chitin (Figure 51). The maximum temperature of degradation for chitin at the second step is recorded at 400.28 ^{0}C for 0.4M treated shell while 403.59 and 402.13 ^{0}C are measured for 0.8 and 1.2M HCl treated samples respectively (Figures 52 and 53).Chitin content of 83.28, 80.77 and 81.89 % are observed for samples demineralized at 0.4, 0.8 and 1.2M HCl respectively. The T_{max} disintegration temperatures of α- chitins extracted from organisms including krill and coral in previous studies ranged from 370 and 372 ^{0}C (Juarez *de* la Rosa *et al*., 2015; Abdou *et al*., 2008). The difference in disintegration temperatures of extracted

chitins compared with this present study (400-403 ^{0}C) shows that different values can be obtained from different aquatic invertebrates.

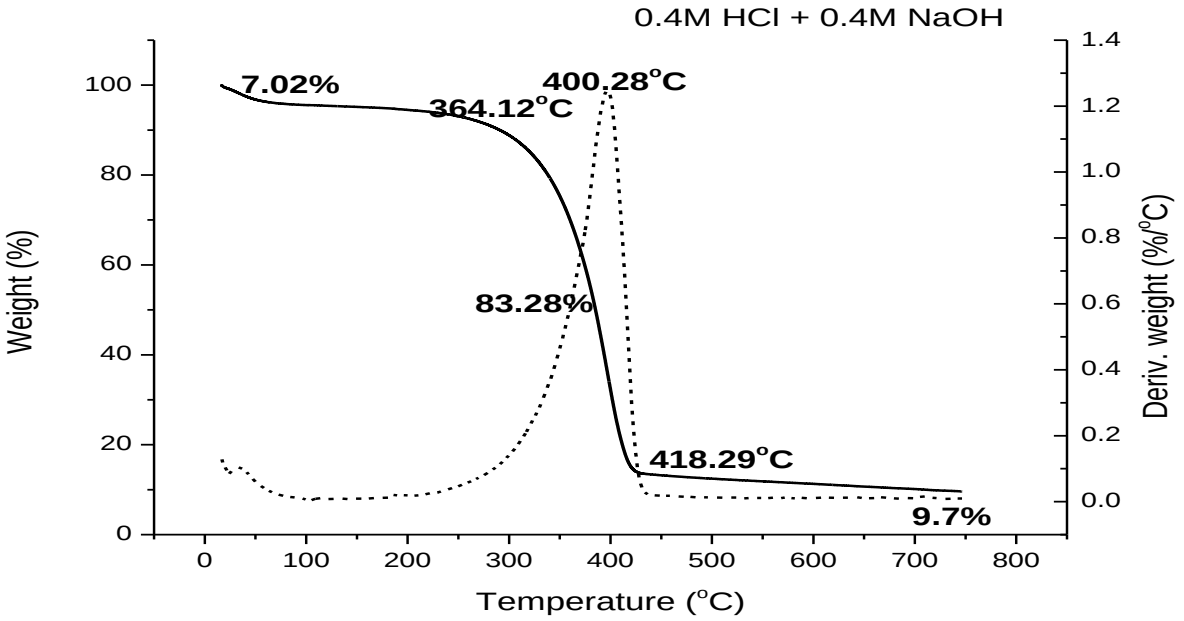

Figure 51: TGA-DTG curves for chitin extracted from shrimp shell at 0.4M HCl and 0.4M NaOH

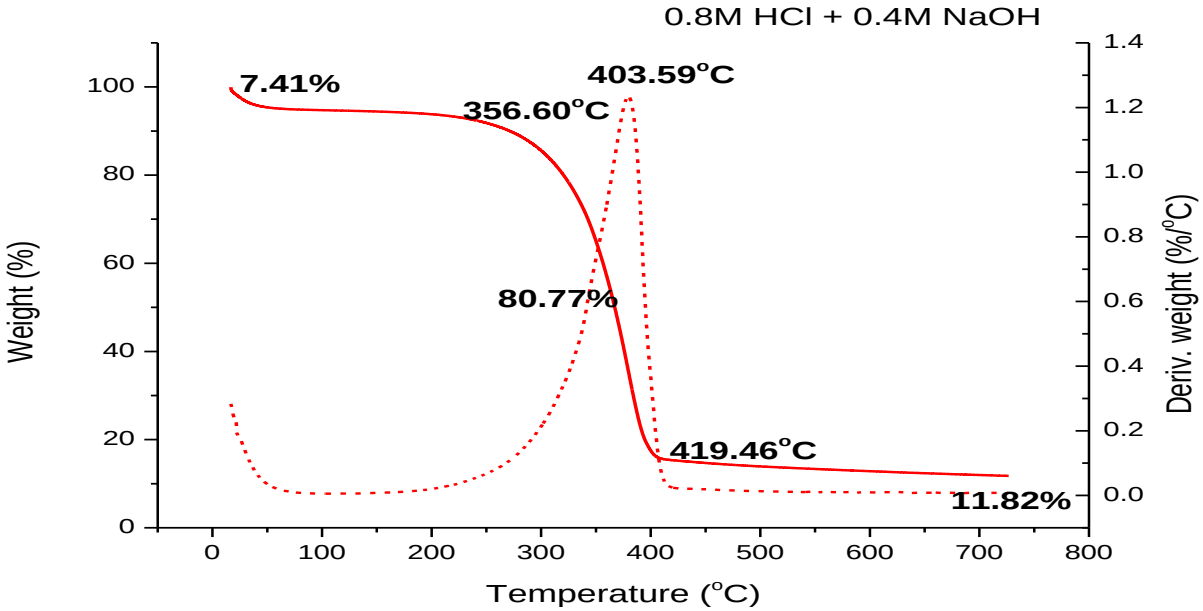

Figure 52: TGA-DTG curves for chitin extracted from shrimp shell at 0.8M HCl and 0.4M NaOH

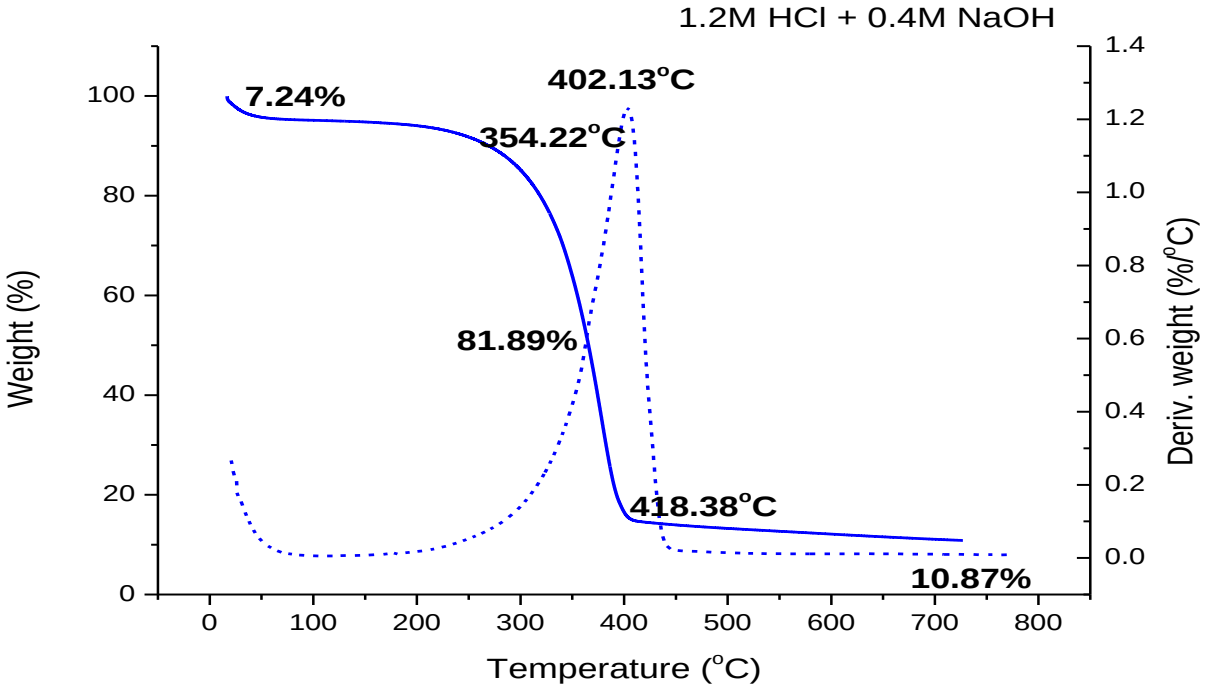

Figure 53: TGA-DTG curves for chitin extracted from shrimp shell at 1.2M HCl and 0.4M NaOH

As shown in Figure 54 – 56, TGA/DTG thermograms for chitin deproteinized with 0.8M alkali reveal mainly two decomposition steps where the first stage occurs in the range 40–100 ^{0}C and attributed to free water evaporation with a 6–9 % weight loss. In the second stage, the degradation of the polysaccharide structure of the molecule commences between 351 and 369 ^{0}C while it ends within 417- 421 ^{0}C, with the highest content of 84.03% recorded for shrimp shell treated with 0.8M HCl and 0.8M NaOH (Figure 55) . Demineralizing with 0.8 and 1.2M HCl results in 83.12 and 82.77 % chitin (Figures 54 and 56). The work of Andrade *et al*., (2012) on shrimp exoskeleton showed that 50 % chitin decomposed between 400 -500 ^{0}C.

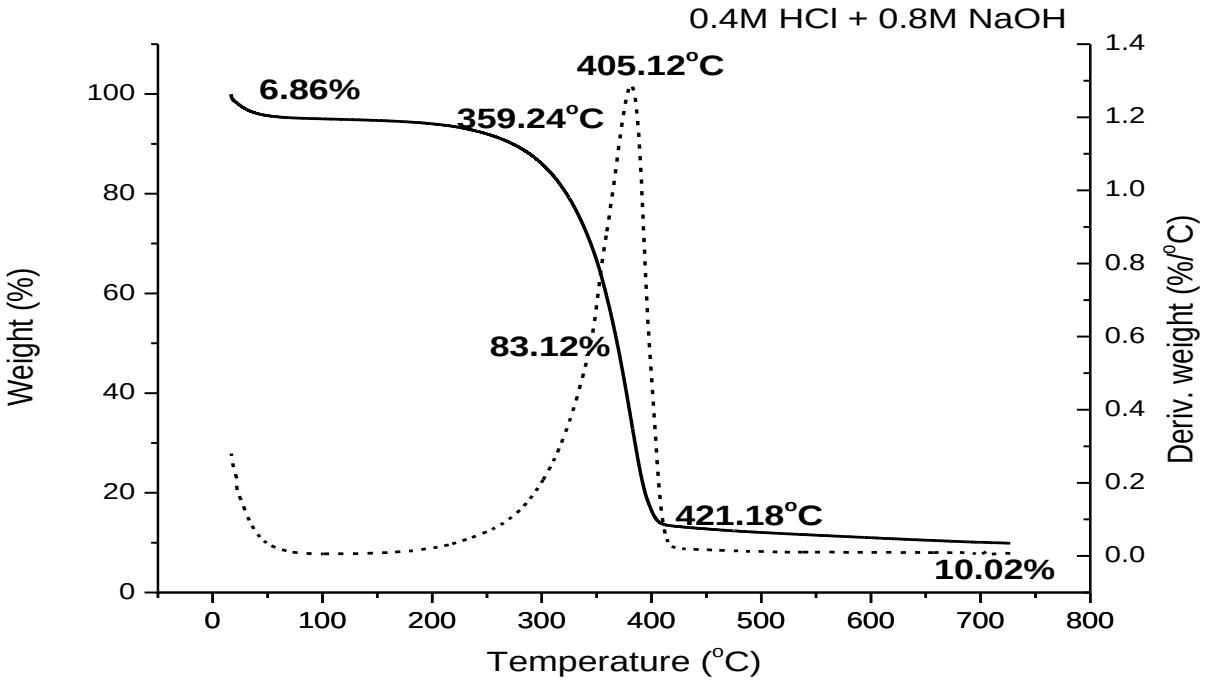

Figure 54: TGA-DTG curves for chitin extracted from shrimp shell at 0.4M HCl and 0.8M NaOH

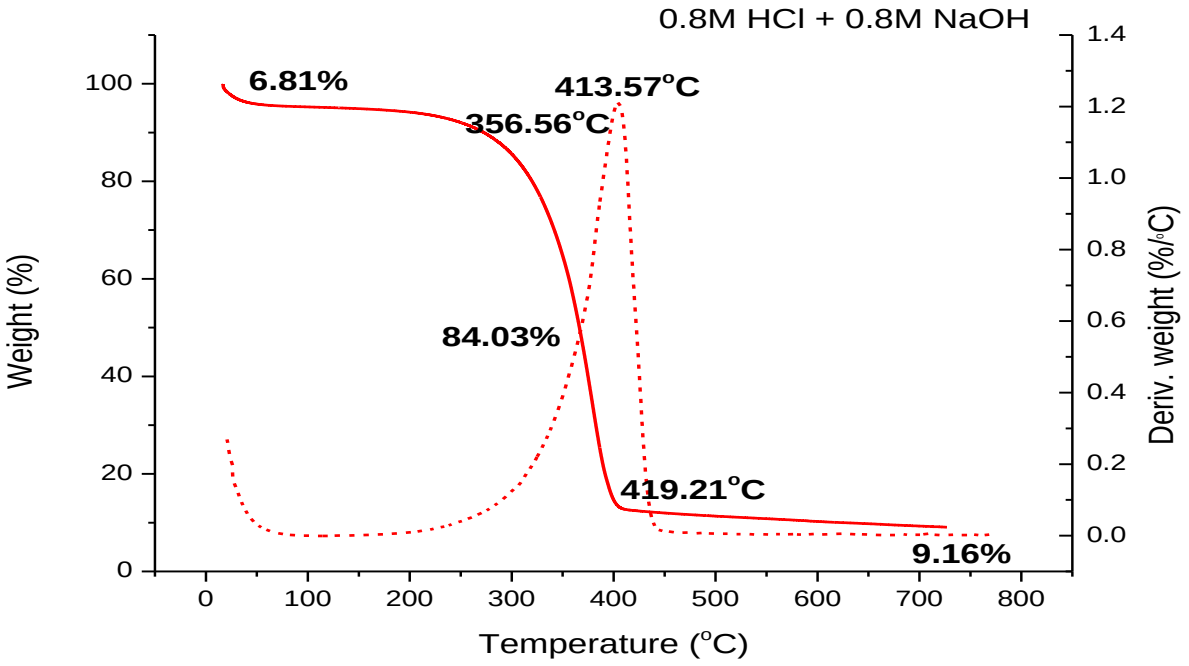

Figure 55: TGA-DTG curves for chitin extracted from shrimp shell at 0.8M HCl and 0.8M NaOH

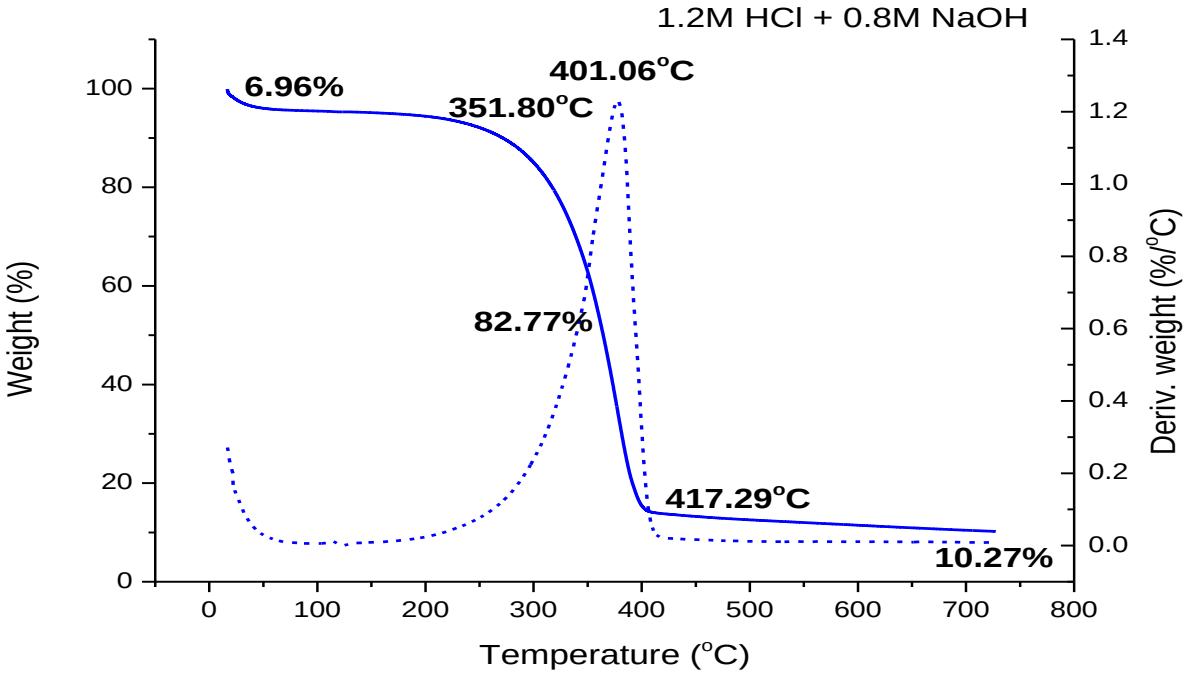

Figure 56: TGA-DTG curves for chitin extracted from shrimp shell at 1.2M HCl and 0.8M NaOH

TGA and corresponding DTG curves of chitin extracted from varying acid concentrations and at 1.2M NaOH are shown in Figures 57 - 59. For these samples, the first step from 40 to 140 ^{0}C is attributed to water evaporation with 6-11 % mass loss. Using 0.4M HCl treatment 83.43 % chitin is obtained and the degradation of its molecular structure occurs in the range 357.10 - 419.15 ^{0}C (Figure 57). The second decomposition stage for 0.8M HCl (Figure 58) treated sample contains 81.77 % chitin as shown by its decomposition, which occurs within 355.48 and 419.37 ^{0}C. Figure 59 shows 79.8 % chitin decomposition when shrimp shell is treated with 1.2M HCl and 1.2M NaOH. Decomposition occurs between 326.97 and 416.60 ^{0}C while the residue produced for the samples are 7.56, 11.35 and 9.7% for 0.4, 0.8 and 1.2M HCl treated samples respectively.

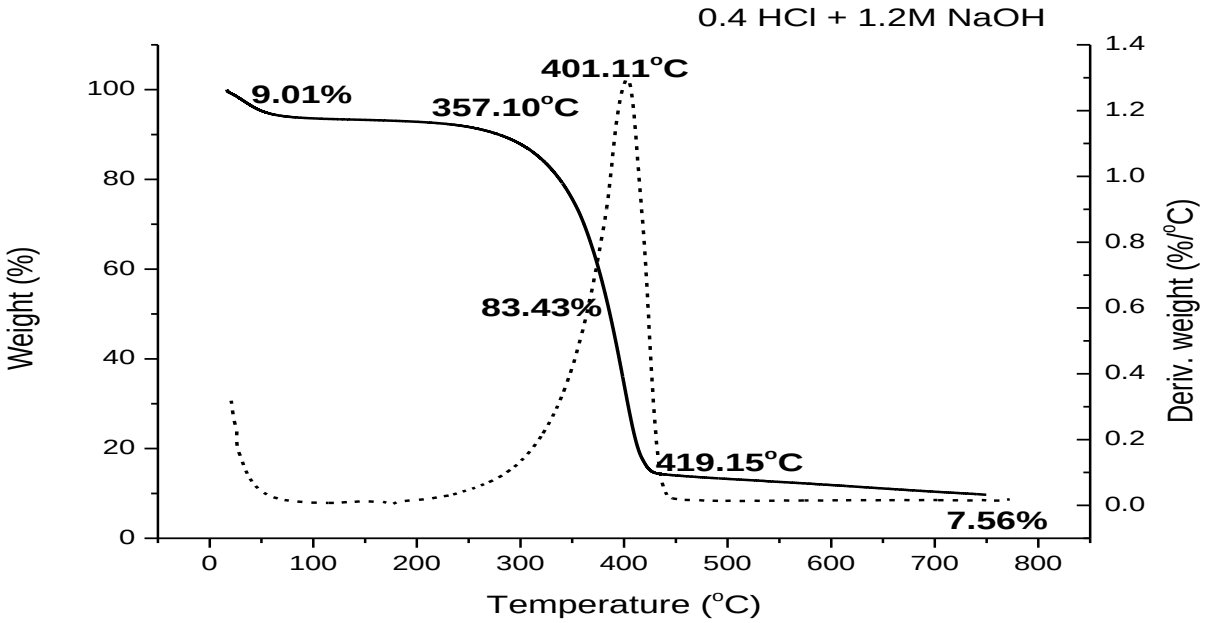

Figure 57: TGA-DTG curves for chitin extracted from shrimp shell at 0.4M HCl and 1.2M NaOH

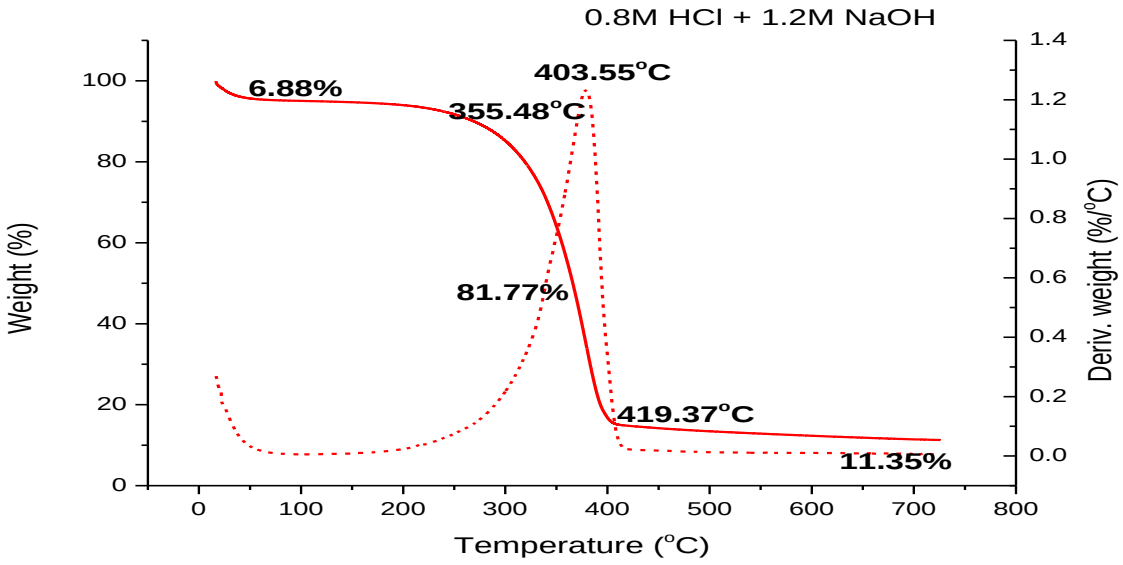

Figure 58: TGA-DTG curves for chitin extracted from shrimp shell at 0.8M HCl and 1.2M NaOH

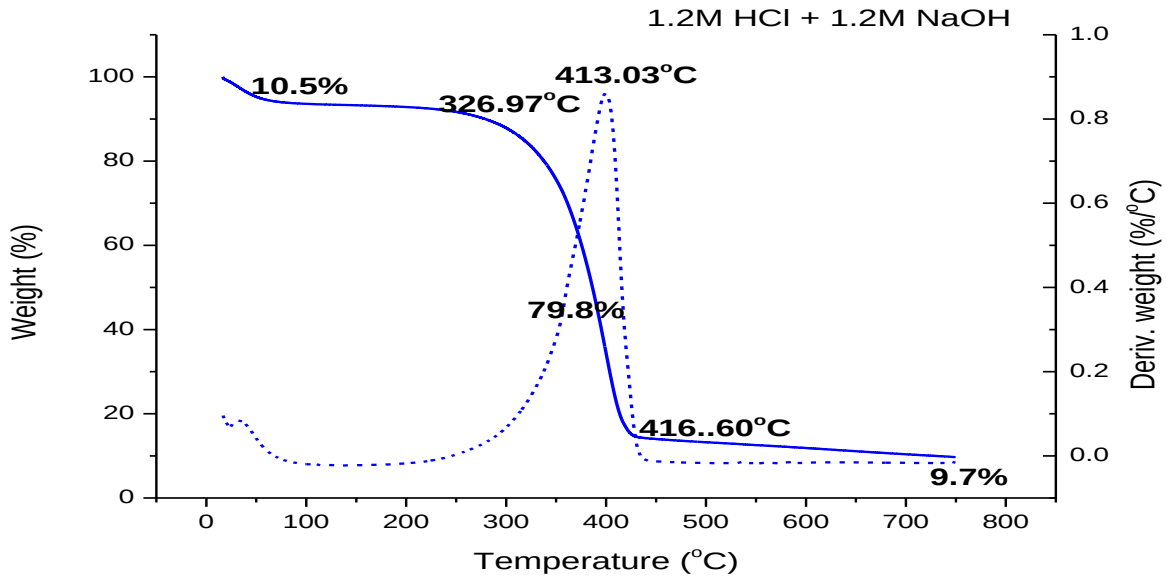

Figure 59: TGA-DTG curves for chitin extracted from shrimp shell at 1.2M HCl and 1.2M NaOH

Thermal stability of chitin bound in each shell is lower compared to their corresponding isolated forms as their T_{onset} possess the least values (316 and 321^{0}C for unextracted chitin in crab and shrimp shells respectively). This is also evident with their DTGmax values. Shrimp shell yields more of chitin than crab shells and thus implying that the harder the shell (as a function of increase in calcite), the lower the yield and stability of chitin. While the DTGmax of shrimp chitin is greater than that of crab chitin, it is also observed that the T_{onset} reduces as HCl and NaOH concentrations increase for each sample. The activation energy, E_a (Figure 60a) of shrimp chitin is higher than that of crab chitin (Figure 60b) owing to the higher thermal stability of the *N*-acetyl (GlcNAc) units in the former. The E_a for the thermal degradation of all shrimp chitin samples is from 139.63 and 106.88 kJ/mol. That from crab lies in 132.54 and 100.12 kJ/mol, at varying concentrations of HCl and NaOH. At higher concentrations of acid and alkali solutions, E_a decreases as the *N*-acetylated units decrease and this in turn lowers the thermal stability of the chitin molecules.

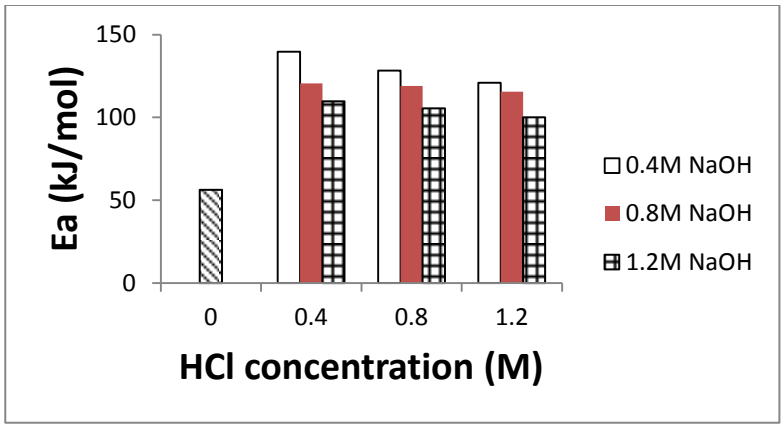

a

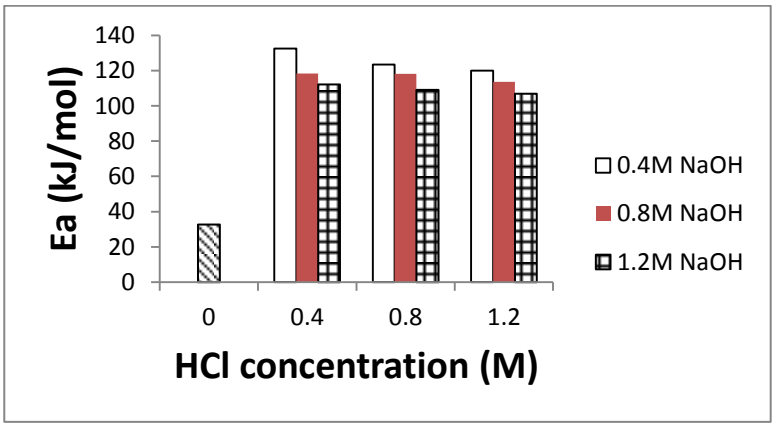

b

Figure 60: Activation energy values of virgin shell and (a) shrimp chitin (b) crab chitin at varying concentrations of HCl and NaOH

4.4 XRD

4.4.1 Crab XRD

The XRD analysis shown in Figure 61 shows that the crystalline form of calcium carbonate in the virgin crab exoskeleton is polycrystalline calcite and the structures designed in the shell are controlled by the organic matrix. The strongest diffraction intensity for the virgin crab shell at 2θ =

29.5° is the calcite (104), which agrees with what Rahman and Halfar (2014) observed in calcified coralline algae. The next to strongest intensities are the calcites occurring at 2θ = 39.59, 48.96, and 47.59^0 while indexed as (11$\bar{3}$), (11$\bar{6}$) and (018) respectively. The chitin present occurs at reflections (013), (012), (110), (202) and (122) representing 2θ = 26.84, 23.33, 36.27, 44.2 and 57.57^0 (Rahman *et al.*, 2013) respectively.

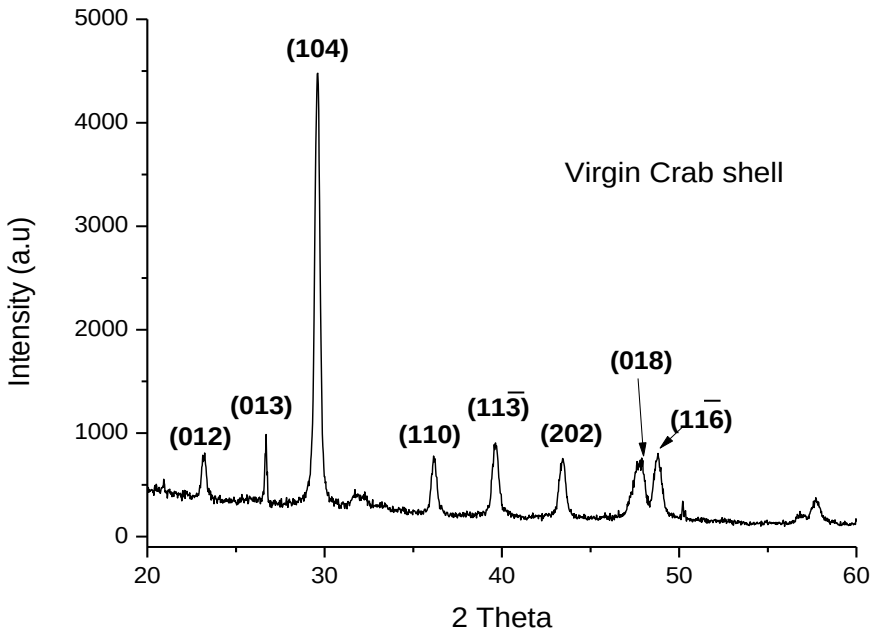

Figure 61: X-ray diffractometry of virgin crab shell

Figure 62 shows the X-ray diffraction patterns of α-chitin obtained from virgin crab shell after demineralization and deproteinization at 0.4, 0.8, and 1.2M HCl and 0.4M NaOH. All chitin samples show strong reflections at 2θ = 26.3, 20.6, 19.0^0 corresponding to (013), (120) and (110) respectively, with minor reflection on (021) plane at 12.5^0. According to Jang *et al.* (2004) α-chitin has four peaks at 9.6°, 19.6°, 21.1°, and 23.7°; β-Chitin has two crystalline peaks at 9.1° and 20.3° and the maximum peaks in γ-chitin are at 9.6 and 19.8^0. Four diffraction peaks of α -chitin nano fibers have been

observed at 2θ= 9.2, 19.1, 20.9, and 23.1^{o} which correspond to 020, 110, 120, and 130 planes, respectively (Ifuku *et al*., 2013). Chen *et al*. (2014) chemically synthesized α -chitin and observed the strongest crystalline peak at 19.1^{0} while other peaks appeared at 2θ = 9.1, 12.6, 23.2, 26.2 and 38.9^{0}. In this current study, CrI of 71.0, 68.8 and 67.6 % are measured for chitin samples extracted using 0.4, 0.8 and 1.2M HCl respectively at 0.4M NaOH. X-ray diffraction results for extracted α -chitin from crab shell using similar range of acid concentrations but at 0.8M alkali is shown in Figure 63. Similar peaks (but different intensities) are diffracted at the same angles, showing that crystallographic planes remain constant for particular marine specie during chemical extraction. Varying concentrations of reagent used caused differences in CrI, which is measured to be 69. 8 % for 0.4M, 68.8 % for 0.8M and 66.6 % for 1.2M HCl at 0.8M NaOH in this present study. In a study by Cárdenas *et al*. (2004), the CrI values were found to be 76.2 % for shrimp α-chitin, 82.7 % for lobster α- chitin, 81.9 % for crab α-chitin, 80.6 % for king crab α-chitin and 66.3 % for squid β-chitin. According to Kaya *et al*. (2014), the CrI value of 90.6 % for *Agabus bipustulatus* is the highest recorded to date. Comparing these with the present study, it has shown that the CrI values of chitins extracted from different organisms vary due to their shell hardness. Similar X-ray pattern (but different intensities) is also observed when extraction is done at 1.2M NaOH at same varying acid concentrations (Figure 64). The highest value for this alkali concentration is calculated as 68.9% for 0.4M HCl followed by 67.9% and 65.5% for 0.8 and 1.2M HCl respectively. In this study, it is observed that increasing both acid and alkali concentrations in the treatment allowed for cleavage of intra and intermolecular hydrogen bonds, thus leading to alterations in chitin crystal structure as demonstrated by the decrease in CrI.

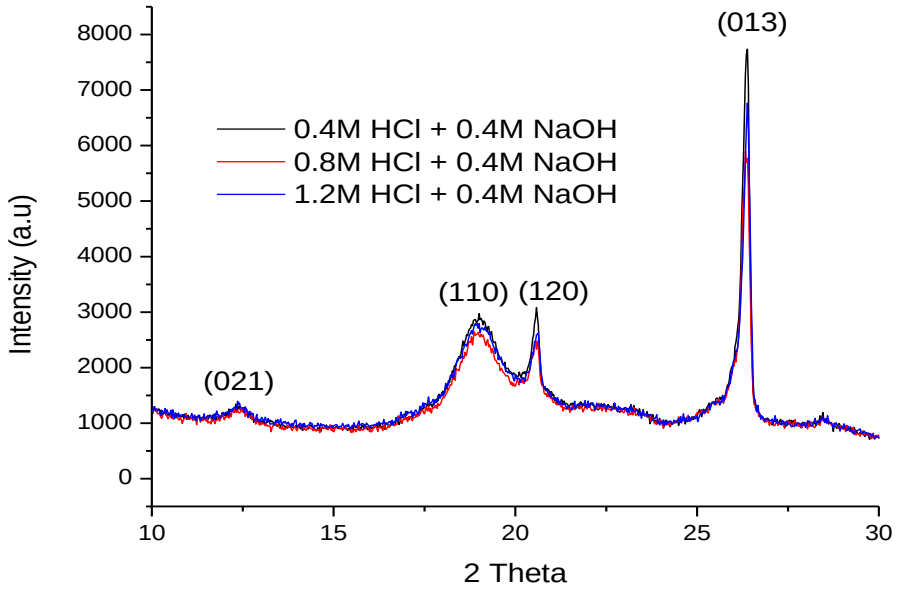

Figure 62: X-ray diffractometry of crab chitin extracted from varying HCl concentrations and 0.4M NaOH

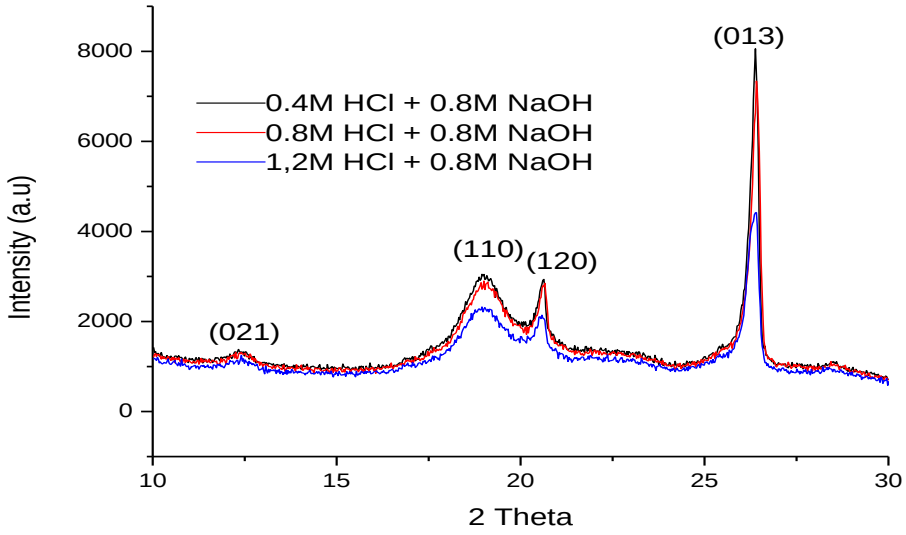

Figure 63: X-ray diffractometry of crab chitin extracted from varying HCl concentrations and 0.8M NaOH

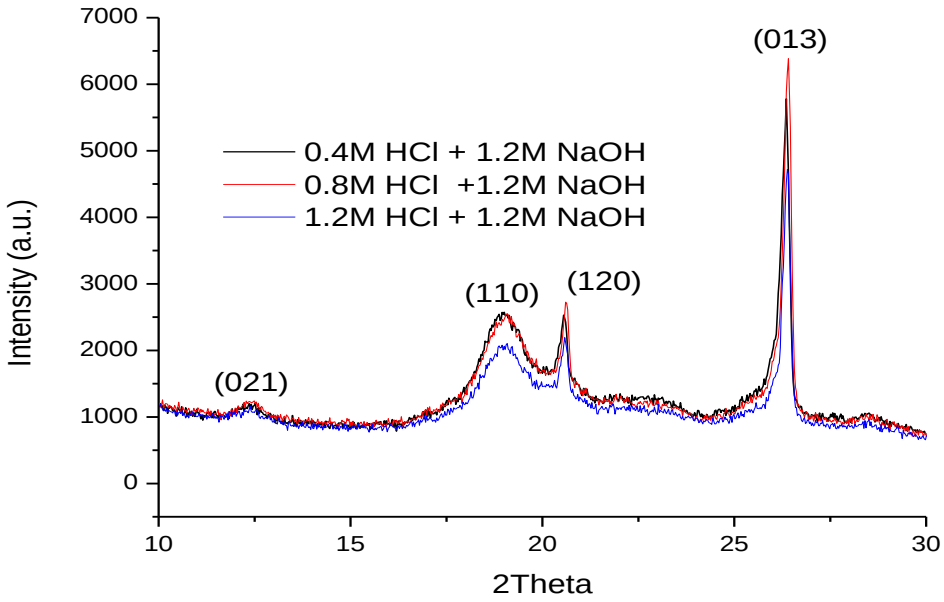

Figure 64: X-ray diffractometry of crab chitin extracted from varying HCl concentrations and 1.2M NaOH

4.4.2 Shrimp XRD

The XRD analysis of shrimp exoskeleton shown in Figure 65 reveals the existence of crystalline form of $CaCO_3$ (calcite) and chitin in the organic material. The $CaCO_3$ peaks are located on (104), $(11\bar{3})$ and $(11\bar{6})$ planes with corresponding 2θ values of 28, 40.7 and 48.2^0 while the rest represent the presence of chitin (Raya *et al*., 2015; Felsen *et al*., 2012; Boßelmann *et al*., 2007). Unlike the virgin crab shell, the chitin shows strongest intensity at $2\theta = 36^0$ (110). In addition, the diffractogram reveals other chitin peaks stronger than the calcite peaks. This justifies the use of less acid baths during demineralization of shrimp shells compared to the virgin crab shells. The FTIR spectrum (see Figure 34) shows weak calcite peak intensities in the shrimp shell than the virgin crab shell while TGA-DTG thermogram (Figure 50) also reveals more of chitin than calcite.

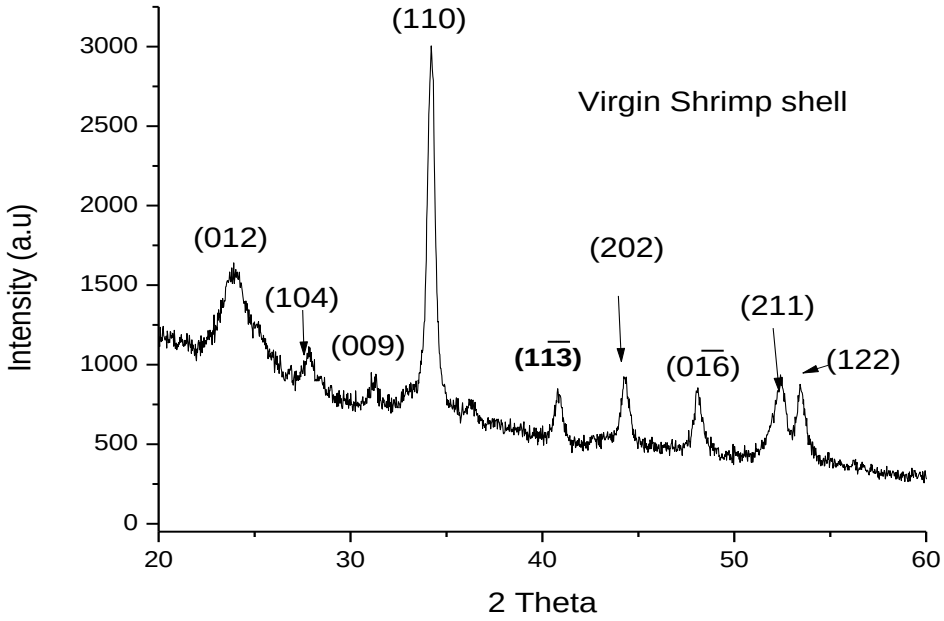

Figure 65: X-ray diffractometry of virgin shrimp shell

X-ray diffraction spectrum of chitin from shrimp exoskeleton is shown in Figures 66-68. One strong peak (19.2º corresponding to (110)), while three weak peaks of 12.6, 23.2 and 26.3^0 diffracting on (021), (130) and (013) are observed. In previous XRD studies conducted on α-chitin from various organisms, two strong peaks at 9 and 19^0, with weak peaks at 12, 21, 23, and 26^0 were observed in the spectra (Yen *et al*., 2009; Sajomsang and Gonil, 2010; Juárez-de La Rosa *et al*., 2012; Liu *et al*., 2012). XRD examination in this study, thus indicates that α-chitin is extracted. Figure 66 shows shrimp chitin extracted from 0.4, 0.8 and 1.2M HCl at 0.4M NaOH. Unlike the crab chitin, the strongest peak is indexed on (110), which is conventionally labeled as the strongest peak for chitin (Isa *et al*., 2012; Wang *et al*., 2013; Uzun and Celik, 2015). This shows that the chitin from shrimp is more structurally stable than its crab equivalent. It is glaring from Figure 66 that the intensity of the peak reduces with increase in acid concentration. The Crl of shrimp chitin for this alkali concentration is measured as 87.4, 86.2 and 83.3% for 0.4, 0.8 and 1.2M HCl respectively. Figure 67

shows that similar crystalline reflections occur on the same planes but at different intensities when deproteinization is done at 0.8M NaOH. Demineralizing with 0.4M HCl produces chitin with Crl 87.4%. Speeding up $CaCO_3$ and protein removal from shrimp shells by irradiation at 20 and 25 kGy after refluxing in 1M HCl and NaOH have been found to yield chitin of 63 and 76% Crl (Nesr *et al*., 2013). Increasing the acid concentration to 0.8 and 1.2 M further reduce the Crl by 1.8 and 5.7%. The most obvious reduction in peak intensities is observed at 1.2M HCl with 1.2M NaOH chitin extract (Figure 68). This is reflected in its Crl being the lowest of all (79.4%), while decrease in acid concentration witnessed increase in Crl of 85.2 and 86.3% for 0.8 and 0.4M respectively. Thus, this study has provided a 13.55 % improvement in the yield of Crl compared to that obtained in the work of Nesr *et al.* (2013). As witnessed for crab chitin, the stability of the chain decreases as a result of gradual removal of *N*-acetyl groups, which eventually scales down its crystallinity. In comparison, higher Crl at each acid and alkali concentrations observed in shrimp chitin buttress the fact that crab chitin is less structurally stable.

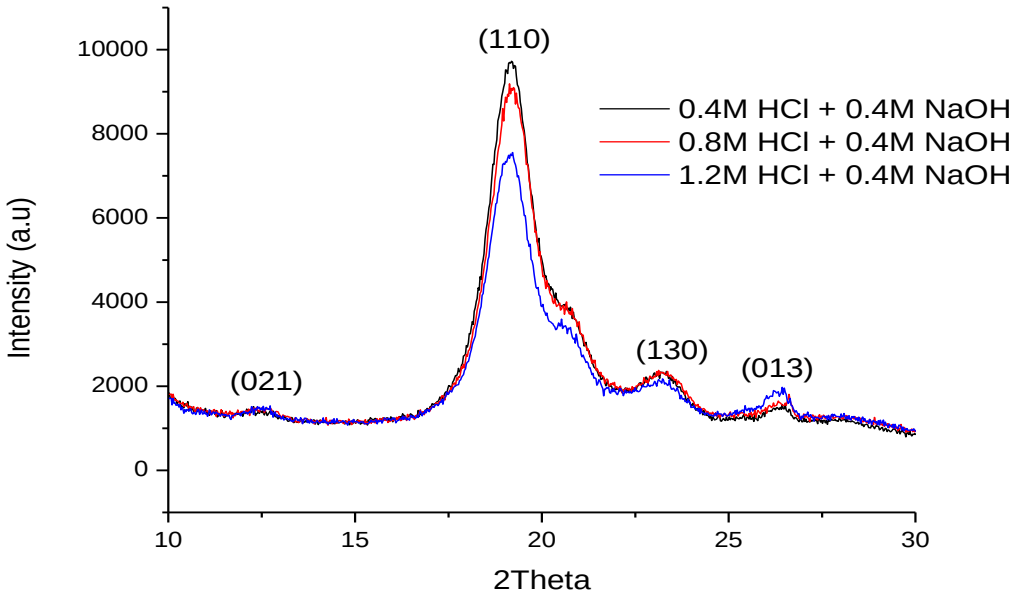

Figure 66: X-ray diffractometry of shrimp chitin extracted from varying HCl concentrations and 0.4M NaOH

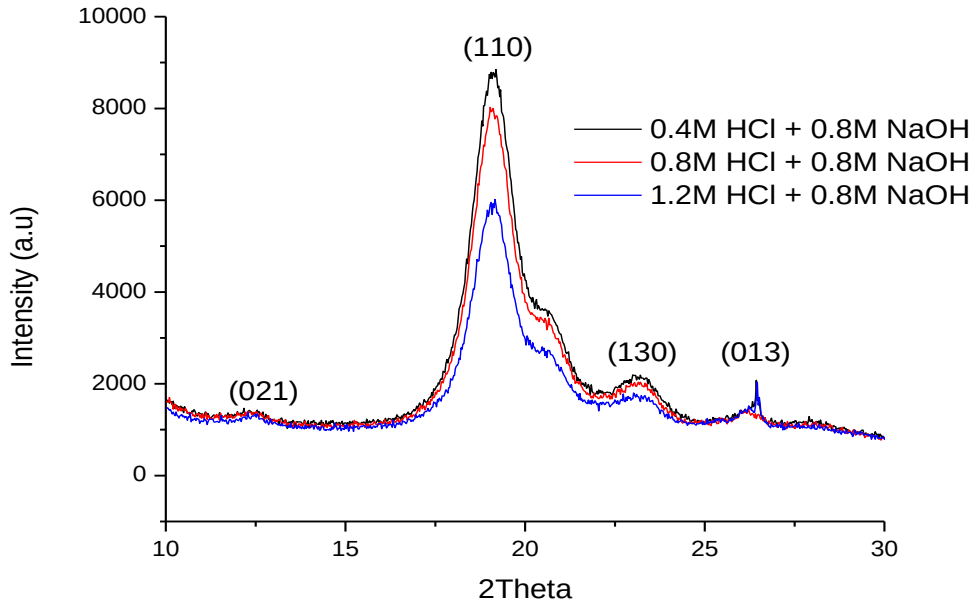

Figure 67: X-ray diffractometry of shrimp chitin extracted from varying HCl concentrations and 0.8M NaOH

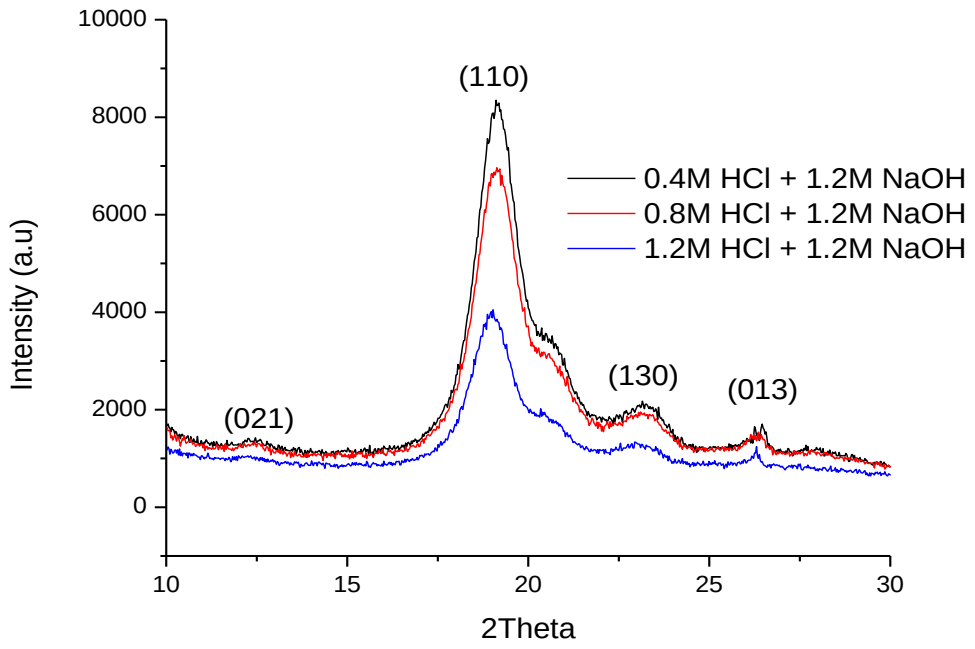

Figure 68: X-ray diffractometry of crab chitin extracted from varying HCl concentrations and 1.2M NaOH

4.5 SEM/EDS

4.5.1 Microanalysis and Morphology of Treated Crab Samples

Figure 69 shows the SEM/EDS of crab shell treated with varying concentration of acid (0.4 - 1.2 M) at fixed molar concentration of base (0.4 M). The EDS of the virgin crab shell shows strong calcium and oxygen peaks (see Figure 69a) similar to that reported by Lee *et al*., (2004) for crab shell before treatment. This implies that the surface of crab shell is composed of $CaCO_3$. Treatment with 0.4 M of acid leads to a significant change in the composition as shown by the EDS microanalysis (see Figure 69b). Calcium is reduced by 96 %, oxygen by 4.8 %, while nitrogen and carbon are increased by 42 and 68 % respectively. This is clear evidence that the $CaCO_3$ is drastically removed and C-N chains of α-chitin are formed. A significant change to the surface of crab shell is observed under 0.8 M acid reaction condition (see Figure 69c). Although the removal of calcium remains at 96 %, the carbon

content is increased by 2 % showing that carbon is enriched as detected by the higher count. A similar change is also noted at 1.2 M HCl treatment (see Figure 69d). Figures 69 (b, c and d) show significant changes to the surface morphology of the shell under the reaction conditions. Small nodule-like fibrils are observed on the surface of the processed samples. The surface morphology has fibrillar and granular structure as opposed to the particulate nature shown in Figure 69a. Samples treated with lower concentrations of HCl (0.4 and 0.8 M) display smooth surface fibrils with uniform fibrillar diameter without agglomeration. However, further increase in the concentration of acid to 1.2M leads to agglomeration of the fibrils (see Figure 69d). Similar morphologies are reported for α- chitin from shrimp and *H. parallela* by Liu *et al*. (2012).

Figure 70 shows the morphology of samples treated at varying concentrations of acid and at 0.8 M of base. In the EDS of Figure 70b the calcium peaks earlier found in the virgin samples had vanished and this indicates the effectiveness of the process in eliminating $CaCO_3$ from the crab shell. The micro-analysis shows a 97 % reduction in the calcium content compared to the virgin sample. The Figure also reveals that carbon and nitrogen contents are enriched by 67 and 37 % respectively. The presence of these peaks shows that $CaCO_3$ is leached out by the acid treatment with conversion of the shell to α-chitin. Increase in concentration to 0.8 M prompts the formation of other peaks and further enrichment of the carbon and nitrogen atoms (see Figure 70c), where calcium is found to reduce by 98 % from the EDS microanalysis. The use of 1.2 M concentration of acid leads to the same reduction (96 %) in calcium content with a higher enrichment in carbon and nitrogen contents (see Figure 70d).

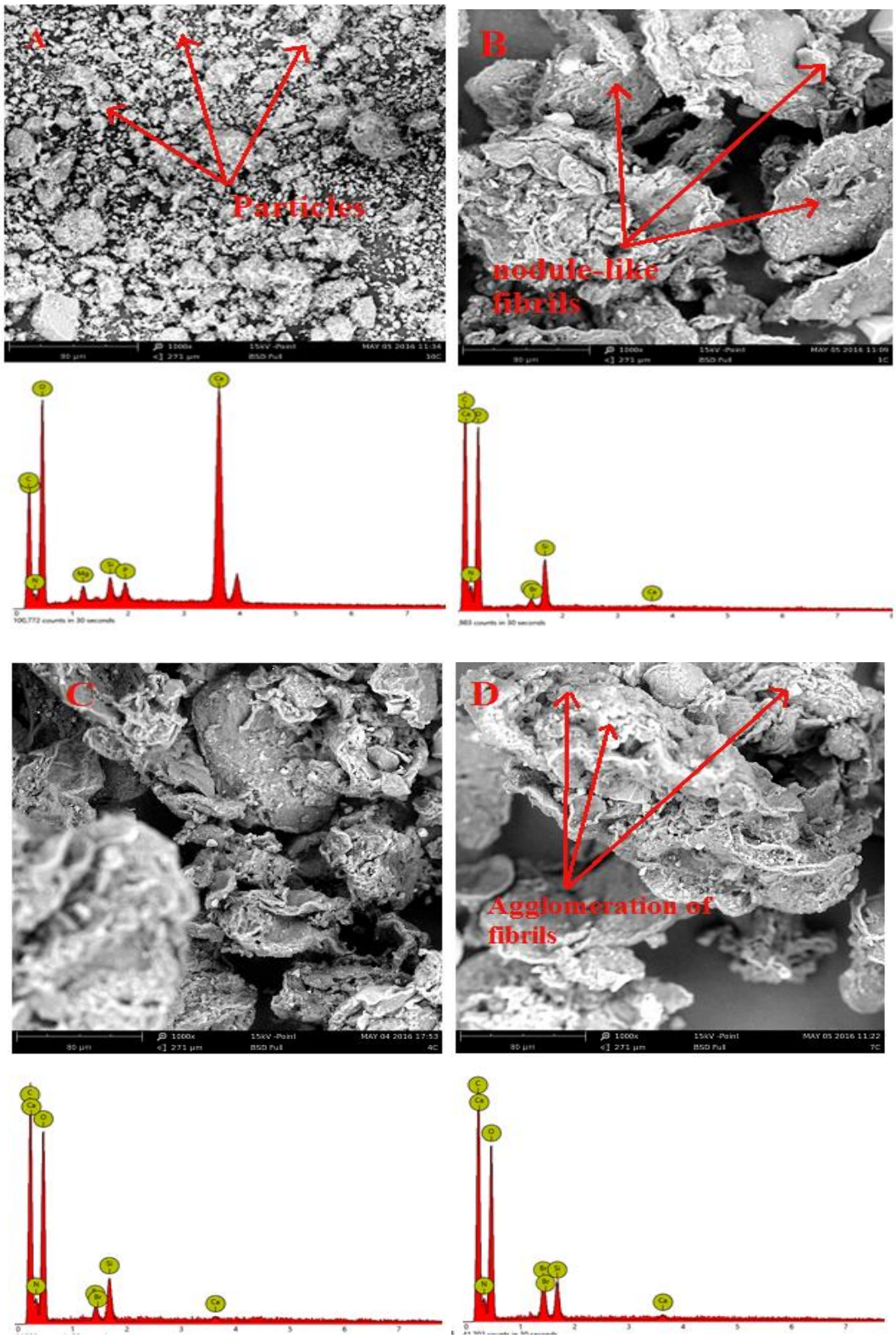

Figure 69: SEM/EDS images of crab shell (a) Virgin (b) treated with 0.4 M HCl (c) t0.8 M HCl (d) 1.2 M HCl at 0.4 M NaOH

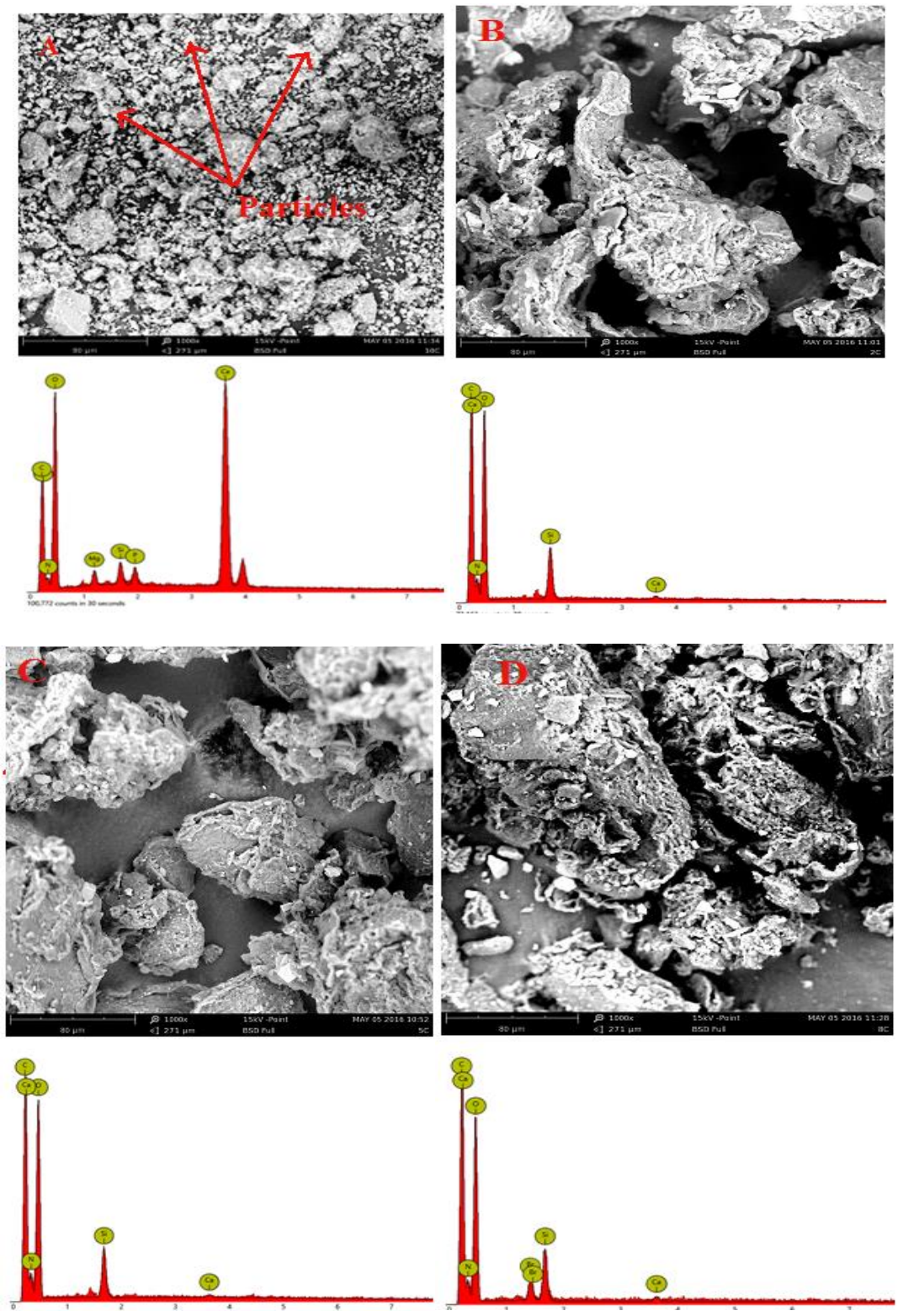

Figure 70: SEM/EDS images of crab shell (a) Virgin (b) treated with 0.4 M HCl (c) 0.8 M HCl (d) 1.2 M HCl at 0.8 M NaOH

The morphology of processed samples (Figures 70b, c and d) clearly indicates a distinct change in the surface morphology compared to that of virgin sample. Smooth and uniformly distributed fibrilla structure characterizes the processed samples as opposed to the particulate nature of the virgin samples. This confirms the conversion of the shells to α-chitin after acid and base treatments. A good uniform structure with a globular organization and less dense structure is observed in Figures 70b-d confirming that the structure is that of α-chitin in agreement with previous reports of Chen *et al*., (2012) and Isa *et al*., (2012). These structures also display a combination of crystalline and amorphous regions.

The SEM and EDS images of samples processed with varying compositions of acid and 1.2 M concentration of base are shown in Figure 71. Microanalysis shows 97, 96 and 98 % reduction in the calcium contents after treatment with 0.4, 0.8 and 1.2 M concentrations of acid respectively. This indicates that process steps adopted in the removal of the calcium carbonate is effective. The analysis further reveals increase in nitrogen contents by 36, 42 and 35 % for 0.4, 0.8 and 1.2 M concentrations of acid respectively and carbon enrichment as it shows the strongest peak in all cases (76, 67 and 67 % for 0.4, 0.8 and 1.2 M concentration of acid respectively). The presence of high carbon and nitrogen contents indicates the formation of N-acetyl groups and C-N chain of α- chitin. The reduction in calcium points to significant removal of calcite resulting to increase formation of α-chitin fibrils. The processed samples have morphology with fibers in circular thread networks. These fibrils form uniform structure with a globular organization that belongs to the chitin family, which was earlier reported by Isa *et al*., (2012). The fibril diameter is found to increase with increases in acid concentrations, while that treated with 1.2 M concentration shows fiber agglomerations. Comparison of Figures 69b, 70b and 71b shows that increasing the base concentrations lead to increase in the sheath-like layers attributed to deacetylation of the chitin. In addition to increase in

layer size as concentration of base increases, the sheaths surfaces' roughness increases and this is attributed to the low degree of deacetylation. This trend in features is repeated in Figures 69c, 69d 70c, 70d, 71c and 71d.

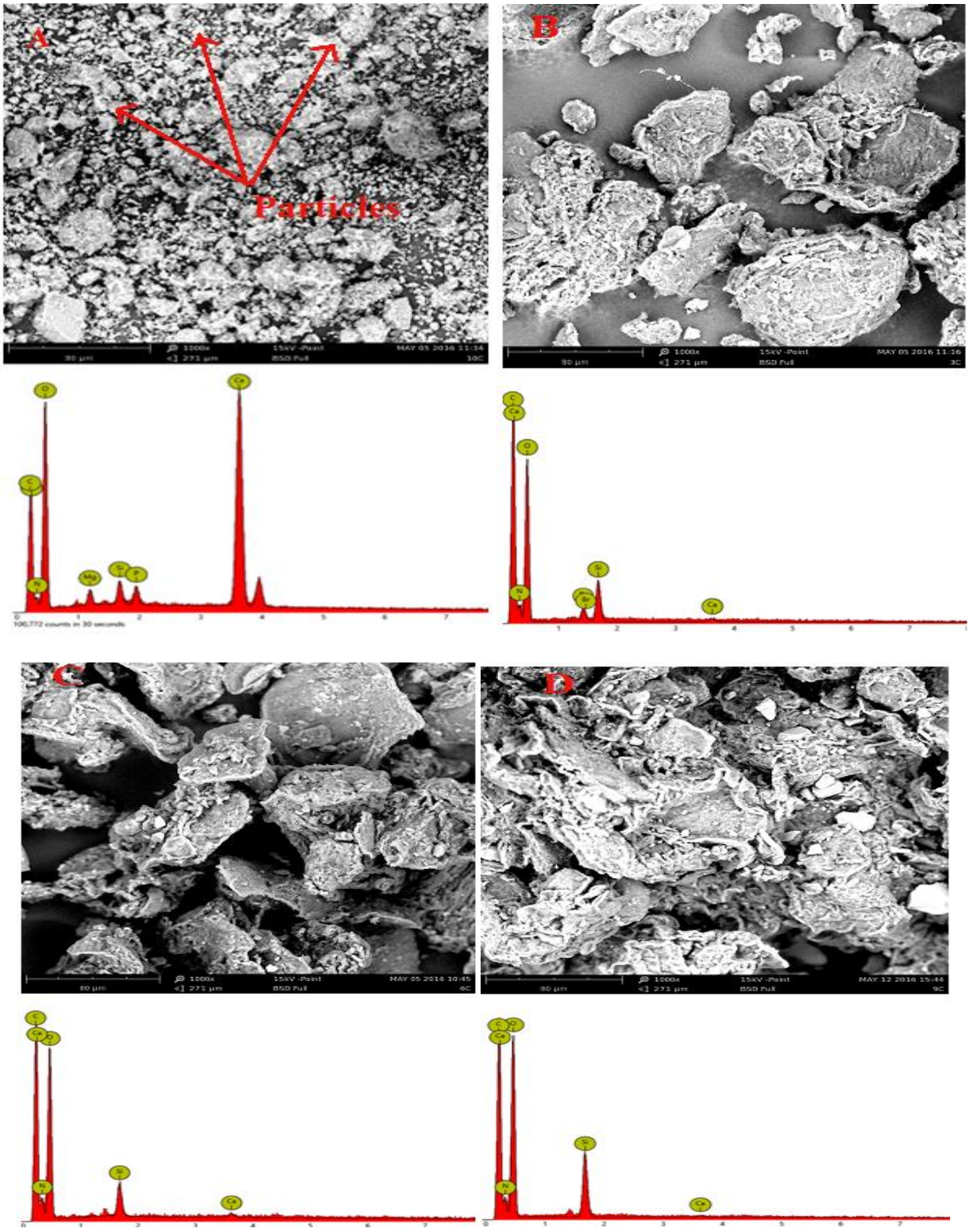

Figure 71: SEM/EDS images of crab shell (a) Virgin (b) treated with 0.4 M HCl (c) 0.8 M HCl (d) 1.2 M HCl at 1.2 M NaOH

4.5.2 Microanalysis and Morphology of Treated Shrimp Samples

Figure 72 is the SEM/EDS of shrimp shells treated with varying concentrations of HCl (0.4 - 1.2 M) at constant molar concentration of NaOH. The EDS of the virgin shrimp shell displays strong calcium and oxygen peaks (see Figure 72a), and the implication of this is that the shrimp shell surface is composed of $CaCO_3$ with other trace elements such as nitrogen and silicon. Treatment with 0.4 M of HCl leads to a significant change in the composition. After acid treatment, the calcium peaks disappears completely giving rise to increase in carbon and oxygen peaks counts (see Figure 72b). The microanalysis from EDS shows that there is a 94.6 % and 4 % reduction in calcium and oxygen contents. However, carbon content increases by 76 %, indicating the formation of α-chitin polymer chains. This confirms that the $CaCO_3$ in the shell dissolved rapidly under the acidic conditions and then removed. This can also be confirmed by the change from relatively rough surface of the shrimp fibers to a relatively smooth surface. Increase in concentration of HCl to 0.8 M leads to significant change in the surface structure of the shrimp shell (see Figure 72c). Rough surfaces of α-chitin are attributed to the low degree of deacetylation. Thus, increase in acid concentrations promotes a high degree of deacetylation as the surface appears smoother than that at 0.4 M with evidence of fibrillar structure. However, the carbon content appears unchanged. The microanalysis shows a total disappearance of calcium after this treatment, which is buttressed by the smoothness of the surface morphology of the treated shells. A similar change is also observed for 1.2 M HCl treatment (see Figure 72d). The difference in surface morphology of the samples suggests that increase in effectiveness is directly related to increase in concentrations of the acids used. The surface smoothness is found to increase with increase in acid concentrations, while 0.4 M concentration leads to formation of large sized sheath-like fibrils. However, further increase in concentration decreases fibril size but with smoother morphology. Similar features were reported for α-chitin from shrimp

and *H. parallela* by Liu *et al*. (2012). The sheath-like nature of chitin was also noted by Isa *et al*. (2012).

The effect of increase in alkaline concentrations to 0.8 M with varying HCl concentrations on the surface morphology and micro-constituents of the treated shells is shown in Figure 73. Figure 73a is the morphology of virgin sample without treatment. Treatment of this sample with 0.8 M base and 0.4 M acid enabled $CaCO_3$ removal and the formation of α-chitin fibril structure as indicated by the SEM/EDS in Figure 73b. Microanalysis shows that the treatment leads to 96 % and 3.2 % removal of calcium and oxygen respectively and a 74.8 % improvement in carbon content. This is a clear indication of calcium removal and the formation of carbon hydrogen chains of the chitin structure. This is also evident from the surface morphology as particle-like substances of the raw shrimp shell (Figure 73a) are changed to plate-like fibrils with improvement in surface smoothness. Further increase in HCl concentrations to 0.8 M produces 4.7 % and 92 % reduction in oxygen and calcium contents respectively and a 75 % increase in carbon content. This result is quite similar to that at 0.4 M acid concentration but with slight improvement in oxygen content while the surface morphology also remains the same. Further increase in acid concentrations to 1.2 M did not result to significant difference relative to that at 0.8 M acid concentration. However, the fibrils declines in size and are not uniform. The surfaces of these samples are not as smooth as those treated with 0.4 M concentration of HCl. This indicates that 0.4 M acid is more effective in the removal of calcium than using 0.8 M and 1.2M of the acid. However, it is noticed that the nitrogen content increases with increase in base concentrations. This is attributed to the formation of more amino groups at higher concentrations of the base.

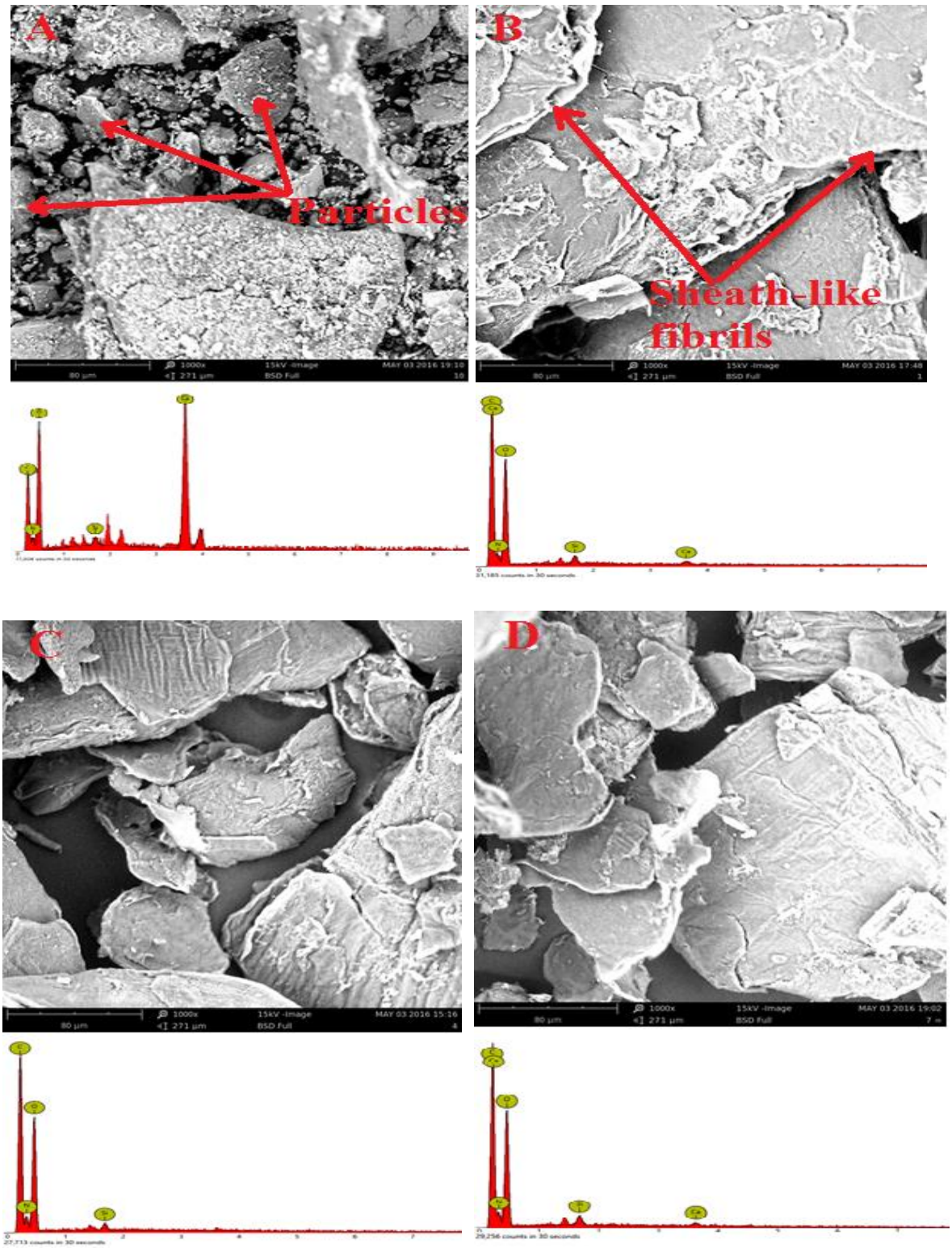

Figure 72: SEM/EDS images of shrimp shell (a) Virgin (b) treated with 0.4 M HCl (c) 0.8 M HCl (d) 1.2 M HCl at 0.4 M NaOH

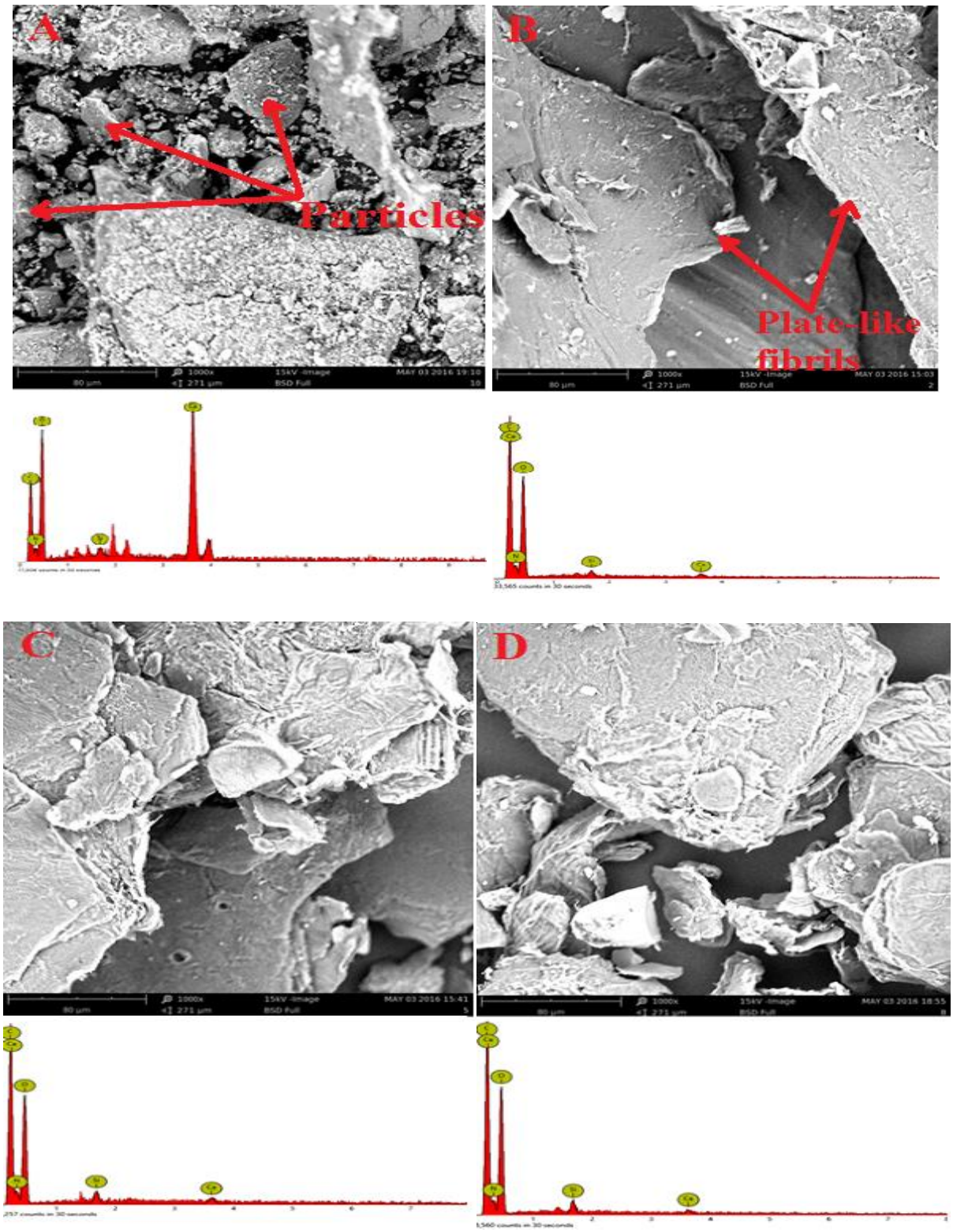

Figure 73: SEM/EDS images of shrimp shell (a) Virgin (b) treated with 0.4 M HCl (c) 0.8 M HCl (d) 1.2 M HCl at 0.8 M NaOH

Figure 74 shows the effect of further increase in concentrations of the base to 1.2 M on the surface morphology and micro-constituents of shrimp shells. The microanalysis shows that there was 98.9 % removal of calcite from the shrimp shells when treated with 0.4 M of the acid (see Figure 74b). The analysis also records 75 % increase in carbon contents showing the formation of α-chitin while oxygen is reduced by 4 %. This is also shown by the change in particle-like structure of the virgin sample to a more fibrilla feature as seen Figure 58b with few small-sized globule having large surface structures compared to virgin shrimp shell. This observation is repeated with further increase in concentration of HCl to 0.8 M, which produces complete removal of calcium. Thus, the treatment leads to the removal of the mineral compounds ($CaCO_3$) resulting in the formation of α-chitin chains and buttressed by the smooth surface morphology of the treated shrimp. Significant increase in the nitrogen content of the sample is observed, which attests to the formation of amino group. This is an explanation for the globular nature of the fibrils in Figure 74c. Figure 74d shows the surface morphology of shrimp treated with 1.2 M HCl. The image shows considerable decrease in $CaCO_3$ content and the formation of fibrillar network of chitin chains. It is evident from Figures 48 b-d that 1.2 M concentration of the base favours the formation of amino groups more than other concentrations.

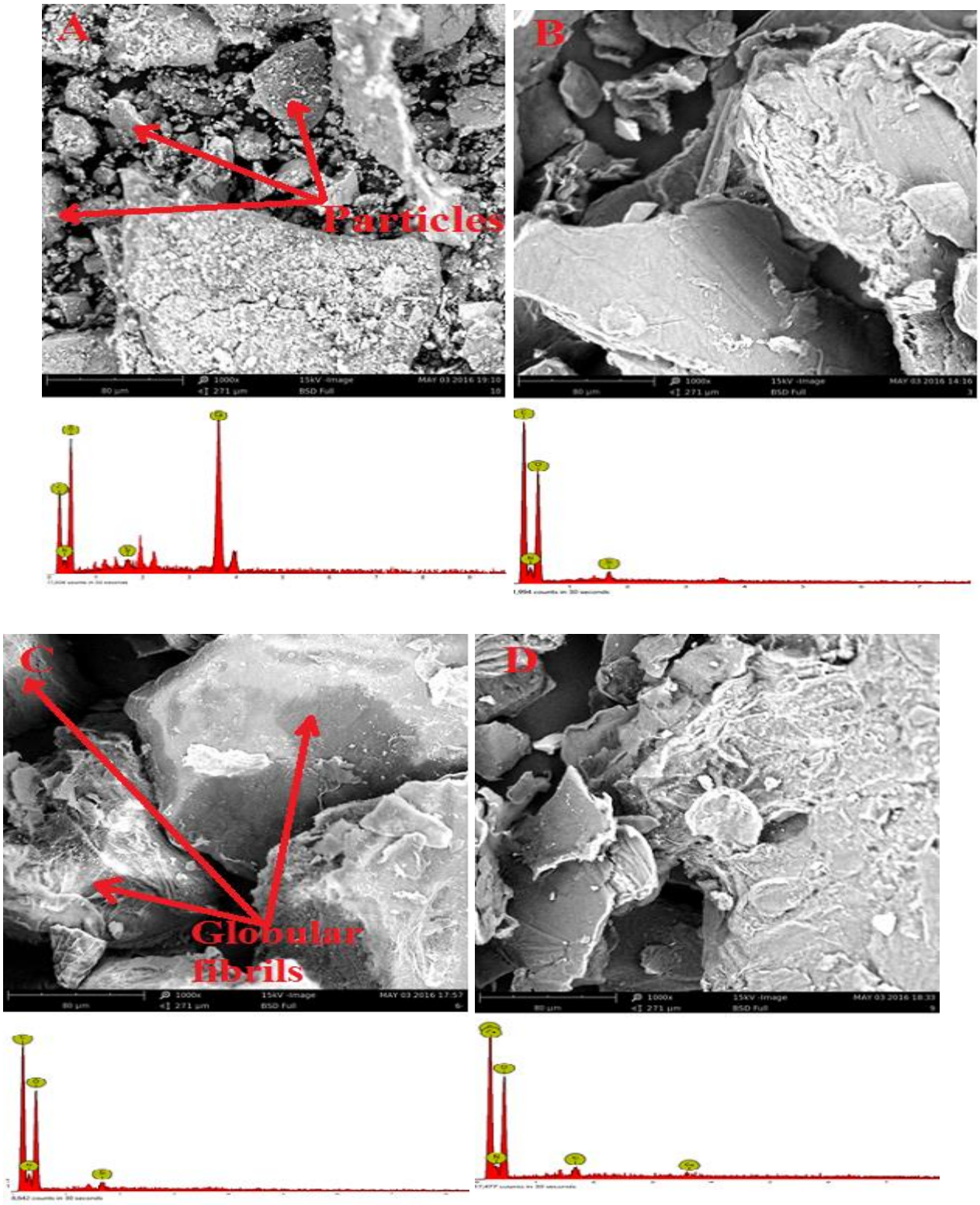

Figure 74: SEM/EDS images of shrimp shell (a) Virgin (b) treated with 0.4 M HCl (c) 0.8 M HCl (d) 1.2 M HCl at 1.2 M NaOH

4.6 Elastic Modulus of PLA and PLA-Chitin Composite

The elastic moduli of PLA and PLA-chitin composites are presented in Figures 75 and 76. It is shown that the modulus of PLA improved with the inclusion of chitin in its matrix. Elastic modulus increases from 3.64 -33GPa when chitin content increased from 10-30 wt. % (Figures 75 and 76). Firooziani *et al.* (2010) stated that elastic modulus of a composite will be higher than the individual polymer if the filler is of a higher stiffness. The high stiffness of chitin that is attributed to the strong hydrogen bond possessed by α- chitin (from both sources) provide its rigidity characteristics (Einbu, 2007; Cui *et al.,* 2016), which controls the mobility of PLA during mechanical deformation. This will increase as the quantity of chitin in the matrix is increased. Biodegradation is exemplified in samples as the gradual loss of modulus on immersion in PBS (pH 7.4, 37^{o}C) for 8 weeks. The appreciable amount of amino groups of approximately 35% from shrimp and crab chitin enhanced hydrogen bond cleavage, which allows the degrading medium diffuse through its structure and hydrolyze the matrix. The alteration of chitin structure therefore, strengthens its ability to hinder the mobility of PLA.

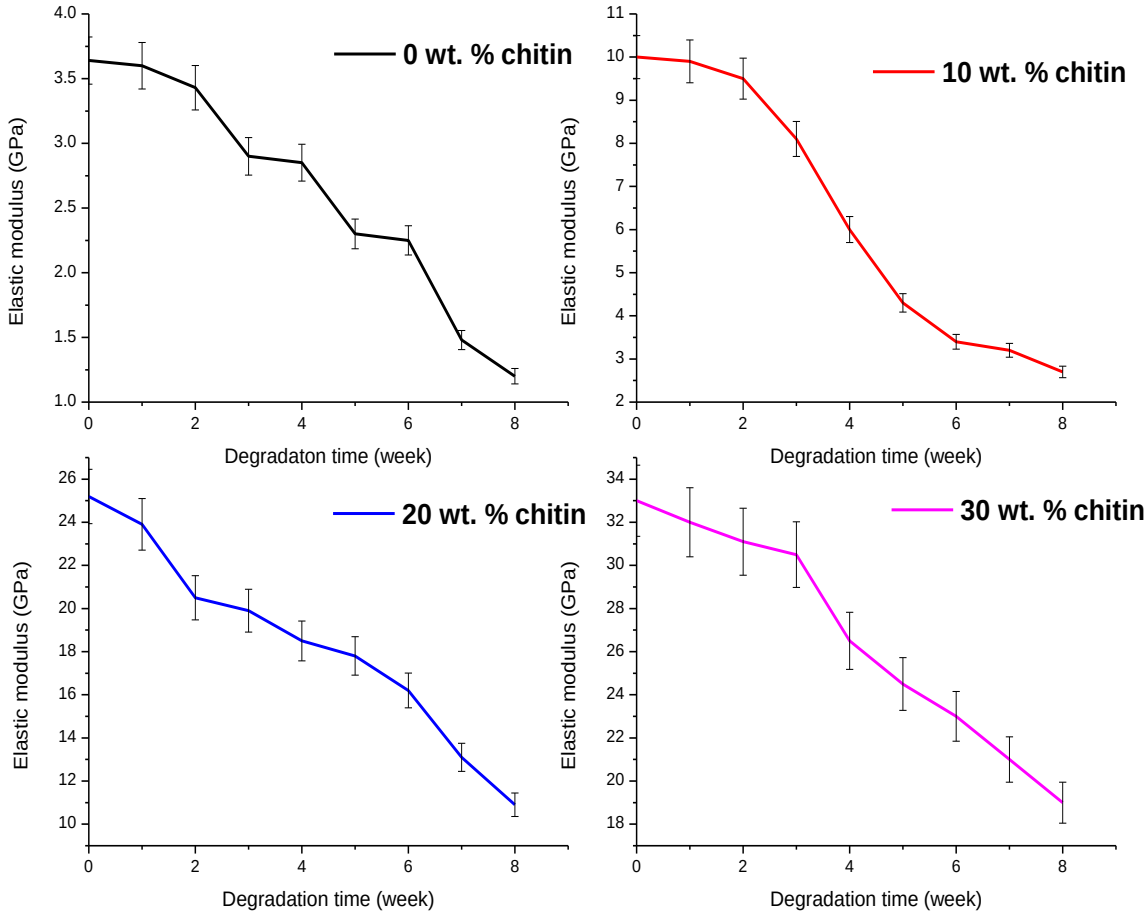

Figure 75: Elastic modulus against degradation time for PLA-chitin composites at varying contents of shrimp chitin

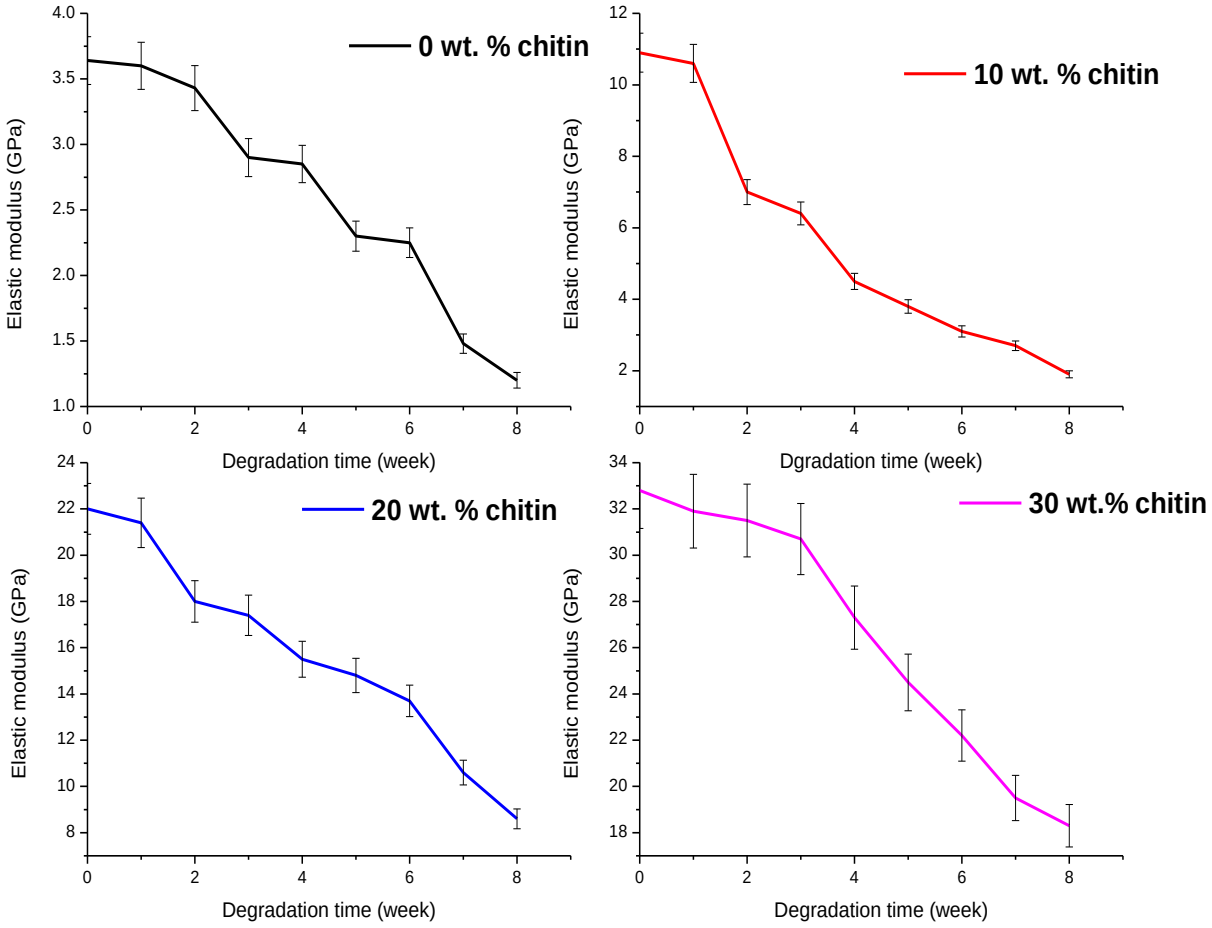

Figure 76: Elastic modulus against degradation time for PLA-chitin composites at varying contents of crab chitin

The empirical equations that show the relationship between elastic modulus (E) and degradation time (T, week) of PLA-chitin composites at varying contents of shrimp (SC) and crab chitin (CC) are given in Equations (13)-(19).

$E_{0\ wt.\ \%\ SC} = 0.0012T^3 - 0.0357T^2 - 0.1036T + 3.6601$ ($R^2 = 0.96650$) (13)

$E_{10\ wt.\ \%\ SC} = 0.04899T^3 - 0.57348T^2 - 0.56995T + 10.00909$ ($R^2 = 0.98652$) (14)

$E_{20\ wt.\ \%\ SC} = -0.04192T^3 + 0.46548T^2 - 2.88871T + 25.48485$ ($R^2 = 0.98078$) (15)

$E_{30\ wt.\ \%\ SC} = 0.03392T^3 - 0.48369T^2 - 0.01235T + 36.86102$ ($R^2 = 0.98203$) (16)

$E_{10\ wt.\ \%\ CC} = 0.0286T^3 + 0.08178T^2 - 1.99373T + 11.36465$ $(R^2 = 0.95565)$ (17)

$E_{20\ wt.\ \%\ CC} = -0.02753T^3 + 0.29762T^2 - 2.35494T + 22.41515$ $(R^2 = 0.97324)$ (18)

$E_{30\ wt.\ \%\ CC} = 0.05093T^3 - 0.74466T^2 + 0.91192T + 32.4202$ $(R^2 = 0.98938)$ (19)

The production of these shorter chains must is seen as promoting the reduction in elastic modulus of PLA. PLA reinforced with 20 wt.% α-chitin from shrimp exoskeleton gradually loses its modulus from 25.2 -10.9GPa after 8 weeks (Figure 75) while that sourced from crab shell with the same content reduces from 22 – 8.6GPa (Figure 76). Maximum modulus of 33 and 32.8GPa is attained at 30 wt. % α-chitin for shrimp and crab respectively and degrade to 19 and 18.3GPa on the 8th week. At these compositions, the composites can serve as a temporary structural device for human cortical bone (20-30GPa), osteonal bone (15GPa) and trabecular bone (11GPa) (Hoffler *et al.,* 2000) depending on the severity of injury/fracture. These materials will pose no danger to the bone and surrounding tissues during remodeling. The strength decrease rate (u_s) measured as a function of strength evolution of samples during degradation is illustrated in Table 4. Polymer strength degradation has been confirmed by Vieira *et al.,* (2015) to follow the same trend as the molecular weight reduction where u_s is directly related to the kinetic constant of the material. Table 4 reveals that the rate at which PLA strength degrades is accelerated by 72% with 10 wt. % α- shrimp chitin addition while allowing for gradual load transfer to the rehabilitee bone and in similar manner the α-crab chitin accelerates the rate by 71%. Thus, the issue of load shielding known with conventional metallic implants is eliminated. Increasing α-chitin contents in PLA further increases the strength degradation rate to a maximum of 77.7 and 79.5% obtained at 30 wt. % α-chitin from crab and shrimp respectively. This implies that the strength of a PLA-chitin composite scaffold will degrade at a slower rate than its unreinforced form (which is then released to the tissue). Rate at which these

composites' strength degrades is faster than that of unreinforced PLA as the load transfer rate to the bone increased.

Table 4: Strength degradation rate of PLA and PLA/chitin composites

	us	
Filler (wt. %)	Crab chitin	Shrimp chitin
0	0.0998	0.0998
10	0.1707	0.1717
20	0.1729	0.1738
30	0.1773	0.1791

4.7 Composite Weight Loss Pattern

In-vitro degradation study of PLA and PLA-chitin composite samples measured in terms of weight loss after immersion in PBS (pH 7.4 and 35^{o}C) for 12 weeks is shown in Figures 77 and 78. There is an increase in weight loss of samples with prolonged degradation time. This indicates that the weight loss is associated with the release of oligomers and monomers diffusing out of the matrix during hydrolysis. Reinforcement with α-chitin from the two exoskeleton sources (shrimp and crab) increases the hydrophylicity of PLA as the degradation of PLA-chitin samples increased rapidly, and is also enhanced by increasing α-chitin contents (wt. %). Weight loss-degradation time response of PLA- chitin follow a similar trend and this implies that chitin sourced from exoskeletons of crustacean shell produces similar characteristics on PLA. The work of Mi *et al.* (2002) states that hydrophilic enhancement of polyester occurred when PLGA50/50 (polylactide-co-glycolide) microspheres were reinforced with chitin. Weight loss of composite increased up to 90 % with increase in hydrophilic chitin content after 40 days. This suggests that the hydrolysis of PLGA was accelerated with incorporation of hydrophilic chitin. However, degradation of materials such as this is very rapid to be considered as bone implants.

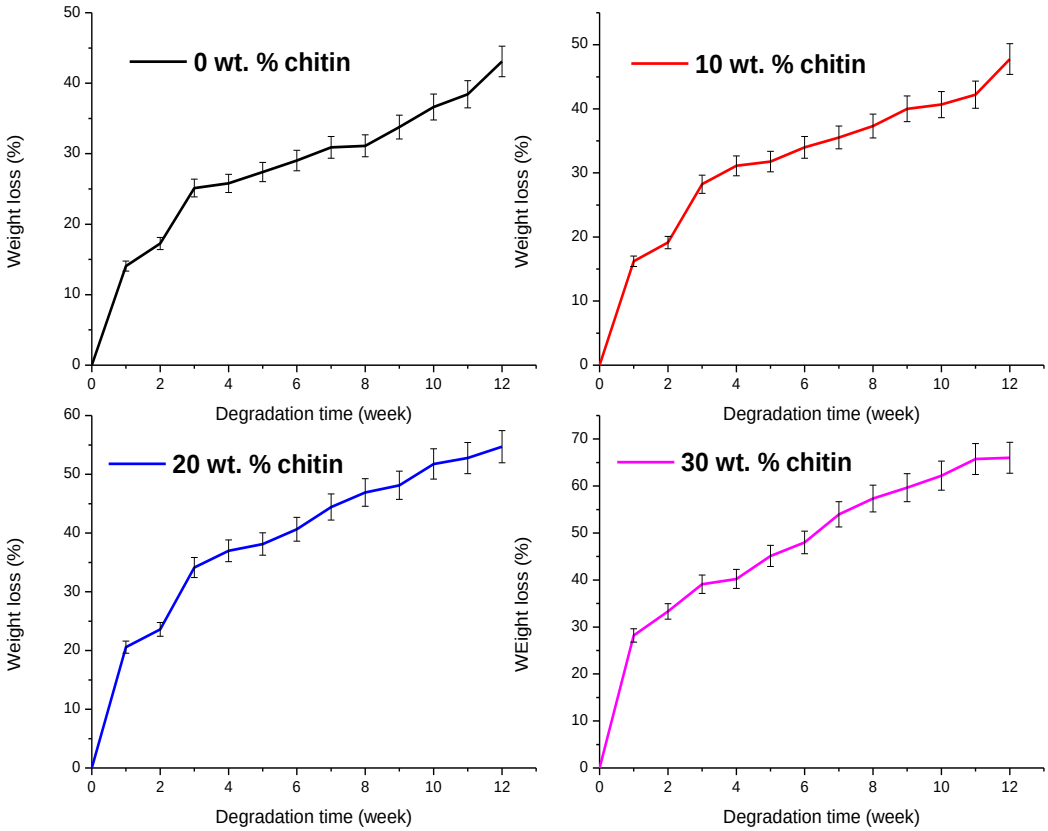

Figure 77: Weight loss against degradation time for PLA-chitin composites at varying contents of shrimp chitin

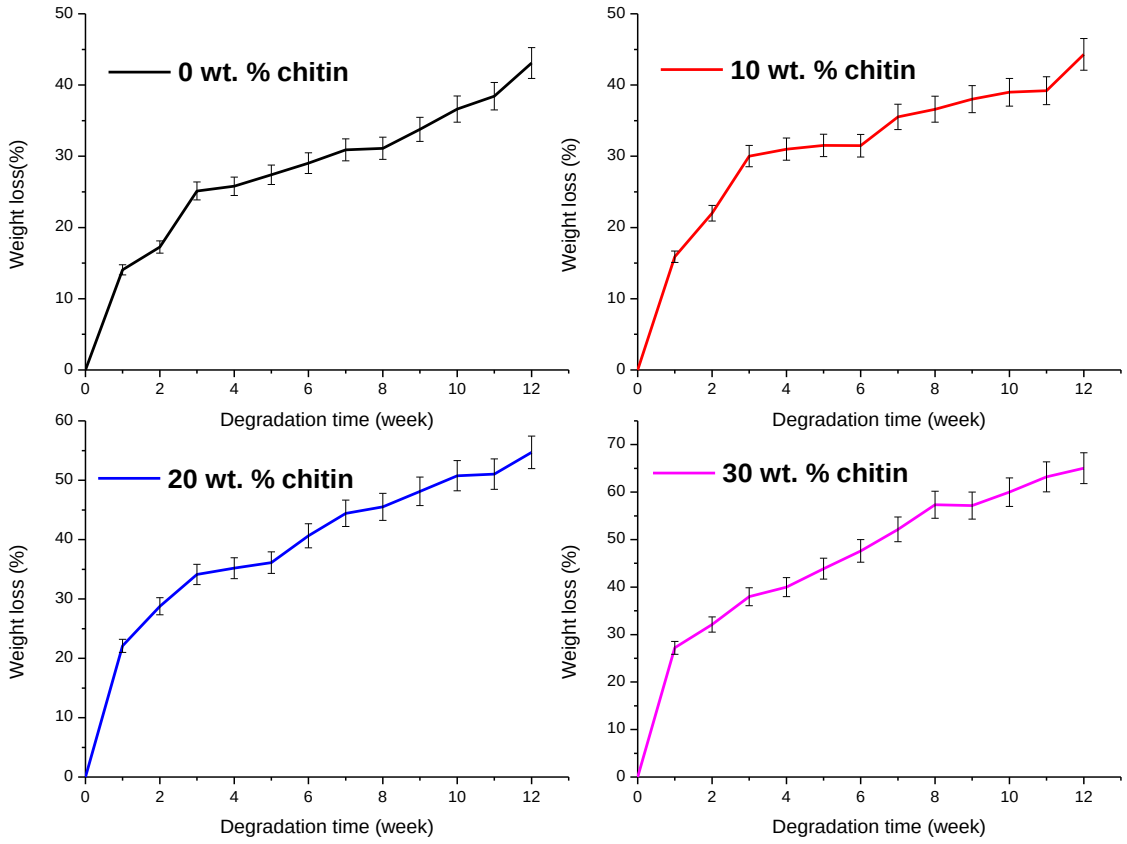

Figure 78: Weight loss against degradation time for PLA-chitin composites at varying contents of crab chitin

Equations (20) – (26) show the empirical model that gives the relationship between weight loss (WL) and degradation time (T, week) of PLA-chitin composites at varying wt. % chitin.

$$WL_{0\ wt.\ \%\ SC} = 0.04787T^3 - 0.98607T^2 + 7.98305T + 6.63394 \quad (R^2 = 0.98205) \quad (20)$$

$$WL_{10\ wt.\ \%\ SC} = 0.04823T^3 - 1.07126T^2 - 9.25128T + 7.10638 \quad (R^2 = 0.97651) \quad (21)$$

$$WL_{20\ wt.\ \%\ SC} = 0.02551T^3 - 0.58531T^2 + 8.11007T + 12.58788 \quad (R^2 = 0.97790) \quad (22)$$

$$WL_{30\ wt.\ \%\ SC} = -0.1234T^3 + 0.12143T^2 + 3.77773T + 25.034165 \quad (R^2 = 0.99239) \quad (23)$$

$$WL_{10\ wt.\ \%\ CC} = 0.07756T^3 + 1.70871T^2 + 12.57851T + 2.21758 \quad (R^2 = 0.96879) \quad (24)$$

$$WL_{20\ wt.\ \%\ CC}: \ 0.07349T^3 - 1.65629T^2 + 13.57263T + 4.79192 \quad (R^2 = 0.94803) \quad (25)$$

$WL_{30\ wt.\ \%\ CC}$: $0.09994T^3 - 1.63365T^2 + 14.62398T + 6.20657$ (R^2 =0.94803) (26)

The study of Engineer *et al.,* (2010) revealed that the In-vitro degradation of 50/50 PLA/PGA in PBS (pH 7.4 and 37 ^{0}C) witnessed 56 and 85 % weight loss after 4 and 12 weeks respectively. Result obtained in this study shows that under a similar condition, PLA loses 25.8 and 43.1% of its weight after 4th and the 12th weeks respectively. Reinforcing PLA with 30 wt. % α- shrimp chitin indicates composite's maximum weight loss of 40.2 and 66% after 4th and 12th weeks respectively (Figure 77). In addition, 40 and 65% weight loss were observed for PLA-chitin using similar α-chitin content sourced from crab shells (Figure 78). The degradation rate of samples investigated by Engineer *et al.,* (2010) was more rapid than those composites achieved in this study (≈29 and 24% faster for the two periods). However, MAST Biosurgery, (2007) earlier confirmed that PGA polymers exhibit tissue reaction as it initiates an inflammatory tissue response. During In-vitro degradation of PLA-PCL (polycaprolactone), Vieira *et al.,* (2015) incubated the blended sample in PBS of pH 7.4 at 37 ^{0}C for 28 weeks and noticed 20% weight loss of sample at the end of this period. In this present study, composite (PLA-chitin 90/10) weight loss of 19.2 and 22% are observed after 2 weeks of degradation with α-chitin sourced from shrimps and crab shells, respectively. This implies that the hydrolytic degradation rate of PLA-PCL sample of Vieira *et al.,* (2015) is much slower with the concern of incomplete dissolution of sample before significant tissue healing. A more rapid hydrolytic degradation of PLA in PBS at pH 7.4 and 80 ^{0}C was observed as 100% weight loss was recorded after 6 days (Tsuji *et al.,* 2011). This also is too rapid for bone healing rate, and besides the temperature is not clinical for humans. Table 5 shows the diffusion coefficient, *D* of PBS into the polymer, hydrolysis time T_H and diffusion time T_D for PLA and PLA-chitin composites. It is observed that for each sample, $T_H >> T_D$, which suggests that the fluid reaches the core of the material before it reacts and the degradation occurs homogenously/uniformly (i.e., bulk erosion). In

this case, diffusion is considered to occur instantaneously. Therefore, the decrease in molecular weights, reduction in mechanical properties and the loss of mass may also occur simultaneously throughout the entire specimen (Vieira *et al.*, 2011).

Table 5: Diffusion coefficient of fluid into samples (*D*), hydrolysis time (T_H) and diffusion time (T_D) of samples

Chitin (wt. %)	PLA-shrimp chitin			PLA-crab chitin		
	$T_H \times 10^6$ (s)	T_D (s)	$D \times 10^{-6}$ (m^2/s)	$T_H \times 10^6$ (s)	T_D (s)	$D \times 10^{-6}$ (m^2/s)
0	21.35	45.6	2.48	21.35	45.6	2.48
10	18.14	31.00	3.47	16.13	33.67	2.84
20	12.5	25.6	4.77	13.96	31.00	3.06
30	10.08	15.00	6.37	11.89	21.68	5.92

Gradual increase in *D* values of PLA-chitin composite is attributed to the inclusion of more hydrophilic filler, which enhances the mobility and fast access of PBS molecules into the polymer matrix. For each sample, diffusion of fluid is faster than the polymer bond degradation, while T_D and T_H reduce with chitin increment. During degradation, pH of PBS lies between 7.4 and 7.37 at 37 ^{0}C (Table 6) with the import that the degradation product of PLA and its composites will have no toxic effect on living cells and tissues during implantation. Hence, the physiological activities in human body may be unaltered during period of implantation.

Table 6: pH values of PLA and PLA-chitin composites in PBS during degradation

	Degradation time (weeks)								
	wt%/ pH	1	2	3	4	5	6	7	8
Shrimp chitin	0	7.40	7.40	7.38	7.39	7.40	7.38	7.39	7.40
	10	7.40	7.40	7.39	7.40	7.40	7.37	7.40	7.38
	20	7.40	7.40	7.37	7.38	7.40	7.40	7.40	7.38
	30	7.40	7.40	7.39	7.38	7.37	7.39	7.38	7.40
Crab chitin	10	7.40	7.37	7.39	7.38	7.37	7.37	7.40	7.37
	20	7.40	7.39	7.40	7.38	7.40	7.38	7.40	7.40
	30	7.40	7.40	7.39	7.37	7.40	7.40	7.38	7.38

CHAPTER FIVE

5.0 SUMMARY OF FINDINGS AND CONCLUSION

5.1. Summary of Findings

S/N	Objective	Finding
`1	To extract α-chitin from crab and shrimp exoskeletons and evaluate the influence of acid and alkali concentrations on its acetylation degree (DA)	The chemical treatment employed in this study is found to effectively extract α-chitin from the two exoskeletons tested. This is confirmed by the presence of amide I bands at 1662 and 1628 cm^{-1} in treated crab shell and in shrimp shell at 1661 and 1626 cm^{-1} in the FTIR spectrum. DA decreases with increase in HCl and NaOH concentrations. Low concentrations of acid and alkali (0.4M HCl with 0.4M NaOH) produces α -chitin with 98.9 and 99.4 % DA from crab and shrimp shells respectively, while 63.7 and 65.6 % (lowest DA) are observed when 1.2M HCl and 1.2M NaOH are used.

2	To study the crystal structure, thermal stability and hydrogen bond energy of extracted α - chitin	Gradual increase in HCl and NaOH concentrations (between 0.4 -1.2M) yield reduction in Crl, which is an indication of increase hydrophylicity of chitin. Crab chitin with the lowest DA possesses 65.5 % Crl when virgin shell is treated with 1.2M HCl and 1.2M NaOH; while for shrimp chitin, 79.4 % Crl is observed with the same concentration. At different concentrations of HCl and NaOH, shrimp chitin Crl ranges from 87.4 -79%, while crab chitin Crl lies between 71- 65.5 %. Thermal stability of chitin gradually reduces as T_{onset} decreases with increasing concentrations of HCl and NaOH. Temperature at which decomposition of shrimp chitin commences ranges between 364.12 - 326.97 ^{0}C, while T_{onse} for crab chitin is between 351.19 and 341.06 ^{0}C as concentrations of HCl and NaOH range between 0.4 – 1.2 M.. In addition, there is reduction in E_a from 139.63 - 106.88 kJ/mol for α- shrimp chitin at increasing concentrations of reagents, while E_a reduces from 132.54 - 100.12 kJ/mol for α-crab chitin.

		E_H for shrimp and crab chitin lies within 5.25 - 4.62 kCal and 4.71 - 4.52 kCal respectively. These values decrease as concentrations of HCl and NaOH increase.
3	To investigate the effect of chitin addition on the stiffness of PLA	Elastic modulus (E) of PLA increased on addition of 10, 20 and 30 wt. % chitin from 3.64 to 10.1, 25.2 and 33 GPa for shrimp-chitin and 10.9, 22 and 32.8 GPa for crab chitin. These are higher than E of PLA composites obtained in literature (1.17 – 9.2 GPa) with 72 – 88% improvement.
4	To study the biodegradation of PLA-chitin composites and their suitability as temporary supporting devices in orthopaedics	PLA-chitin composites degrade via bulk hydrolysis as $T_H >> T_{D.}$ Degradation (weight loss) of PLA rises from 14.06-43.09 % at 37 ^{0}C and pH7.4. Reinforcement with 10-30 wt. % chitins for both sources further elevates its weight loss from 16.22-66.02% under human physiological conditions (pH 7.4 and 37 ^{0}C). pH of fluid is maintained between 7.4 and 7.37.

		This implies that the degradation products are non-toxic and will not trigger inflammatory issues. Thus, PLA-chitin composites can serve as a potential substitute for metallic and fossil based polymers femoral scaffolds in orthopaedics.

5.2 Conclusion

In this work, α-chitin with varying proportions of amino groups from 0.5 - 36.3% have been produced via chemical extraction treatment using varying concentrations of HCl and NaOH. Observations from FTIR, XRD and TGA reveal that α-chitin content present in shrimp shell is higher than that in crab shell and this is the reason for the use of lower number of acid baths during demineralization, with resultant high CrI, E_a and E_H. For both chitin sources, the OH (6)…OC intra and CO…HN intermolecular hydrogen bonds are most dominant in the hydrogen bonds. Gradual reduction of *N*-acetyl proportions reduces the high occupancy of hydrogen bonds and creates a biopolymer with good mechanical properties and bioactivity. The extensive hydrogen bonding of α-chitin with 34.4 and 36.3% deacetylation has improved the elastic modulus of PLA (3.64GPa) such that PLA-chitin composites' modulus ranges between 10-33 GPa. This makes them a potential material that can be used as temporary supporting device for the human bone whose elastic modulus is between 10-

30GPa. On the 8th week of healing, results have shown that PLA-chitin implant would gradually loose its stiffness to a level where the fractured bone would be able to withstand loads. The pH of PBS fluctuates between 7.4 and 7.37 at 37 ^{0}C throughout the immersion period. This implies that degradation products of PLA-chitin composites are non-toxic and, hence, there will be no noticed tissue inflammation during the implantation period.

5.3 Contributions to Knowledge

1. This study has shown that 1.2M HCl and 1.2M NaOH are suitable combination of process parameters for the extraction of α- chitin with improved hydrophylicity without compromising crystallinity and thermal stability.

2. This research has developed α- chitin reinforced PLA with stiffness comparable to the human bone.

3. The In-vitro investigation revealed that α- chitin increases the degradation rate of PLA to allow for steady healing of the rehabilitee bone and also enhances hydrophylicity with non-toxic degradation products.

5.4 Recommendation

An In-vivo study on the efficacy of PLA-chitin composite as femoral scaffold should be carried out to authenticate the efficacy of the In-vitro results obtained in this study.

REFERENCES

Abdel Hai, F., Abdel Wahab, H., and Ibrahim, A. (2014). Synthesis, characterization and thermal properties of thiazole containing polymers. *Malaysian Polymer Journal*, ***9*** **(1)**, 1-9.

Abdou, E.S., Nagy, K.S.A., and Elsabee, M.Z. (2008). Extraction and characterization of chitin and chitosan from local sources. *Bioresource Technology*, **99**, 1359–1367.

Abdulkarim, A., Isa, M.T., Abdulsalam, S.A., Muhammad, A.T., and Ameh, A.O. (2013). Extraction and characterisation of chitin and chitosan from mussel shell. *Civil and Environmental Research*, ***l3*****(2)**, 108-114.

Abdul Razak, S.I., Sharif, N.F.A. and Abdul Rahman, W.A., (2012). Biodegradable polymers and their bone applications: A review. *International Journal of Basic and Applied Sciences, **12*** **(1),** 31-49.

Adeosun, S.O., Akpan, E.I., Gbenebor,, O.P., Peter, A.A., and Olaleye, S.A. (2016). Mechanical behavior of electrospun palmfruit bunch reinforced polylactide composite fibe. *The Journal of The Minerals, Metals & Materials Society*, ***68*** **(1)**, 265-270.

Ali, N.A., and Noori, F.T. (2014). Crystallinity, mechanical, and antimicrobial properties of polylactic acid / microcrystalline cellulose /silver nanocomposites. *International Journal of Application or Innovation in Engineering & Management*, ***3*****(1)**, 77 – 81.

Al Sagheer, F.A., Al-Sughayer, M.A., Muslim, S., and Elsabee, M.Z. (2009). Extraction and characterization of chitin and chitosan from marine sources in Arabian Gulf. *Carbohydrate Polymers*, ***77***, 410–419.

Alsaheb, R.A., Aladdin1, A., Othman1, N.Z., Malek1, B.A., Leng, O.M., Aziz1, R., and El Enshasy, H.A. (2015). Recent applications of polylactic acid in pharmaceutical and medical industries. *Journal of Chemical and Pharmaceutical Research*, ***7*** **(12)**, 51-63.

Alvarez, F.J., (2014).The effect of chitin size, shape, source and purification method on Immune recognition. *Molecules*,19, 4433-1451.

Ambati, R.R., Phang, S.M., Ravi, S., and Aswathanarayana, R.G. (2014). Astaxanthin: sources, extraction, stability, biological activities and its commercial applications—A review. *Marine Drugs*, ***12***, 128-152.

Ameh A. O., Isa M. T., Adeleye T. J. and Adama K. K., (2013). Kinetics of demineralization of shrimp exoskeleton in chitin and chitosan synthesis. *Journal of Chemical Engineering and Materials Science*, ***4*****(3)**, 32 -37.

Andrade, S.M.B., Ladchumananandasivam, B., Rocha, B.G., Belarmino, D.D., and Galvão, A.O. (2012). The use of exoskeletons of shrimp (Litopenaeus vanammei) and crab (Ucides cordatus) for the extraction of chitosan and production of nanomembrane. *Materials Sciences and Applications*, ***3***, 495-508.

Anith, A. and Rabeeth, M. (2010). Degradation of fungal cell walls of phytopathogenic fungi by lytic enzyme of streptomyces griseus. *African Journal of Plant Science*, ***4*** **(3)**, 61-66.

Arakane, Y.,Specht, C.A., Kramer, K.J., Muthukrishnan, S., and Beeman, R.W. (2008). Chitin synthases are required for survival, fecundity and egg hatch in the red flour beetle, Tribolium castaneum. *Insect Biochemistry and Molecular Biology*, ***38***, 959–962.

Aranaz I, Mengíbar M, Harris R, Paños I, Miralles B, Acosta N, Galed G. and Heras Á. (2009). Functional characterization of chitin and chitosan. *Current Chemical Biology*, ***3***, 203–230.

Arbia, W.., Arbia, L., Adour, L., and Amrane, A. (2013). Chitin extraction from crustacean shells using biological methods-A review. *Food Technology and Biotechnology*, ***51***, 12–25.

Azuma, K. Izumi, R., Osak, T., Ifuku, S., Morimoto, M., Saimoto, H., Minami, S., and Okamoto, Y. (2015). Chitin, chitosan, and its derivatives for wound healing: old and new materials. *Journal of Functional Materials*, ***6***, 104-142.

Barauna, G., Huberb, D.C.C. and Dueka, E.A.R. (2013). In vitro degradation of poly-L-co-D, L-lactic acid membranes. *Materials Research*, ***16***, 221-226.

Barriere, F., Mahmood, T., Degroot, K., and Vanblitterswijk, C., (2008). Advanced biomaterials for skeletal tissue regeneration: instructive and smart functions. *Materials Science and Engineering Reports*, ***59*****(1–6)**, 38–71.

Bhargava, R., Wang, S. and Koening, J. L.(2003). FTIR microspectroscopy of polymeric systems. *Advances in Polymer Science*, ***163***, 137-191.

Bijarimi, M., Ahmad, S., and Rasid, R. (2012). Mechanical, thermal and morphological properties of poly(lactic acid)/epoxidized natural rubber blends. *Journal of Elastomers and Plastics*, ***46*** **(4)**, 338-354.

Biskup, R.C., Jarosińska, D., Rokita, B., Ulański, P., Rosiak, J.M. (2012). Determination of degree of deacetylation of chitosan - comparision of methods. *Progress on Chemistry and Application of Chitin and Its Derivatives*, ***17***, 5-20.

Boßelmann, F., Romano, P., Fabritius, H., Raabe, D., and Epple, M. (2007). The composition of the exoskeleton of two crustacea: The American lobster Homarus americanus and the edible crab Cancer pagurus. *Thermochimica Acta*, ***463***, 65–68.

Broido, A. (1969). Simple, sensitive graphical method of treating thermogravimetric analysis data. *Journal of Polymer Science Part A: Polymer Physics*, ***27***, 1761– 1774.

Bropp, R.C. (2012). Natureworks ingeo polylactide: past, present and future. Biopolymers and *Biocomposites workshop,IOWA State University*, 1-24.

Brugnerotto, J. Lizardi, J., Goyoolea, F.M., Argülles-Monal, W., Desbrières, J. and Rinaudo, M. (2001). An infrared investigation in relation with chitin and chitosan characterization. *Polymer*, ***42,*** 3569–3580.

Brunner, E., Ehrlich. H., Schupp, P., Hedrich, R., Hunoldt, S., Kammer, M., Machill, S., Paasch, S., Bazhenov, V., Kurek, D., Arnold, T., Brockmann, S., Ruhnow, M. and Born, R. (2009). Chitin-based scaffolds are an integral part of the skeleton of the marine demosponge Ianthella basta. *Journal of Structural Biology*, ***168*** **(3)**, 539–547.

Burkersrod, F.V., Schedl, L., and Gopferich, A., (2002). Why degradable polymers undergo surface erosion or bulk erosion. Biomaterials, ***23***, 4221–4231.

Bose, S., Roy, M., and Bandyopadhyay, A., (2012). Recent advances in bone tissue engineering scaffolds. *Trends in Biotechnology*, ***30*****10)**, 546–554.

Cárdenas, G., Cabrera, G., Taboada, E. and Miranda, S.P. (2004). Chitin characterization by SEM, FTIR, XRD, and 13C cross polarization/mass angle spinning NMR. *Journal of Applied Polymer Science, **93*(4)**, 1876–1885.

Casiday, A., R., and Fray, R. (2012). Blood, sweat and buffers: pH regulation during exercise acid base equilibra during experiment. *Department of Chemistry, Washington University*, 1-22.

Chen, X., Chew, S.L., Kerton, F.M. and Yan, N. (2014). Direct conversion of chitin into a N-containing furan derivative. *Green Chemistry, **16***, 2204–2212.

Ciambelli, G.S., Perez, M.O., Siqueira, G.V., Candellaa, M.A., Mottaa, A.C., Duartea, M.A.T., Rincon, M.C.A. and Duekb, E.A.R. (2013). Characterization of poly (L-co-D,L lactic acid) and a study of polymer-tissue interaction in subcutaneous implants in wistar rats. *Materials Research*, **16**, 28-37.

Ciolacu, D., Kovac, J., and Kokol, V. (2010). The effect of the cellulose-binding domain from clostridium cellulovorans on the supramolecular structure of cellulose fibres. *Carbohydrate Research, **345***, 621-630.

Correia, L.M., Saboya, R.M.A., Campelo, N.S., Cecilia, J.A., Castellón, E.R., Cavalcante, C.L. and Vieira, R.S. (2014). Characterization of calcium oxide catalysts from natural sources and their application in the transesterification of sunflower oil. *Bioresource Technology*, ***151***, 207–213

Cui, J., Yu, Z., and Lau, D. (2016). Effect of acetyl group on mechanical properties of chitin/chitosan nanocrystal: A molecular dynamics Study. International Journal of *Molecular Sciences, **7*** **(61)**, 1-13.

Daraghmeh, N.H., Chowdhry, B.Z., Leharne, S.A., Al Omari, M.M. and Badwan, A.A.(2011). Chitin. *Profiles of Drug Substances, Excipients and Related Methodology, **36***, 35-102.

Drumright, R.E., Gruber, P.R., and Henton, D.E., (2000). Polylactic acid technology. *Advanced Materials, **12*** **(23)**, 1841 - 1847.

Duarte, M. L., Ferreira, M. C., Marvão, M.R. and Rocha, J. (2002). An optimized method to determine the degree of acetylation of chitin and chitosan by FTIR spectroscopy. *International Journal of Biological Macromolecules, **31***, 1–8.

Ehrlich H. (2010). Chitin and collagen as universal and alternative templates in biomineralization. *International Geology Review, **52***, 661-699.

Einbu, A. (2007). Characterisation of chitin and a study of its acid-catalysed hydrolysis. *Ph.D thesis, Department of Biotechnology, Norwegian University of Science and Technology, Trondheim*, 1-75.

Elias, C.N., Lima, J.H.C., Valiev, R., and Meyers, M.A. (2008). Biomedical applications of mtitanium and its alloys. *Biological Materials Science*, 46-48.

Engineer, C., Parikh, J., and Raval, A., (2010). Hydrolytic degradation behavior of 50/50 poly lactide-co-glycolide from drug eluting stents. *Trends Biomaterials and Artificial Organs, **24*(3)**, 131- 138.

Farrar, D. (2005). Bioresorbable polymers in orthopaedics. Medical Device *Manufacturing and Technology*, 1 – 4.

Felsen, J., Žalga, A., and Kareiva, A. (2012). Characterization of naturally derived calcium compounds used in food industry. *CHEMIJA*, ***23(*2)**, 76–85.

Fricke, O., Sumnik, Z., Tutlewski, B., Stabrey, A., Remer, T., and Schoenau, E., (2008). Local body composition is associated with gender differences of bone development at the forearm in puberty. *Hormone Research*, ***70*(2)**, 105–111.

Firoozian P., Hazizan M.A,. and Khalil, H.P.S.A. (2010). Prediction of Mechanical Properties of Mica-filled Epoxy cCmposite using various Mechanical Models. *Journal of Reinforced Plastics and Composites*, **29**, 2368-7268.

Fuchs, M., Vosshenrich, R., Dumont, C., and Sturmer, K.M. (2003). Refixation of osteochondral fragments using absorbable implants. *First results of a retrospective study. Chirurg* ***74****(6),* 554-561.

Gallego, R., Arteaga, J.F., Valencia, V.C., and Franco, J.M., (2013). Isocyanate-functionalized chitin and chitosan as gelling agents of castor oil. *Molecules*, ***18***, 6532-6549.

Gao, Q. W., Lan, P., Shaou, H., and Hu, X., (2002). Direct synthesis with melt polycondensation and microstructure analysis of poly(L-lactic acid-co-glycolic acid). *Polymer Journal*, ***34*(11)**, 786-793.

Garlotta, D.A., (2001). literature review of poly(lactic acid). *Journal of Polymers and the Environment*, ***9***, 63 – 64.

Ge, Z., Tian, X., Heng, B.C., Fan, V., Yeo, J.F. and Cao,T. (2009). Histological evaluation of osteogenesis of 3D-printed poly-lactic-coglycolic acid (PLGA) scaffolds in a rabbit model. *Biomedical Materials*, ***4*** **(2**), 1748-6041.

Gerstenfeld, L.C.., Alkhiary, Y.M., Krall, E.A., Nicholls, F.H., Stapleton, S..N., Fitch, J.L., Bauer, M., Kayal, R., Graves, D.T., Jepsen, K.J., and Einhorn, T.A., (2006). Three-dimensional reconstruction of fracture callus morphogenesis. *Journal of Histochemistry & Cytochemistry*, ***54*(11**),1215–1243.

Glarner, M. and Gogolewski, S. (2004). Degradation in vitro of new bioresorbable terpolymers of lactides. European Cells and Materials, ***7*** **(2)**, 36.

Gunatillake, P.A., and Adhikari, R. (2003). Biodegradable synthetic polymers for tissue engineering. *European Cells and Materials*, ***5***, 1-16.

Gortari, M.C. and Hours, R.A. (2013). Biotechnological processes for chitin recovery out of crustacean waste. *A mini-review. Electronic Journal of Biotechnology*, ***16***, 1–14.

Guo, F., Kikuchi, K., Matahira, Y., Sakai, K., and Ogawa, K. (2002). Water-soluble chitin of low degree of deacetylation. . *Journal of Carbohydrate Chemistry*, ***21***, 149-161.

Gupta. B., Revagade, N., and Hilborn, J., (2007). Poly(lactic acid) fiber: an overview. *Progress in Polymer Science*, ***34***,455–482.

Gopferich, A., and Tessmar, J., (2002). P olyanhydride degradation and erosion. *Advanced Drug Delivery Reviews*, ***54***, 911–931.

Hajji, S., Younes, I., Bellaaj, O., Hajji, R., Rinaudo, M.,cNasri, M. and Jellouli, K. (2014). Structural differences between chitin and chitosan extracted from three different marine sources. *International Journal of Biological Macromolecules*, ***65***, 298– 306.

Huang, L., Juszkiewicz, M., Jeu, W.H., Cerda, E., Emrick, E., Menon, N. and Russell, P.T. (2007). Synthesis and characterization of electroactive and biodegradable ABA block copolymer of polylactide and aniline pentamer. *Biomaterials*, ***28*** **(10)**, 1741-1751.

Hansen, D.C., (2008). Metal corrosion in the human body: the ultimate bio-corrosion scenario. *The Electrochemical Society Interface*, 31-34.

Haris, A.M., and Lee, E.C.(2006). Injection molded polylactide (PLA) composites for automotive applications. *Materials Research and Advanced Engineering, Food Motor Company*, 1-9.

Hoffler, C.E., Moore, K.E., Kozloff, K., Zysset, P.K., and Goldstein, S.A. (2000). Age, gender and bone lamellae elastic moduli. *Journal of Orrhopuedic Rmearch*, ***18***, 132-437.

Huertas, C.E., Fessi, H. and Elaissari, A. (2010). Polymer-based nanocapsules for drug delivery. *International Journal of Pharmaceutics*, **385**, 113–142.

Ifuku, S.,Shervani, Z. and Saimoto, H., (2013). Chitin nanofibers, preparations and applications. *INTECH*, 85-101.

Isa, M.A., Ameh, A.O., Gabriel, J.O. and Adama, K.K. (2012). Extraction and characterization of chitin from Nigerian Sources. *Leonardo Electronic Journal of Practices and Technologies*, ***21***, 75 -81.

Islam, K.N., Abu Bakar, M.Z., Noordin, M.M., Hussein, M.Z., Abd Rahman, N.S. and Ali, M.E. (2011). Characterisation of calcium carbonate and its polymorphs from cockle shells (Anadara granosa). *Powder Technology*, ***213***, 188–191.

Jaafarzadeh, N., Mengelizadeh, N., Takdastan, A., Farsani, M.H., Niknam, N., Aalipour, M., Hadei, M. and Bahrami, P. (2015). Biosorption of heavy metals from aqueous solutions onto chitin. *International Journal of Environmental Health Engineering*, ***4*****(1)**, 1-7.

Jiang, T., Khan, Y. and Nair, S.L, (2010). Chitosan-poly(lactide-co-glycolide) microsphere-based scaffolds for bone tissue engineering: In vitro degradation and In vivo bone regeneration studies. *Acta Biomaterialia, **6*** **(9)**, 3457-3470.

Jiang, T., Kim, B.S., Kang, S.W., Kwon, J.H., Leea, Y.M., Kim, S.H. and Kim, Y.H. (2006). In vitro evaluation of chitosan/poly(lactic acid-glycolic acid) sintered microsphere scaffolds for bone tissue engineering. *Biomaterials*, ***27*** **(28)**, 4894-4903.

Jang, M.K., Byeong-Gi, K., Young-Il, J., Chang, HL. and Woon, N. (2004). Physicochemical characterization of α-chitin, β-chitin, and γ-chitin separated from natural resources. *Journal of Polymer Science A1*, ***42***, 3423–3432.

Jeong, S.I., Kim, B.S., Lee, Y.M., Ihn, K.J., Kim, S.H., and Kim, Y.H., (2004). Morphology of elastic poly(l-lactide-co-ε- caprolactone) copolymers and in vitro and in vivo degradation behavior of their scaffolds. *Biomacromolecules* ***5***,1303-1309.

Juarez-de la Rosa, B.A., Crespo, J.M., Owen, Q., Gónzalez-Gómez, W.S.,Yañez-Limón, J.M. and Alvarado-Gil, J.J. (2015). Thermal analysis and structural characterization of chitinous exoskeleton from two marine invertebrates. *Thermochimica Acta*, ***610***, 16–22.

Juarez-de la Rosa, B.A., Quintana, P., Ardisson, P.L., Ya´nez-Limon, J.M. and Alvarado-Gil, JJ. (2012). Effects of thermal treatments on the structure of two black coral species chitinous exoskeleton. *Journal of Materials Science*, ***47***, 990–998.

Kaleas, I.S. and FACS, M.D., (2001). Principles of bone healing. *Neurosurg Focus*, ***1***, 1-4.

Kasaai, M.R. (2010). Determination of the degree of N-acetylation for chitin and chitosan by various NMR spectroscopy techniques: A review. *Carbohydrate Polymers*, 79, 801–810.

Kaya, M.,Lelešius, E., Nagrockait, R., Sargin, I., Arslan, G., Mol, A., Baran, T., Can, E. and Bitim, B.(2015). Differentiations of chitin content and surface morphologies of chitins extracted from male and female grasshopper species. *PLOS ONE*, 1-14.

Kaya, M., Baran, T., Mentes, A., Asaroglu, M., Sezen, C. and Tozak, K.O. (2014). Extraction and characterization of α-chitin and chitosan from six different aquatic invertebrates. *Food Biophysics*, ***9***, 145–157.

Khong, T.T. (2013). Vietnamese chitin raw material, the chitin de-N-acetylation reaction, and a new chitosan alginate gelling concept. *Thesis for the degree of Philosophiae Doctor, Norwegian University of Science and Technology*, 1 -1 19.

Kim, S.(2011). Chitin, chitosan, oligosaccharides and their derivatives; biological and their applications. *CRC Press, Taylor & Francis Group*, 3-633.

Kittle, J.D. (2012). Characterization of cellulose and chitin thin films and their interactions with bio-based polymers. *Dissertation submitted to Virginia Polytechnic Institute and State University*, 1 186.

Kumirska, J., Weinhold, M.X., Czerwicka, M.C., Kaczyński, Z., Bychowska, A., Brzozowski, K.,Thöming, J. and Stepnows, P. (2011). Influence of the chemical structure and physicochemical properties of chitin- and chitosan-based materials on their biomedical activity. *Biomedical Engineering, Trends in Materials Science*, 25-64.

Kumirska, J., Czerwicka, M., Kaczyński, Z., Bychowska, A., Brzozowski, K., Thöming, J. and Stepnowski, P.(2010). Application of spectroscopic methods for structural analysis of chitin and chitosan. *Marine Drugs*, ***8***, 1567-1636.

Kurita, K. (2001). Controlled functionalization of the polysaccharide chitin. *Progress in Polymer Science*, ***26***, 1921-1971.

Lee, M.Y., Hong, K.J., Kajiuchi, T., and Yang, J.W., (2004)., Determination of the efficiency and removal mechanism of cobalt by crab shell particles. ***J****ournal of Chemical Technology & Biotechnology, **79*****(12)***, 1388 – 1394.

Lima, C.A., Goulart, V.P., Côrrea, L., Pereira, T.M., and Zezell, D.M., (2015). ATR-FTIR spectroscopy for the assessment of biochemical changes in skin due to cutaneous squamous cell carcinoma. International Journal of Molecular Sciences, 16, 6621-6630.

Liman, Z., Selmi, S., Sadok, S. and El Abed, A. (2010). Extraction and characterization of chitin and chitosan from crustacean by-products: Biological and physicochemical properties. *African Journal of Biotechnology*, ***10*** **(4)**, 640-647.

Li, M., Shi, X., Guo, C. and Lin1, S. (2016). Phosphorus deficiency inhibits cell division but not growth in the dinoflagellate amphidinium carterae. *Frontiers in Microbiology*, ***7*(826)**, 1-11.

Li, H., Chang, J., Qin, Y., Wu, Y., Yuan, M. and Zhang, Y. (2014). Poly(lactide-co-trimethylene carbonate) and polylactide/polytrimethylene carbonate blown films. *International Journal of Molecular Sciences*, ***15***, 2608-2621.

Liu, N., Liu, B., Yao, C., and Cui, D., (2016). Immortal ring-opening polymerization of rac-lactide using polymeric alcohol as Initiator to prepare graft copolymer. *Polymers*, ***8*(17)**, 2-9.

Liu, S., Yu, J., Bi, C., Zhu, F., Qu, M., Jiang, C. and Yang, Q. (2012). Extraction and Characterization of chitin from the beetle holotrichia parallela motschulsky. *Molecules*, ***17***, 4604-4611.

Liu, Y., Liu, Z., Pan, W. and Wu, Q. (2008). Absorption behaviors and structure changes of chitin in alkali solution. *Carbohydrate Polymers*, ***72***, 235-239.

Lopes, S.M., Jardini, A.L., and Filho, R.M., (2014). Synthesis and characterizations of poly (lactic acid) by ring-opening polymerization for biomedical applications. *Chemical Engineering Transactions*, ***38***, 331 – 336.

Liu, X., and Ma, P. X.,(2004). Polymeric scaffolds for bone tissue engineering. *Annals of Biomedical Engineering*, 32(3), 477-486.

Lopes, S.M., Jardini, A.L., and Filho, R.M., (2012). Poly (lactic acid) production for tissue engineering applications. *Procedia Engineering*, ***42***, 1402 – 1413.

Luquet, G., Fernández, M.S., Badou, A., Guichard, N., 1Le Roy, N., Corneillat, M., 4, Alcaraz, G. and Arias, J.L. (2013). Comparative ultrastructure and carbohydrate composition of gastroliths from astacidae, cambaridae and parastacidae freshwater crayfish (grustacea, decapoda). *Biomolecules*, ***3***, 18-38.

Maharana, T., Mohanty, B., and Negi, Y.S., (2009). Melt-solid polycondensation of lactic acid and its biodegradability. *Progress in Polymer Science*, ***34*(1)**, 99-124.

Mahmoud, N.S., Ghaly, A.E. and Arab, F.(2007). Unconventional approach for demineralization of deproteinized crustacean shells for chitin Production. *American Journal of Biochemistry and Biotechnology*, ***3* (1)**, 1-9, 2007.

Malinovsky F.G., Fange. J.U. and Willats, W.T.G. (2014).The role of the cell wall in plant immunity. *Frontiers in Plant Science*, ***5*(178)**, 1-12.

Marsell, R., and Einhorn, T.A., (2011). The Biology off fracture healing. National Institute of Health Public Access, ***42*(6)**, 551–555.

MAST Biosurgery Inc. (2006). MAST Biosurgery resorbable technology: An overview. www.mastbio.com, 1-6.

Mi, F.L., Lin, Y.M., Wu, Y.B., Shyu, S.S. and Tsai, Y.H. (2002). Chitin/PLGA blend microspheres as a biodegradable drug-delivery system: phase-separation, degradation and release behavior. *Biomaterials*, ***23***, 3257–3267.

Mitchell, A. and Shrotriya, P., (2007). Onset of nanoscale wear of metallic implant materials: Influence of surface residual stresses and contact loads. *Wear*, ***263***, 1117-1123.

Mobedi, H., Nekoomanesh, M., Orafaei, H., and Mivehchi, H., (2006). Studying the degradation of poly(*L*lactide) in presence of magnesium hydroxide. *Iranian Polymer Journal*, ***15***,31-39.

Mobedi, H., Mashak, A., Nekoomanesh, M. and Orafai, H., (2011). *l*-Lactide additive and in vitro degradation performance of poly(*l*-lactide) films. Iranian Polymer Journal, ***20*** (3), 237-245.

Moon, S. I., Taniguchi, I., Miyamoto, M., Kimura, Y., and Lee, C.W., (2001). Synthesis and properties of high-molecular-weight poly(L-lactic acid) by melt/solid polycondensation under different reaction conditions. *High Performance Polymers,* ***13*****(2),** 189-196.

Morimoto, Y.V., Kami-ike, N., Miyata, T., Kawamoto, A., Kato, T., Namba, K., and Minamino, T., (2016). High-resolution pH imaging of living bacterial cells to detect local pH differences. Jamaican Society for Microbiology, 7(6), **1-8.**

Morrison, S.J., and Scadden, D.T., (2004). The bone marrow niche for haematopoietic stem cells. *Nature*, ***505*****(7483)**, 327– 334.

Muzzarelli, C., Francescanheli, O., Tosi, G., and Muzzarelli, R.A.A.,(2004). Susceptibility of dibutyryl chitin and regenerated chitin fibres to deacylation and depolymerization by lipases. *Carbohydrate Polymers, **56***, 137–146.

Nam, Y.S., Park, W.H., Ihm, D., and Hudson, S.M., (2010). Effect of the degree of deacetylation on the thermal decomposition of chitin and chitosan nanofibers. *Carbohydrate Polymers, **80***, 291-295.

Nampoothiri, K.M., Nair, N.R., and John, R.P., (2010). An overview of the recent developments in polylactide (PLA) research. *Bioresource Technology, **101***, 8493–8501.

Nair, L.S. and Laurencin, C.T., (2007). Biodegradable polymers as biomaterials. Progress in Polymer Science, ***32,*** 762–798.

Ndazi, B.S. and Karlsson, S. (2011). Characterization of hydrolytic degradation of polylactic acid/rice hulls composites in water at different temperatures. *eXPRESS Polymer Letters*, ***5*****,(2)**, 119–131.

Negrea, P., Caunii, A., Sarac, I., and Butnariu, M. (2015). The study of infrared spectrum of chitin and chitosan extract as potential sources of biomass. *Digest Journal of Nanomaterials and Biostructures, **10*** **(4)**, 1129 – 1138.

Nemtsev, S.V., Zueva, O.Y., Khismatullin, M.R., Albulov, A.I., and Varlamov, V.P. (2004). Isolation of chitin and chitosan from honeybees. *Applied Biochemistry and Microbiology*, ***40***, 39–43.

Nesr, E.M., Raafat, A.I., Nasef, S.M., Soliman, E.A., and Hegazy, E.A., (2013) Chitin and chitosan extracted from irradiated and non-irradiated shrimp wastes (comparative analysis study). *Arabian Journal of Nuclear Sciences and Applications, **46***, 53–66.

Nikolov, S., Fabritius, H., Petrov, M., Friák, M., Lymperakis, L., Sachs, C., Raabeb, D. and Neugebauer, J. (2011). Robustness and optimal use of design principles of arthropod exoskeletons studied by ab initiobased multiscale simulations. *Journal of the Mechanical Behaviour of Biomedical Materials, **4***, 129 – 145.

Nordstrom, P., Pohjonen, T., Tormala, P. and Rokkanen, P., (2001). Shear-load carrying capacity of cancellous bone after implantation of self-reinforced polyglycolic acid and poly-L-lactic acid pins: experimental study on rats. *Biomaterials*, ***22***, 2557-2561.

Nugroho, P. and Mitomo, H., (2008). Study of Biodegradation and Improvement of Heat Stability of Poly(lactic acid) by Irradiation at High Temperature. *Malaysian Polymer Journal*, ***3*****(1)**, 27 - 37.

Ohta, M., Obuchi, S., and Yoshida, Y.,(1995). Preparation process of polyhydroxycarboxylic acid. *US Patent*, ***5***,143-144.

Paulino, A.T., Simionato, J.I., Garcia, J.C. and Nozaki, J. (2006). Characterization of chitosan and chitin produced from silkworm chrysalides. *Carbohydrate Polymers*, ***64***, 98–103.

Park, S.D., Todo, M., Arakawa, K. and Koganemaru, M., (2006). Effect of crystallinity and loading-rate on mode I fracture behavior of poly(lactic acid). *Polymer*, ***47***, 1357–1363.

Pawlikowski, M., Klasztorny, M., and Skalski, K., (2008). Studies on constitutive equation that models bone tissue. *Acta of Bioengineering and Biomechanics/Wrocław University of Technology*, ***10*****(4)**, 39–47.

Penczek, S., Duda, A., ,Szymanski, R., and Biela, T., (2000). What we have learned in general from cyclic esters polymerization.*Macromolecular Symposia*, ***153*****(1)**, 1-15.

Pina, S. and Ferreira, J.M.F., (2012). Bioresorbable plates and screws for clinical applications: A review. *Journal of Healthcare Engineering*, ***·3*** **(2),** 243–260.

Pinto, A.M., Moreira, S., Gonialvesc, I.C., Gama, F.M., Mendes, A.M. and Magalhaes, F.M. (2013). Biocompatibility of poly(lactic acid) with incorporated graphene-based materials. Colloids and Surfaces B: *Biointerfaces*, ***104***, 229– 238.

Piper, K., and Valentine, G., (2012). Bone pathology. *Methods in Molecular Biology*, ***915***, 51 88.

Pluta, M., Galeski, A., Alexandre, M., and Dubois, P., (2002). Polylactide/montmorillonite nanocomposites and microcomposites prepared by melt blending: Structure and some physical properties. *Journal of Applied Polymer Science*, ***86*****(6)**, 1497-1506.

Porpino, K.K., Barreto, M.C., Cambuim, K.B., Carvalho, J.R. and Toscano, F.A. (2011). Fe (II) adsorption on ucides cordatus crab shells. *Quim. Nova*, ***34*****(6)**, 928-932.

Prokop, A., Jubel, A., Helling, H.J., Eibach, T., Peters, C.,Baldus, S.E. and Rehm, K.E., (2004). Soft tissue reactions of different biodegradable polylactide implants. Biomaterials, 23, 259-267.

Raposo, J.F., Sobrinho, L.G., and Ferreira, H.G., (2002). A minimal mathematical model of calcium homeostasis. *Journal of Clinical Endocrinology and Metabolism*, ***87*****(9)**, 4330–4340.

Rahman, M.A. and Halfar, J. (2014). First evidence of chitin in calcified coralline algae: new insights into the calcification process of Clathromorphum compactum. *Scientific Reports*, 1-11.

Rahman, M.A., Halfar, J. and Shinjo, R., (2013). X-Ray diffraction is a promising tool to characterize coral skeletons. *Advances in Materials Physics and Chemistry*, ***3***, 120-125.

Rahn, BA., (2002). Bone healing: histologic and physiologic concepts. *Fackelman, GE., editor. Bone in clinical orthopedics*, 287-326.

Rasal, R. M., Janorkar, A. V., and Hirt, D. E., (2010). Poly(lactic acid) modifications. *Progress in Polymer Science*, ***35*****(3)**, 338-356.

Rathi, S.R., Coughlin, E.B., Hsu, S.L., Golub, C.S., Ling , G.H. and Tzivanis, M.J., (2014). Maintaining structural stability of poly(lactic acid): Effects of multifunctional epoxy based reactive oligomers. *Polymers*, ***6***, 1232-1250.

Raya, I., Mayasari, E., Yahya,, A., Syahrul, M. and Latunra, A., (2015). Shynthesis and characterizations of calcium hydroxyapatite derived from crabs shells (Portunus pelagicus) and its Potency in safeguard against to dental demineralizations. *International Journal of Biomaterials*, 1-9.

Rhim, J.W., Mohanty, A.K., Singh, S.P., and Ng, P.K.W., (2006). Effect of the processing methods on the performance of polylactide films: thermocompression versus solvent casting. *Journal of Applied Polymer Science*, ***101*****(6)**, 3736 - 3742.

Rojas, J., Hernandez, C. and Trujillo, D., (2014). Effect of the alkaline treatment conditions on the tableting performance of chitin obtained from shrimp heads. *African Journal of Pharmacy and Pharmacology*, ***8*** **(7)**, 211-219.

Sajomsang, W. and Gonil, P., (2010). Preparation and characterization of α-chitin from cicada sloughs. *Materials Science and Engineering*, C, ***30***, 357–363.

Seal, C.K, Vince, K. and. Hodgson, M.A. (2009). Biodegradable surgical implants based on magnesium alloys – A review of current research. *IOP Science*, ***4***, 1-4.

Shakoor, A., Muhammad, R., Thomas, N.L and Silberschmidt, V.V. (2013). Mechanical and thermal characterisation of poly (l-lactide) composites reinforced with hemp fibres. *Journal of Physics: Conference Series*, ***451***, 1-10.

Sharp, R.G. (2013). A Review of the Applications of chitin and Its derivatives in agriculture to modify plant-microbial interactions and improve crop yields. *Agronomy*, ***3***, 757-793.

Shervani, Z.,Taisuke, Y., Ifuku, S., Saimoto, H., and Morimoto, M., (2012). Preparation of gold nanoparticles loaded chitin nanofiber composite. *Advances in nanoparticles*, ***1*****(3)**, 71-78.

Shih, A.T., (2008). Bone healing. *American College of Food and Ankle Surgeons*, 1-2.

Sreedhar, B., Vani, C.S., Devi, D.K., 1, Rao, M.V. and Rambabu, C. (2012). Shape controlled synthesis of barium carbonate microclusters and nanocrystallites using natural polysachharide – gum acacia. *American Journal of Materials Science*, ***2*****(1)**, 5-13.

Stuart, B.,(2004).Infrared spectroscopy: fundamentals and applications. *John Wiley & Sons, Ltd, ISBNs: 0-470-85427-8*, 1-203.

Sultana, N. and Abdul Kadir, M.R., (2011). Study of in vitro degradation of biodegradable polymer based thin films and tissue engineering scaffolds. African Journal of *Biotechnology*, ***10*** **(81)**, 18709-18715.

Takayama, T., Todo, M. and Tsuj, H. (2011). Effect of annealing on the mechanical properties of PLA/PCL and PLA/PCL/LTI polymer blends. *Journal of the Mechanical behavior of biomedical materials*, ***4***, 255-260.

Todo, M., Park, S.D., Takayama, T. and Arakawa, K. (2007). Fracture micromechanisms of bioabsorbable PLLA/PCL polymer blends. *Engineering Fracture Mechanic*s, ***74***, 1872 –1883.

Tsuji, H., Eto, T. and Sakamoto, Y. (2011). Synthesis and hydrolytic degradation of substituted poly(DL-lactic acid)s. *Materials*, ***4***, 1384-1398.

Uzun, I. and Celik, O., (2005). Physicochemical characterization and the comparison of chitin and chitin modified with maleic anhydride, *Oriental Journal of Chemistry*, ***31*****(2)**, 619-627.

Veerasingam1, S., and Venkatachalapathy, R. (2014). Assessment of carbonate concentration and characterization of marine sediments by fourier transform infrared spectroscopy. *Infrared Physics and Technology*, ***66***, 136-140.

Vieira, A.C., Vieira, J.C., Guedes, R.M. and Marques, A.T. (2015). Experimental degradation characterization of PLA-PCL, PGA-PCL, PDO and PGA fibers. *Materials Science Forum*, ***636***, 825-832.

Vieira, A.C., Vieira, J.C., Ferra, J.M., Magalhães, F.D., Guedes, R.M. and Marques, A.T. (2011). Mechanical study of PLA-PCL fibers during In vitro degradation. *Journal of Mechanical Behaviour of Biomedical materials, **3*** **(4)**, 451-460.

Vink, E.T., Ra´bago, K.R., Glassner, D.A., Springs, B., Connor, R.P.O., Kolstad, J. and Gruber, P.R., (2004). The sustainability of natureworks polylactide polymers and ingeo polylactide fibers: an update of the future. *Molecular Bioscience, **4***, 551–564.

Wang, X. and Uchiyama, S.(2013). Polymers for biosensors construction. *INTECH*, 67-86.

Wang, Y., Chang, Y., Yu, L., Zhang, C., Xu, X., Xue, Y., Li, Z. and Xue, C. (2013). Crystalline structure and thermal property characterization of chitin from Antarctic krill (Euphausia superba). *Carbohydrate Polymers*, ***92***, 90– 97.

Weiner, S., and Wagner, H.D.,(1998). The material bone: structure mechanical function relations. *Annual Review of Materials Science*, 28(1), 271–298.

Weiss, I.M. and Schönitzer, V. (2006). The distribution of chitin in larval shells of the bivalve mollusk mytilus galloprovincialis. *Journal of Structural Biology, **153***, 264–277.

Witzke, D.R,, Narayan, R, and Kolstad, J.J., (1997). Reversible kinetics and thermodynamics of the homopolymerization of L-lactide with 2-ethylhexanoic acid tin (II) salt. *Macromolecules, **30***, 7075–7085.

Xiao, L., Wang, B., Yang, G. and Gauthier, M., (2012). Poly(lactic acid)-Based biomaterials: synthesis, modification and applications, *InTech*, 247-282.

Yen, M.T., Yang, J.H. and Mau, J.L. (2009). Physicochemical characterization of chitin and chitosan from crab shells. *Carbohydrate Polymers*, ***75***, 15–21.

Younes, I. and Rinaudo, M., (2015). Chitin and chitosan preparation from marine sources, structure, properties and applications. *Marine Drugs*, ***13***, 1133-1174.

Zaku, S.G., Emmanuel, S.A., Aguzue, O.C. and Thomas, S.A. (2011). Extraction and characterization of chitin; a functional biopolymer obtained from scales of common carp fish (*Cyprinus carpio* l.): A lesser known source. *African Journal of Food Science*, ***5*****(8)**, 478 – 483.

Zhang, M., Haga, A,, Sekiguchi, H., and Hirano, S., (2000). Structure of insect chitin isolated from beetle larva cuticle and silkworm (Bombyx mori) pupa exuvia.International Journal of Biological Macromolecules, ***27*****(1),** 99-105.

Zhao, Y., Ju, W.T., Jo, G.H., Jung, W.J. and Park, R.D., (2011). Perspectives of chitin deacetylase research. *Biothechnology of Polymers*, 131-144.

Zhao, Y., Park, R.D. and Muzzarelli, R.A.A. (2010). Chitin deacetylases: properties and applications. *Marine Drugs*, ***8***, 24-46.

APPENDIX

A. Thermogravimetric Results of Samples

Table A1: TGA of Virgin shrimp shell

Chitin T_{onset} (^{0}C)	$CaCO_3$ T_{onset} (^{0}C)	Chitin T_{finish} (^{0}C)	$CaCO_3$ T_{finish} (^{0}C)	Chitin T_{max} (^{0}C)	$CaCO_3$ T_{max} (^{0}C)	Chitin Mass loss (%)	$CaCO_3$ Mass loss (%)	Residue (%)
321.01	666.03	397.93	712.81	387.54	712.81	33.71	18.85	38.67

Table A2: TGA of shrimp chitin

S/N	Acid: Alkali (M)	T_{onset} (^{0}C)	T_{finish} (^{0}C)	T_{max} (^{0}C)	Mass loss (%)	Yield (%)	Residue (%)
1	0.4:0.4	364.12	418.29	400.28	83.28	49.57	9.69
2	0.4:0.8	359.24	421.18	405.12	83.12	49.41	10.02
3	0.4:1.2	357.1	419.15	401.11	83.43	49.72	7.562
4	0.8:0.4	356.6	419.46	403.59	80.77	47.06	11.82
5	0.8:0.8	356.56	419.21	413.57	84.03	50.32	9.157
6	0.8:1.2	855.48	419.37	403.55	81.77	48.06	11.35
7	1.2:0.4	354.22	418.38	402.13	81.89	48.18	10.87
8	1.2:0.8	351.8	417.29	401.06	82.77	49.06	10.27
9	1.2:1.2	326.97	416.6	413.03	79.8	46.09	9.706

Table A3: TGA of virgin crab shell

Chitin T_{onset} (^{0}C)	$CaCO_3$ T_{onset} (^{0}C)	Chitin T_{finish} (^{0}C)	$CaCO_3$ T_{finish} (^{0}C)	Chitin T_{max} (^{0}C)	$CaCO_3$ T_{max} (^{0}C)	Chitin Mass loss (%)	$CaCO_3$ Mass loss (%)	Residue (%)
316.03	682	397.33	729	356.8	717.07	10.38	30.93	54.89

Table A4: TGA of crab Chitin

S/N	Acid: Alkali (M)	T_{onset} (^{0}C)	T_{finish} (^{0}C)	T_{max} (^{0}C)	Mass loss (%)	Yield (%)	Residue (%)
1	0.4:0.4	351.19	416.65	398.42	62.3	51.92	30.819
2	0.4:0.8	350.12	415.08	397.58	67.74	57.36	23.97
3	0.4:1.2	348.34	413.62	395.29	67.5	57.12	25.011
4	0.8:0.4	346.6	412.81	395.33	61.65	51.27	28.24
5	0.8:0.8	346.1	416.19	398.23	64.48	54.1	25.92
6	0.8:1.2	345.36	413.69	394.52	64.12	53.74	26.71
7	1.2:0.4	343.7	415.66	393.16	61.47	51.09	31.55
8	1.2:0.8	342.16	413.61	394.56	65.19	54.81	22.56
9	1.2:1.2	341.06	409.91	367.74	65.22	54.84	22.29

B. Crystalline Properties of Samples

Table B1: Crystalline properties of shrimp chitin

S/N	Acid: Alkali (M)	D_{110} (Å)	D_{130} (Å)	D_{013} (Å)	CrI (%)
1	0.4:0.4	0.0544	0.0757	0.124	87.4
2	0.4:0.8	0.0548	0.076	0.126	87
3	0.4:1.2	0.0552	0.0762	0.128	86.3
4	0.8:0.4	0.0568	0.0805	0.141	86.2
5	0.8:0.8	0.0602	0.0883	0.176	85.4
6	0.8:1.2	0.0747	0.128	1	85.2
7	1.2:0.4	0.0766	0.134	1.22	83.3
8	1.2:0.8	0.0768	0.135	1.34	82
9	1.2:1.2	0.0798	0.142	3.64	79.4

Table B2: Crystalline properties of crab chitin

S/N	Acid: Alkali (M)	D_{110} (Å)	D_{120} (Å)	D_{013} (Å)	CrI (%)
1	0.4:0.4	0.0273	0.0759	0.0296	71
2	0.4:0.8	0.02745	0.077	0.0298	69.8
3	0.4:1.2	0.02828	0.0847	0.0312	68.9
4	0.8:0.4	0.0286	0.0878	0.0316	68.8
5	0.8:0.8	0.0287	0.0887	0.0318	68
6	0.8:1.2	0.0293	0.0961	0.033	67.9
7	1.2:0.4	0.02957	0.0989	0.0334	67.56
8	1.2:0.8	0.02964	0.0997	0.0335	66.6
9	1.2:1.2	0.0311	0.1216	0.03626	65.5

C. Acetylation Degree (DA) of Samples

Table C1: Shrimp chitin DA

S/N	Acid: Alkali (M)	DA (%)
1	0.4:0.4	99.4
2	0.4:0.8	79.5
3	0.4:1.2	74.3
4	0.8:0.4	84.7
5	0.8:0.8	79.1
6	0.8:1.2	73.8
7	1.2:0.4	81.1
8	1.2:0.8	77.4
9	1.2:1.2	65.6

Table C2: Crab chitin DA

S/N	Acid: Alkali (M)	DA (%)
1	0.4:0.4	98.9
2	0.4:0.8	88.6
3	0.4:1.2	78.4
4	0.8:0.4	89.4
5	0.8:0.8	83.8
6	0.8:1.2	75.9
7	1.2:0.4	87.9
8	1.2:0.8	82.1
9	1.2:1.2	63.7

D. Elastic Modulus

Table D1: Elastic modulus of PLA and PLA-chitin composites using varying contents of shrimp chitin at different degradation time

	Elastic Modulus (GPa)			
	Shrimp chitin (wt %)			
Time (wk)	0	10	20	30
0	3.64	10	25.2	33
1	3.6	9.9	23.9	32
2	3.43	9.5	20.5	31.1
3	2.9	8.1	19.9	30.5
4	2.85	6	18.5	26.5
5	2.3	4.3	17.8	24.5
6	2.25	3.4	16.2	23
7	1.48	3.2	13.1	21
8	1.2	2.7	10.9	19

Table D2: Elastic modulus of PLA and PLA-chitin composites using varying contents of crab chitin at different degradation time

	Elastic Modulus (GPa)			
	Crab chitin (wt %)			
Time (wk)	0	10	20	30
0	3.64	10.9	22	32.8
1	3.6	10.6	21.4	31.9
2	3.43	7	18	31.5
3	2.9	6.4	17.4	30.7
4	2.85	4.5	15.5	27.3
5	2.3	3.8	14.8	24.5
6	2.25	3.1	13.7	22.2
7	1.48	2.7	10.6	19.5
8	1.2	1.9	8.6	18.3

E. Biodegradation

Table E1: Weight loss of PLA and PLA-chitin composites using varying contents of shrimp chitin at different degradation time

Weight loss (%)				
	Shrimp chitin (wt. %)			
Time (wk)	0	10	20	30
1	14.06	16.22	20.56	28.21
2	17.25	19.14	23.59	33.32
3	25.13	28.24	34.12	39.09
4	25.79	31.11	36.99	40.23
5	27.41	31.78	38.12	45.12
6	29.03	33.98	40.65	47.98
7	30.89	35.54	44.43	53.98
8	31.12	37.31	46.91	57.34
9	33.78	40.01	48.12	59.67
10	36.63	40.67	51.76	62.21
11	38.43	42.21	52.76	65.76
12	43.09	47.77	54.7	66.02

Table E2: Weight loss of PLA and PLA-chitin composites using varying contents of crab chitin at different degradation time

Weight loss (%)				
	Crab chitin (wt. %)			
Time (wk)	0	10	20	30
1	14.06	15.9	22.1	27.21
2	17.25	22	28.76	32.12
3	25.13	30.02	34.12	37.98
4	25.79	31	35.19	40.01
5	27.41	31.52	36.12	43.87
6	29.03	31.48	40.65	47.6
7	30.89	35.54	44.43	52.14
8	31.12	36.61	45.51	57.34
9	33.78	38.01	48.12	57.17
10	36.63	38.99	50.76	60
11	38.43	39.21	51.03	63.23
12	43.09	44.31	54.7	65.02

Table F: Vibration modes of samples from FTIR

Vibration modes	Wavenumber (/cm) Crab chitin	Shrimp chitin	Crab shell	Shrimp shell
OH stretching	3496,3446	3496,3445	3431	3444
NH stretching	3266	3266	3279	3390
NH stretching	3107	3107	-	3109
Symmetric Ch3 stretching and asymetric CH2 stretching	2933	2934	-	2924
CH stretching	2891	2878	2895	2852
C=O secondary amide stretch (amide I)	1662	1661	1655	1653
C=O secondary amide stretch (amide I)	1628	1626	-	-
NH bend, CN stretch (amide II)	1559	1559	-	-
CH2 bending and CH3 deformation	1417	1416	1419	1423
CH bending and Ch3 symmetric deformation	1379	1379	-	-
CH2 wagging (amide III)	1314	1312	-	1327
Asymmetric bridge oxygen stretching	1157	1157	1153	1153
Asymmetric in -phase ring stretching mode	1114	1117	-	-
C-O-C asymetric stretch in phase ring	1074	1074	1069	1072
CO stretching	1028	1028	1030	-
CH3 wagging along chain	953	953	-	953
CH stretching (saccharide rings)	893	897	-	-
NH out-plane bending	750	750	700	713
OH out-of -plane bending	694	694	38.6	-
Calcium carbonate	-	-	1794. 1473, 874	1796. 1456, 874

G. FTIR OF SAMPLES

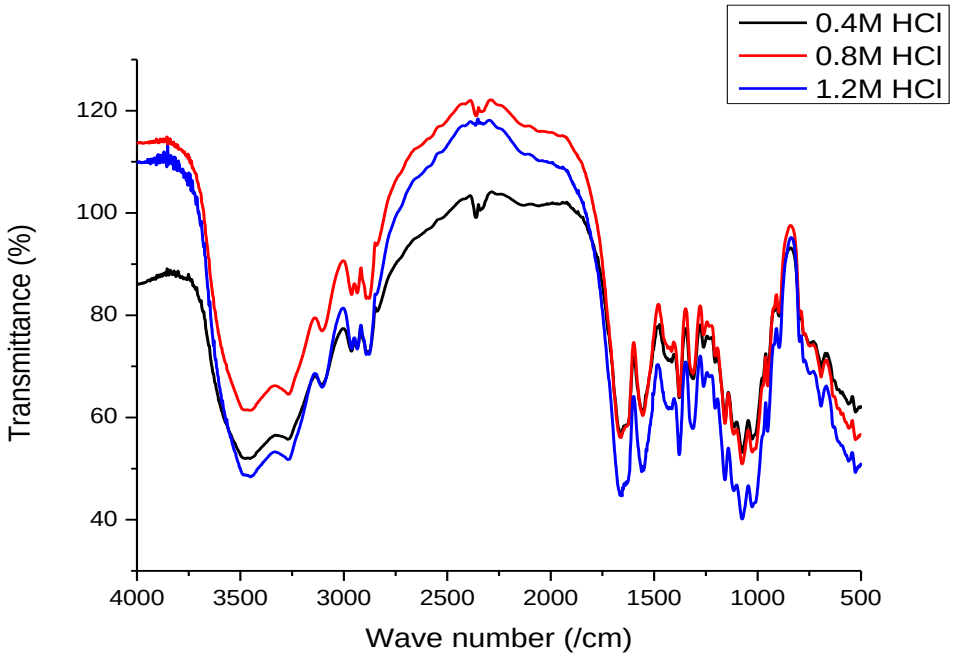

Figure G1: FTIR spectra of crab shell demineralized only at 0.4, 0.8 and 1.2M HCl

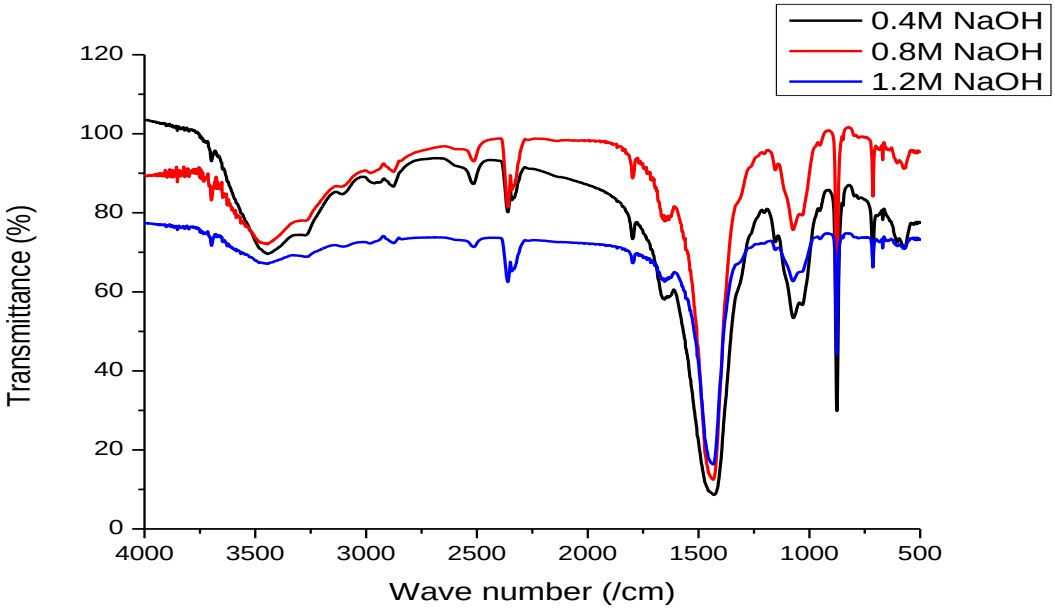

Figure G2: FTIR spectra of crab shell demineralized only at 0.4, 0.8 and 1.2M NaOH

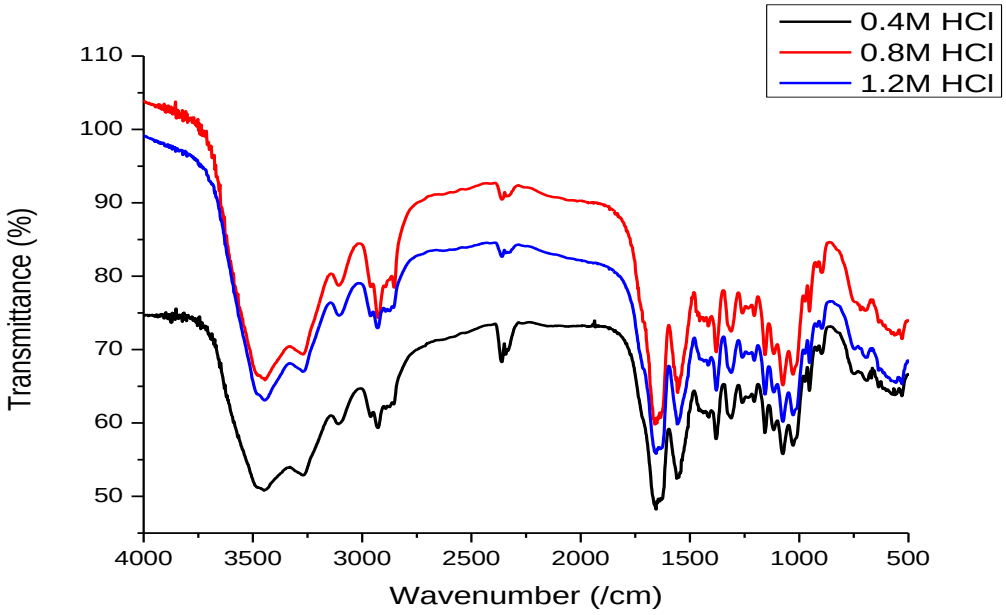

Figure G3: FTIR spectra of shrimp shell demineralized only at 0.4, 0.8 and 1.2M HCl

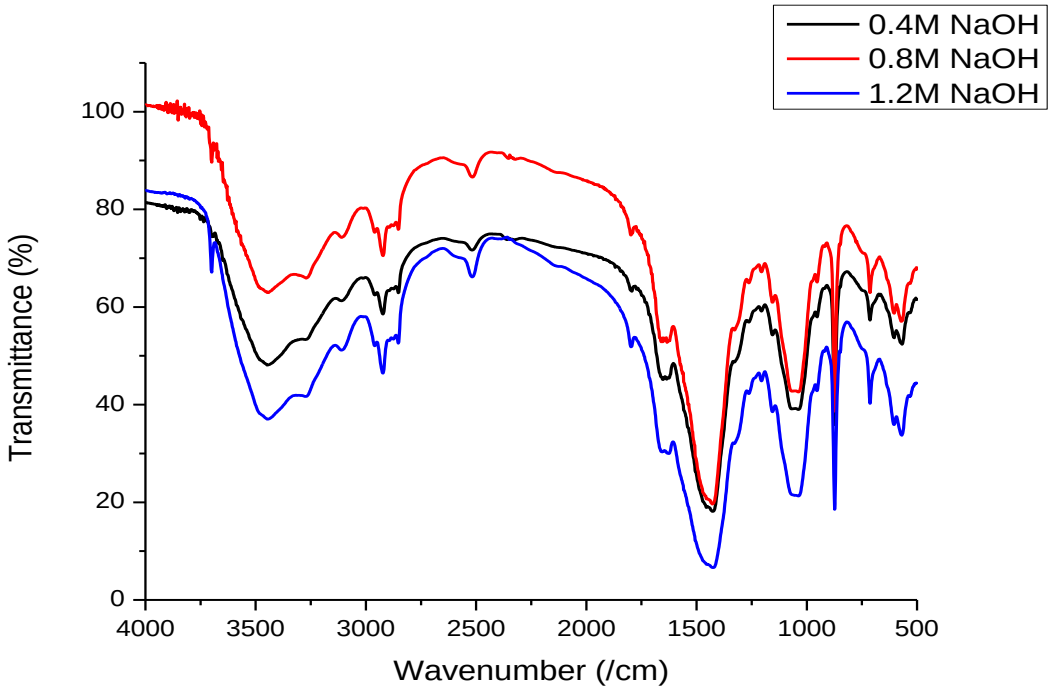

Figure G4: FTIR spectra of shrimp shell demineralized only at 0.4, 0.8 and 1.2M NaOH

H. PAPERS PUBLISHED

Gbenebor, O.P., Adeosun, S.O., Lawal, G.I., Jun, S. and Olaleye, S.A. (2017). Acetylation, crystalline and morphological properties of structural polysaccharide from shrimp exoskeleton. *Engineering Science and Technology, an International Journal*, ***20***, 1155–1165.

Gbenebor, O.P., Adeosun, S.O., Lawal, G.I., and Jun, S. (2016). Role of $CaCO_3$ in the physicochemical properties of crustacean-sourced structural polysaccharides. *Materials Chemistry and Physics*, ***184***, 203-209.

Adeosun, S.O., Lawal, G.I. and **Gbenebor, O.P**. (2014). Characteristics of biodegradable implants. *Journal of Minerals and Materials Characterization and Engineering*, ***2*****(2)**, 88-107.